Real Mirror Symmetry

and

The Real Topological String

Daniel Krefl

München 2009

Real Mirror Symmetry
and
The Real Topological String

Daniel Krefl

Dissertation

an der Fakultät für Physik

der Ludwig–Maximilians–Universität

München

vorgelegt von

Daniel Krefl

aus Bergisch Gladbach

München, Mai 2009

Erstgutachter: Prof. Dr. Dieter Lüst

Zweitgutachter: Prof. Dr. Wolfgang Lerche

Tag der mündlichen Prüfung: 02.07.2009

Abstract

This thesis is concerned with real mirror symmetry, that is, mirror symmetry for a Calabi-Yau 3-fold background with a D-brane on a special Lagrangian 3-cycle defined by the real locus of an anti-holomorphic involution. More specifically, we will study real mirror symmetry by means of compact 1-parameter Calabi-Yau hypersurfaces in weighted projective space (at tree-level) and non-compact local $\mathbb{P}^2$ (at higher genus).

For the compact models, we identify mirror pairs of D-brane configurations in weighted projective space, derive the corresponding inhomogeneous Picard-Fuchs equations, and solve for the domainwall tensions as analytic functions over moduli space, thereby collecting evidence for real mirror symmetry at tree-level. A major outcome of this part is the prediction of the number of disk instantons ending on the D-brane for these models.

Further, we study real mirror symmetry at higher genus using local $\mathbb{P}^2$. For that, we utilize the real topological string, that is, the topological string on a background with O-plane and D-brane on top. In detail, we calculate topological amplitudes using three complementary techniques. In the A-model, we refine localization on the moduli space of maps with respect to the torus action preserved by the anti-holomorphic involution. This leads to a computation of open and unoriented Gromov-Witten invariants that can be applied to any toric Calabi-Yau with involution. We then show that the full topological string amplitudes can be reproduced within the topological vertex formalism. Especially, we obtain the real topological vertex with trivial fixed leg. Finally, we verify that the same results arise in the B-model from the extended holomorphic anomaly equations, together with appropriate boundary conditions, thereby establishing local real mirror symmetry at higher genus. Significant outcomes of this part are the derivation of real Gopakumar-Vafa invariants at high Euler number and degree for local $\mathbb{P}^2$ and the discovery of a new kind of "gap" structure of the closed and unoriented topological amplitudes at the conifold point in moduli space.

Contents

Part I

Overview

Chapter 1

Introduction

1.1 Motivation

During the last century, two complementary, but fundamentally different theories describing very successfully particular corners of the physical world emerged. Namely, Einstein's general relativity and quantum field theory (to which we will sometimes refer to just as QFT). Over the time, both theories have passed many experimental tests to very high accuracy and nowadays there is no doubt that at least in certain regions of parameter space these theories form the framework to describe the fundamental laws of nature.

Einstein's theory describes gravity, the weakest of the four fundamental forces we observe, by promoting space-time, more precisely the metric, to be a dynamical field itself with equations of motion given by Einstein's field equations (which reduce to Newton's law of gravity in an appropriate approximation). Roughly speaking, the major conceptual idea behind Einstein's theory is that matter (=energy) backreacts on the geometry in a way that it curves the surrounding space-time. The force of gravity we observe is in this sense just an artifact of a non-trivial space-time geometry.

However, general relativity starts to break down for large curvatures, respectively strong gravitational fields. Perhaps the most impressive example being the formation of black holes. The pure existence of these singularities in the classical theory points towards the existence of a more complete fundamental theory which remains valid even at strong curvature and for which general relativity constitutes only an effective description.

Quantum field theory, on the other hand, is the framework in which to describe the remaining three fundamental forces we observe, that is the strong, weak, and electro-magnetic interactions. As the name suggests, it is intrinsically quantum, that means quantum me-

chanics forms its conceptual foundation. Here, the basic idea behind is that the forces are mediated via the exchange of specific particles, more precisely field quanta. These are the gluons for the strong interaction, the W and Z bosons for the weak interaction and the photon for the electro-magnetic interaction. All three interactions are summarized in the so-called Standard Model, a gauge theory with gauge group $SU(3) \times SU(2) \times U(1)$. Up to some minor issues, like for example the still to be observed Higgs-field, responsible for the generation of the gauge boson masses via spontaneous symmetry breaking (however expected to be discovered at latest with the next generation of particle accelerators), and non-vanishing Neutrino masses (pointing towards a slight extension of the Standard Model), all predictions made by the Standard Model have been verified with excellent accuracy.

However, there are many indications that the Standard Model is again only an effective theory which has to be replaced at high energies by some more fundamental underlying theory. Besides more aesthetical reasons, like for example the many parameters one needs to put in by hand or, more specifically, the hierarchy and naturalness problems, the whole process of regularization and renormalization needed to make sense of loop amplitudes (by introducing an ultra-violett (for short UV) cutoff) points towards the existence of a more complete theory which is effectively described by the Standard Model at low energies. The more aesthetical open questions in the Standard Model might be (at least partially) answered by a grand unified theory (practically meaning the embedding of the Standard Model gauge group into some bigger gauge group, for example into $SU(5)$) or some kind of supersymmetric extension thereof (usually, however, the many parameter problem becomes even worse with supersymmetry). Besides phenomenological reasons, like for example the prediction of gauge coupling unification, supersymmetric theories are appealing because they are usually better behaved in the UV. However, even with supersymmetry, in general quantum field theories describing point-like particles are not UV finite. One might see the source of the divergences in the fact that in such theories interactions are localized at points in space-time, and thus they can not be avoided as long as one stays in this formalism.

The upshot is, that it is more than evident that both, general relativity and quantum field theory (*i.e.*, the Standard Model) are just effective theories approximately describing a more fundamental underlying theory. The best hope one might have is that both theories are an effective description of a single underlying theory, albeit describing different aspects of it. The existence of a single underlying theory, unifying general relativity and quantum field theory, is not obvious at all but not totally un-expectable. In order to make this a

bit more precise, recall that general relativity is a purely classical field theory, valid for weakly curved space-time. In the regime of quantum physics, space-time is locally flat and gravity negligible. On the other hand, in the large scale domain (which is naturally weakly curved), where gravity becomes relevant, quantum effects and hence a quantization of gravity become negligible. Only if we leave the range of validity, that is, going to strong curvature, respectively very high energies, we should introduce some kind of quantum field theory of gravity (which then naturally should unify with the Standard Model or some extension thereof). However, most likely this will not be a consistent theory, because the gravitational interaction becomes too divergent in this regime. Rather, a new theory needs to be introduced, which reconciles the interactions in a unified, intrinsically UV finite, framework.

Luckily, we already have a promising framework at hand into which such a theory might fit. Namely, (super) string theories, about which we will say a bit more in the next section. However, before doing that, let us conclude this motivation by saying some words on why it is interesting at all to look for such a theory, besides pure intellectual curiosity.

From a high energy experimental physicist's point of view, the question for such a unified theory incorporating quantum gravity might at first look very irrelevant, since on the one hand, gravity becomes strong at the Planck scale, which is far out of reach of any (foreseeable) accelerator experiment, and on the other hand, it seems more likely that many of the immediate questions left open by the Standard Model will be answered by an extension (UV completion) thereof in terms of an ordinary quantum field theory. However, one should always keep in mind that nothing is set in stone as long as we haven't probed higher energy scales via experiment. The underlying assumptions for the large separation of scales used in this argument are in fact quite conservative. For example, there are theoretical ideas in terms of extra-dimensional theories, which allow to lower the scale at which gravity becomes strong to scales accessible by future accelerator technology. So it might be that already at (soon) observable energy scales something interesting happens which calls for a theory of quantum gravity to be fully explained.

Whereas it is very likely that we can still make a lot of progress in physics beyond the Standard Model without a full fledged unified theory, the question of a theory of quantum gravity becomes more pressing if we want to understand better the physics of the (very) early universe or black hole physics. These are systems in extreme conditions, in the sense that we are at very high energies, respectively strongly curved space-time, where, as outlined before, the conventional physical theories start to break down and a

new formulation is needed. Turning things around, if at all, most likely experimental evidence or constraints on a unified theory might come from (indirect) cosmological or astrophysical observations.

Finally, one should also keep in mind that the quest for such a theory, especially research in string theory, is a trigger and accelerator for research in mathematics, unveiling many unexpected relations and leading to many new and beautiful mathematical structures and methods, which will finally find their way to applications in other (perhaps practically more useful) scientific fields.

1.2 (Super) string theory

As mentioned in the previous section, we would like to have a UV finite theory, however ordinary quantum field theories, describing point-like particles, intrinsically diverge due to point-like interaction regions. Perhaps the most conservative approach to write down a (possibly) UV finite theory would be to consider extended objects instead (the interaction regions are then naturally spread out over space, implying a better UV behavior), but still sticking to general principles, like for example the Hamiltonian principle, Lorentz invariance, unitarity, *etc.*. In this sense, the simplest conceptual change to resolve the UV divergence problem would be to give up the picture of point-like particles and instead promote 1-dimensional objects (strings) to be the fundamental identities of matter (whose length is so small that they look effectively 0-dimensional at currently achievable energies).

More concretely, a string possesses a tension $T = (2\pi\alpha')^{-1}$, where α' is the so-called Regge-slope related to the length l_s of the string via $l_s^2 = \alpha'$, which constitutes the only fundamental constant of a theory describing strings. Naturally, there is a (low-energy) limit, *i.e.*, $\alpha' \to 0$, in which the string shrinks to a point and there we should recover an effective description in terms of quantum field theory.

Besides the center of mass motion, strings have in comparison to point-like particles additional degrees of freedom in terms of an infinite tower of (quantized) oscillator modes. Different oscillation modes of a string give rise to different kinds of particles in the low-energy limit.

Theories describing such strings as fundamental entities are called (super) string theories (and the scientific field is usually referred to just as string theory). String theories are indeed not only intrinsically UV finite, but automatically include a spin-2 particle in their spectra, identifiable with the graviton. Hence, string theories predict gravity and are

therefore (for this and other reasons) currently the most promising candidates for a more fundamental theory underlying general relativity and the Standard Model.

The simplest string theory one may consider is the so-called bosonic string. Since it does not contain fermions in its massless spectrum and is further unstable due to a tachyon, it should be seen rather as a toy-model than as a realistic candidate for the unified theory we are after.

In better shape are the so-called super string theories (of which there are five types known of: Type I with $SO(32)$ gauge group, Type IIA, Type IIB and two heterotic theories with gauge group $SO(32)$ and $E_8 \times E_8$, respectively). These theories are intrinsically supersymmetric and as a consequence possess space-time fermions. Further, tachyons are not present (due to the so-called GSO projection).

The super string theories of relevance for this thesis are the two Type II theories. Everything that follows in the remainder of this section should be thought of in this context (albeit much of it translates one-to-one to the other theories). For completeness, we just mention that super string theories are not the end of the story, in the sense that they are not fundamental by themselves. In detail, the different super string theories are related by a web of dualities (for a definition of duality, see the next section) and are expected to constitute just effective descriptions for different aspects of a single underlying theory, dubbed M-theory.

In order to set the stage and introduce some notations, let us briefly recall some (for our purposes sufficient) basics of string theory (for more complete textbook treatments, see for instance [1]). Similar to a point particle that sweeps out a worldline during time evolution and whose classical (relativistic) action is basically equal to the length of the wordline, a string sweeps out a 2-dimensional worldsheet, usually denoted as Σ, with classical action being proportional to the area of Σ. The action defines a classical 2-dimensional (super-) conformal field theory, which, after quantization, becomes a 2-dimensional (super-) conformal QFT. From the worldsheet point of view, topologically non-trivial worldsheets correspond to interactions of strings, since such non-trivial worldsheets arise by joining and splitting of propagating strings. Note that a string, as a 1-dimensional object, can have two different topologies. Namely, it can be either a line or a circle, hence there are two basic types of strings to consider. Open strings (lines) and closed strings (circles). Further, a string can be oriented or unoriented.

The sum over all possible worldsheet topologies defines string perturbation theory, where higher topologies are suppressed by powers of the string coupling constant g_s (which,

however, is not a fundamental constant, but rather determined by the vacuum expectation value of the so-called dilaton field). In more detail, the worldsheets are Riemannian surfaces classified according to their Euler number $\chi = 2 - 2g - h - c$, where g is the genus, h the number of boundaries (holes) and c the number of crosscaps (making a surface non-orientable). The weighting of a surface in terms of g_s is simply g_s^χ.

Roughly speaking, closed strings can be associated with the background space-time geometry (the bulk), that is, they mediate the gravitational interaction and ultimately should (in a background independent formulation of string theory, which we, however, do not possess yet) dynamically create the space-time background it propagates in. Physically, one might expect (or hope) that the vacuum (target-) space the string propagates in is approximately flat four dimensional Minkowski space. However, this is not the case. Consistency of the quantization of the string requires that space-time has more than four dimensions (ten for superstring theories). Hence, string theory predicts extra dimensions, with all the wide-ranging consequences coming with it (for one amazing possible consequence, see for example the end of the last section)!

In order to account for this apparent mismatch with observation, one assumes that the extra six dimensions are compact and very small (at least smaller than the length scale accessible with currently available accelerators), as is familiar from Kaluza-Klein theory.

In the weak coupling ($g_s \to 0$) and low energy limit ($\alpha' \to 0$), the (perturbative) closed string sectors of the Type II theories are effectively described by supergravity. In this formalism, one makes an Ansatz for the non-trivial space-time background of the form $\mathbb{R}^{1,3} \times X$, where X denotes the (internal) compact space formed by the extra six dimensions. Consistency, in terms of preservation of ($\mathcal{N} = 2$) supersymmetry, constrains X to be a Calabi-Yau 3-fold, that is, a complex Kähler manifold with vanishing first Chern class (more general solutions are also possible if one allows for a non-trivial 3-form background). Note that each member of the large (perhaps infinite) set of possible internal background configurations, *i.e.*, Calabi-Yau 3-folds, comes with additional degrees of freedom. Namely, the choice of Kähler class (volumes), and choice of a complex structure (shape) of X.

In the effective four dimensional theory arising after Kaluza-Klein reduction of the original theory on X, these additional degrees of freedom will be parameterized by massless fields (moduli) in the effective action, which one ultimately needs to get rid of for phenomenological consistency (usually referred to as stabilizing the moduli, a topic on which there has been lots of progress in recent years; however, for our purposes bulk moduli stabilization is not of concern and we refer the interested reader to [2] for a comprehensive

review on this topic.). In detail, in Type IIA, the Kähler structure is represented by $h^{(1,1)}$ massless vector multiplets and the complex structure in terms of $h^{(2,1)}$ massless hypermultiplets, while in Type IIB the role of vector and hypermultiplets are exchanged. Here, $h^{(p,q)}$ denote the Hodge numbers of X (which are topological invariants).

Note that the total moduli space factorizes locally (at least at the two-derivative level) as $\mathcal{M}_{tot} = \mathcal{M}_H \times \mathcal{M}_V$, where $\mathcal{M}_H$ denotes the moduli space of the hypermultiplets and $\mathcal{M}_V$ of the vectormultiplets. Since the dilaton field (determining the value of g_s) belongs to the hypermultiplets and can not couple to the vectormultiplets (since $\mathcal{M}_{tot}$ factorizes), we deduce that $\mathcal{M}_V$ does not receive any perturbative corrections in g_s. Thus, in Type IIA, the moduli space $\mathcal{M}_K$ of the Kähler structure can only receive corrections perturbative in α' and non-perturbative corrections, while in Type IIB, the moduli space $\mathcal{M}_{CS}$ of the complex structure is corrected only non-perturbatively.

One should note that in order to stay in the supergravity approximation, not only the overall volume of X, but also the volumes of all cycles therein need to be relatively large in comparison to l_s. The reason for this is that with decreasing volumes of cycles, quantum corrections (for example in Type IIA due to non-perturbative worldsheet instantons) become stronger and start to blur classical notions of geometry until finally near l_s, classical concepts totally break down and have to be replaced by some sort of stringy geometry.

Open strings perturbatively describe Dp-branes, *i.e.*, $(p+1)$ dimensional subspaces of space-time where they can end on (often we will suppress the p and just say D-branes). However, despite this perturbative description in terms of open strings, one should always keep in mind that Dp-branes themselves are dynamical objects which intrinsically are of non-perturbative nature.

The massless open string spectrum contains a $U(1)$ gauge field, which can be thought of as living on the respective D-brane. If multiple, say N, D-branes overlap, the massless open string spectrum gives rise to a non-abelian $U(N)$. In addition, the spectrum contains a set of complex scalars, which parameterize the normal degrees of freedom of the D-brane *i.e.*, the D-brane moduli (in some cases the normal directions need to be complexified, for example via Wilson-lines in the case of D6-branes).

In the supergravity approximation, D-branes can be seen as wrapped over cycles of X and give rise to supersymmetric gauge theories in the low-energy limit (under certain conditions on the cycles, *i.e.*, the D-brane needs to be a $\frac{1}{2}$-BPS state in the bulk theory).

From the low-energy effective theory point of view, D-branes are sources for certain Ramond-Ramond (for short RR) fields of the (low-energy) bulk theory. From Gauss law

we infer that their total charge (with compact support) needs to cancel. Since D-branes are always positively charged, we can either introduce none of them in a compact background, or we need some other negatively charged objects. From a string theoretic point of view, one can see the requirement of charge cancellation in the low-energy theory as reminiscent of cancellation of tadpoles in string loop amplitudes (therefore one usually refers to charge cancellation also as tadpole cancellation). The prototypical example is given by the total 1-loop amplitude in Type I theory (that is the sum of torus, Klein-bottle, annulus and Möbius-strip). In detail, while the torus amplitude is itself intrinsically UV finite, the remaining amplitudes are only finite as sum, with a specific choice of number of D9-branes and sign in the Möbius-strip amplitude, explaining the famous $SO(32)$ group for Type I strings mentioned above.

The Type I example immediately tells us how to find the negatively charged objects to chancel the D-brane charge. Namely, instead of considering a purely oriented theory, we need to consider in addition an unoriented sector. For that, we perform a so-called orientifold projection of the Type II theories, that is, we mod out by $I \circ P$, where P denotes worldsheet orientation reversal and I is an involutive symmetry of the target space X (that means, we project to states invariant under the combined action of P and I). Note that this introduces open strings in the Type II theories as well, which are otherwise only theories of closed strings. For Type IIB, the involution I needs to be holomorphic, while for Type IIA anti-holomorphic. The fixed-point locus in X under the action of I defines an orientifold plane (for short Op-plane, where p denotes the dimensionality). These planes are not dynamical (at least at weak coupling), however, they are sources for RR-fields and constitute the negatively charged objects we are looking for.

To be more explicit, let us stick in the following to the Type IIA theory. Note that the Type IIA string supports only even dimensional D-branes (while the Type IIB string only odd dimensional ones, wrapped on holomorphic cycles). For a space-time filling D6-brane (which is wrapped on a 3-cycle of X), the $\frac{1}{2}$-BPS supersymmetry condition is that the wrapped 3-cycle is special Lagrangian (for short sLag). In physical terms, the Lagrangian property tells us that the D6-brane can only host a flat $U(1)$ bundle, while special means that the D6-brane needs to minimize its volume. Note that for general X, the only systematic construction of sLag cycles is in terms of fixed-point loci of anti-holomorphic involutions.

For an appropriate choice of wrapped cycles, different D-branes may intersect. The strings spanned between two different D-branes (actually the strings are localized to the

intersection area) give rise to chiral matter charged under the respective gauge groups. Thus, the open string sector possesses all necessary ingredients for the Standard Model, and one might hope that one can engineer it in the effective theory via a suitable choice of D-brane setup. However, despite a lot of effort, so far this hope has not been fully materialized. Besides some more down to earth problems like unwanted (exotic) matter or unrealistic couplings, there are as well some deeper unsolved conceptual issues, like for example gauge coupling unification or breaking of supersymmetry.

Time has to show if one can overcome these issues, or if other approaches to perform model building in string theory, like for example the recent F-theory attempts, are more promising.

However, one should always keep in mind, that so far model building in Type II theories is limited to a very small region (presumably of measure zero) in the full space of possible solutions (usually referred to as landscape). In detail, technical limitations constrain the accessible part to the weakly coupled region and either to special points in moduli space of X where an explicit worldsheet CFT description is available (for instance orbifold points) or to regions with large radii X where the supergravity approximation is applicable and classical notions like D-branes wrapping cycles, *etc.*, apply.

Hopefully, some of the model building issues mentioned above might be resolved via models sitting deeper in moduli space (for which recent F-theory developments indeed give some hints to). Thus, it would be very desirable to develop technologies to enter this regime.

The motivation and aim of this thesis is, however, not directly concerned with extending Type II model building perspectives (although it certainly does provide new insights for that), but rather to understand better the notion of quantum, respectively stringy geometry, that is, how classical geometric notions are modified due to non-perturbative quantum corrections. In this thesis, we focus on one specific sector of quantum effects, namely worldsheet instantons. Basically, a worldsheet instanton is a worldsheet wrapped over an element of $H_2(X, \mathbb{Z})$ (or an appropriate generalization thereof for open string worldsheets, *i.e.*, relative homology groups). Mathematically, the worldsheet instantons correspond to maps from the string worldsheet (at tree-level a sphere for the closed string and a disk for the open string) into X. Hence, determining them amounts to count all those maps appropriately, which forms a mathematically non-trivial problem in enumerative geometry (for certain types of backgrounds, there are however mathematical techniques to explicitly calculate them, see chapter 7).

The physicist's tool to study/determine these wordsheet instanton corrections is mirror symmetry and the topological string, as we will outline in the next section.

1.3   Mirror symmetry

Perhaps the simplest example of a duality in super string theory is T-duality, which played a major role in uncovering the web of dualities between the superstring theories mentioned in the last section. Especially, T-duality is the equivalence of Type IIA string theory compactified on a circle of radius R with Type IIB on a circle of radius $1/R$ (or vice versa). Generally, the term duality stands for a non-trivial equivalence of seemingly different physical theories. Some dualities may even relate theories which are in the deep quantum regime to pure classical ones. Thus, dualities may open up regions in parameter space of some theories, which have not been accessible before. Albeit not of relevance for our purposes, Maldacena's AdS/CFT correspondence is nowadays perhaps the most known example of such a duality (with overwhelming evidence, but still unproven). In detail, Maldacena's original conjecture is the equivalence of Type IIB supergravity on $AdS_5 \times S^5$ and (strongly coupled) $\mathcal{N} = 4$ super (conformal) Yang-Mills.

The duality that forms the underlying conceptual core of this thesis, is mirror symmetry (for textbook level introductions, see for instance [3]). It conjectures that for every Calabi-Yau 3-fold, X, there exists a different ("mirror") Calabi-Yau 3-fold, Y, such that Type IIB compactified on the one, is equivalent to Type IIA on the other (if the Strominger-Yau-Zaslow conjecture is true, *i.e.*, that one can see every Calabi-Yau 3-fold as a $\mathbb{T}^3$ fibration, mirror symmetry may actually boil down to T-duality). Especially, the cohomology dimensions of X and Y are related via $h_X^{(p,q)} = h_Y^{(3-p,q)}$, *i.e.*, via a diagonal reflection of the Hodge diamond. Thus, the Kähler structure of X is swapped with the complex structure of Y (cf. previous section) and vice versa.

As a side remark, one should note that while the statement of mirror symmetry seems to be generally true, there are some subtle cases like rigid manifolds for which there is no obvious geometric mirror, but rather the mirror is expected to be given by some kind of non-geometric compactification, of which (presumably) there is only a CFT description available.

Recall from the previous discussion that in Type IIA on X the Kähler moduli space $\mathcal{M}_K$ (parameterizing the volumes of cycles) is corrected only perturbatively in α' and non-perturbatively, especially by worldsheet instantons (wrapped on elements of $H_2(X, \mathbb{Z})$).

Under mirror symmetry, $\mathcal{M}_K$ is identified with $\mathcal{M}_{CS}$ of Type IIB on Y which is corrected only non-perturbatively. However, under mirror symmetry, the even homology of X gets mapped to $H_3(Y, \mathbb{Z})$, and since there are no D2-branes in Type IIB, there are no corresponding non-perturbative corrections and the classical moduli space is exact! Thus, using mirror symmetry, we can determine the effect worldsheet instantons have on the geometry. To be more explicit, in terms of the period integrals (which one may view as quantum volumes), the statement of (closed string) mirror symmetry can be summarized in a single equation:

$$
\begin{array}{ccc}
\text{IIB on } Y & & \text{IIA on } X \\
\Pi^\alpha = \displaystyle\int_{\Gamma_\alpha} \Omega & = & \displaystyle\int_{\Gamma_i^{(2k)}} (\wedge J^{(1,1)})^k + \text{n.p.} \\
\sim (\ln z_a)^k + \mathcal{O}(z) & & \sim t_i^k + \mathcal{O}(e^{-t}) \,,
\end{array}
\tag{1.1}
$$

where Π^α stands for the period integral, $\Gamma_i^{(2k)}$ is a $2k$-cycle of X, Γ_α a 3-cycle of Y, J denotes the Kähler form of X, t the Kähler parameters of X, Ω the unique holomorphic 3-form of Y, z the complex structure parameter of Y and n.p. stands for the non-perturbative corrections in terms of worldsheet instantons.

Especially, for $k = 1$, this equation includes the map between the Kähler moduli of X and the complex structure moduli of Y, the so-called mirror map. Note that the Kähler parameters t_i determine flat-coordinates of the complex structure moduli space of Y, *i.e.*, the coordinates $z_a(t_i)$ are flat.

For example, the periods Π^α form the building block out of which the $\mathcal{N} = 2$ prepotential $\mathcal{F}^{(0)}$ can be constructed, which encodes the gauge coupling and the Kähler potential in the four-dimensional low-energy effective space-time theory. In the Type IIB side, $\mathcal{F}^{(0)}(z)$ can be calculated exactly. Especially, the periods $\Pi^\alpha(z)$ fulfill a system of (higher order) differential equations, usually called Picard-Fuchs system (as one easily infers from variation of the Hodge structure, see for instance [4] for a short introduction to this topic),

$$
\mathcal{L}_a \Pi^\alpha(z) = 0 \,,
\tag{1.2}
$$

where $\mathcal{L}_a$ are the Picard-Fuchs (differential-) operators with $a \in \{1, \ldots, h_X^{(1,1)}\}$, allowing for a straight forward computation of $\Pi^\alpha(z)$.

Having obtained the periods, we can express the prepotential in terms of the Type IIA Kähler parameters via the mirror map and extract the (tree-level) worldsheet instanton contributions, that is, the number of maps $\mathbb{P}^1 \to X$.

The upshot is, using mirror symmetry, we can extract the quantum corrections in the Type IIA theory from a purely classical computation in Type IIB.

1.4   Overview and outline

The consideration so far was purely in terms of the bulk, *i.e.*, pure closed string, sector. However, as outlined in section 1.2, the Type II models of interest possess in addition an open and unoriented sector. Whereas mirror symmetry for the pure bulk theory has been studied very extensively over the years and is nowadays well established and understood, mirror symmetry including D-branes in contrast is still very elusive, especially on compact backgrounds. However, important progress has been made in recent years.

The inclusion of D-branes breaks the bulk $\mathcal{N} = 2$ supersymmetry down to $\mathcal{N} = 1$ and the quantity of interest becomes the space-time superpotential $\mathcal{W}$ of the D-brane gauge theory, which is generally a holomorphic function of the closed and open string moduli. Recall from section 1.2 that the open string moduli parameterize the possible deformations of the D-brane embedding inside X. Especially, we are interested in Type IIA D-branes, which we will also refer to as A-type branes. The possible deformations are counted by the first Betti number of L, *i.e.*, $b_1(L)$, where L denotes the (sLag) cycle wrapped by the (A-type) D-brane.

If we for example take a D-brane with a single open string modulus u, the supersymmetric vacua of the D-brane theory sitting at two different points, say at u_1 and u_2, are expected to be separated by a domainwall, whose tension $\mathcal{T}$ is given by

$$\mathcal{T} = \mathcal{W}(u_2) - \mathcal{W}(u_1)\,. \tag{1.3}$$

If u is a modulus and hence a flat-direction of the superpotential, we have that $\mathcal{T} = 0$. However, generally, for A-type D-branes the deformations are obstructed by quantum effects, which is reflected in a non-vanishing $\mathcal{T}$. In other words, the classical geometry gets replaced by some sort of quantum geometry which possesses less degrees of freedom. Thus, in order to stabilize the D-brane moduli (to obtain a phenomenologically viable model), it is very important to quantify such quantum effects.

Especially, in the open string sector we have (non-perturbative) worldsheet instantons with the topology of a disk, where the boundary is located on the D-branes. For a single D-brane, these are counted by all maps $f : D \to X$, with $f(\partial D)$ on $L \subset X$ (where D stands for a disk), *i.e.*, with image in the relative homology group $H_2(X, L; \mathbb{Z})$.

Intuitively, it is clear why disk instantons lift (at least some) of the open string moduli. The reason is simply that the worldsheet energetically prefers to minimize its volume, that is, prefers a representative in the relative homology group with this property and, if possible, the D-brane adjusts accordingly.

In (toric) non-compact models, it has been known already for some time how to determine exactly the disk instanton contributions to the domainwall tension, respectively superpotential for a specific class of branes, namely toric branes. As in the pure closed string case, mirror symmetry plays a major role, since the statement of open string mirror symmetry translates the computation of $\mathcal{T}$ to a purely classical computation on the mirror B-side. More specifically, the mirror D-branes are D5-branes wrapped on holomorphic curves, denoted as C (whose explicit parameterization is easy to deduce for toric branes in local models), and the computation of $\mathcal{T}$ boils down to dimensional reduction of Witten's holomorphic Chern-Simons functional on the D5-branes, which just yields Abel-Jakobi type integrals evaluated on 3-chains Γ with boundary $\partial\Gamma = C - C_*$ (equal to the difference of two possible positions of a D5-brane) [5], *i.e.*, one has

$$\mathcal{T} = \mathcal{W}(C) - \mathcal{W}(C_*) = \int_\Gamma \Omega . \tag{1.4}$$

As has been worked out in [6, 7], one can as well take the Hodge theoretic point of view in this context, and derive an associated extended Picard-Fuchs system for a relative period vector which includes in addition the superpotential/domainwall tension.

For compact geometries, however, the story is more involved. First of all, as mentioned previously, in Type IIA, the only systematic construction of sLag 3-cycles in general X known so far is as fixed-point loci of anti-holomorphic involutions. Therefore, for the time being, one has to stick to D-branes on such 3-cycles, usually referred to as real branes. The question then arises what the appropriate mirror configuration is. Since general B-type D-branes are best described via matrix factorizations (for a nice overview, see [8]), the question boils down to find the corresponding matrix factorization of the real brane. But even with the mirror matrix factorization at hand, it is a priori not clear how to extract the corresponding curves wrapped by the mirror D5-branes and what the analog of the Chern-Simons functional should be. However, important progress has been made recently.

As pioneered by Walcher and Morrison [9] on the basis of the quintic, for a real brane with $H_1(L, \mathbb{Z}) = \mathbb{Z}_2$ (hence with discrete modulus), the appropriate (mathematical) concept (in the B-model geometry) is that of a Hodge theoretic normal function. In more detail, from a matrix factorization one can extract algebraic curves representing the brane vacua

via the algebraic second Chern class. If the algebraic cycle is homologically trivial, it yields a normal function ν such that $\mathcal{T} = \nu$. Especially, for holomorphic curves, $\mathcal{T}$ reduces to (1.4). Furthermore, one can then show that $\mathcal{T}$ fulfills an inhomogenous Picard-Fuchs equation of the form

$$\mathcal{L}\mathcal{T}(z) = c\sqrt{z}\,, \tag{1.5}$$

where $\mathcal{L}$ is the Picard-Fuchs operator of the bulk geometry, and c a normalization constant. That $\mathcal{T}$ fulfills (1.5) has been argued already before by Walcher [10]. Especially, c was determined there via monodromy considerations and localization on the moduli space of stable maps.

Solving (1.5) and plugging in the mirror map, one obtains the quantum corrected A-model domainwall tension, thereby establishing real mirror symmetry (that is, mirror symmetry for the bulk plus a D-brane on the real locus).

In part II of this thesis, based on the publication [11] done in collaboration with J. Walcher, we pick up this approach and generalize the concept of real mirror symmetry to the remaining 1-parameter Calabi-Yau hypersurfaces (in weighted projective space). One of the outcomes will be explicit integer numbers for disk instantons (or better BPS states) ending on the real brane, *i.e.*, in terms of Ooguri-Vafa invariants (see table 2.1).

So far, our considerations were purely at tree-level. However, as is clear, there will be worldsheet instanton corrections of higher genus as well, *i.e.*, maps of a genus g Riemannian surface $\Sigma^{(g)}$ for the closed string, and maps of a genus g surface with h boundaries (ending on L), denoted as $\Sigma^{(g,h)}$, into X. These corrections again possess an integer expansion, *i.e.*, into Gopakumar-Vafa invariants [12, 13], respectively Ooguri-Vafa invariants [14], counting certain BPS states (see section 9.3).

It is by now well known that the generating function counting maps $\Sigma^{(g)} \to X$ is given by the closed string topological string free energy $\mathcal{F}^{(g)}$ (we postpone a basic introduction to topological strings to chapter 9). Similarly, the open topological string free energy $\mathcal{F}^{(g,h)}$ is the generating function for counting maps $\Sigma^{(g,h)} \to X$. Thus, the quantification of worldsheet instantons amounts to compute the topological amplitudes.

There has been a lot of progress in closed and open topological string theory in the last couple of years. The improved understanding concerns in particular local (non-compact) backgrounds defined by toric Calabi-Yau manifolds together with toric branes on top. However, while many lessons were learned (for reviews see for instance [15, 16]), it has long been unclear how they would apply to compact backgrounds, which indeed remains the challenging case to understand in general.

Recently, it has become clearer that there are significant qualitative distinctions between the non-compact and compact settings. Perhaps the most dramatic additional ingredient is a topological analogue [17] of the tadpole cancellation condition familiar from the type II superstring. In particular, a satisfactory BPS interpretation of the topological string amplitudes requires that one considers topological string orientifolds, whose charge precisely cancels that of the background D-branes (similar as for the superstring, as outlined in the previous section). Thus, we have to consider O-planes and D-branes defined via the fixed locus of an anti-holomorphic involution. We will refer to the resulting theory as the real topological string, and we will investigate various aspects of it in part III of this thesis, which is based on the publication [18] done in collaboration with J. Walcher.

Specifically, we will study the real topological string on the local Calabi-Yau manifold given by the canonical bundle over the projective plane (local $\mathbb{P}^2$). Among our main findings are several parallels both with the usual toric story, as well as with the real topological string on a compact manifold (cf. [17]). We hope that these connections will prove useful for both lines of investigation.

A physical motivation for the importance of the real topological string comes from considering the combined open and closed type IIA superstring with orientifold projection, which is a well-known playground for string phenomenology (recall the short outline in the previous section). As stated previously, the orientifold projection is the gauging of a discrete symmetry $I \circ P$, where I is an anti-holomorphic involution of the internal background X and P denotes parity reversal on the string world-sheet.

The world-sheets of the orientifolded theory then have general topology, in the sense that they can be oriented or unoriented and may possess boundaries and/or cross-caps. As is well known, one can represent these world-sheets as quotients $\hat{\Sigma}/\sigma$ of a closed oriented world-sheet $\hat{\Sigma}$ by an anti-holomorphic involution σ. The equivalence class of σ determines the topology of $\hat{\Sigma}/\sigma$. In the non-perturbative (in α') sector of such orientifolded type IIA, one has to consider world-sheet instantons with general topology, *i.e.*, maps from Riemann surfaces with or without boundaries and cross-caps into target-space equipped with involution.

This is what the real topological string is taylored for, *i.e.*, it includes in addition unoriented topological amplitudes capturing the unoriented maps, as will become clear in chapter 6.

A nice property of the real topological string is that local and compact backgrounds are more closely related (the real brane is usually non-toric in local settings), and hence

one can learn more for the compact case from the local real case than from the usual toric open topological string. On the other hand, some calculational techniques from the local toric case remain applicable, as we will explain in part III of this thesis.

The main outcome of this part of the thesis is the explicit calculation of a sort of "real" Gopakumar-Vafa invariants for the local model under consideration (listed in appendix C). In addition, we will observe a specific gap condition at the conifold point in moduli space, useful for the calculation of the topological amplitudes, which is expected to persist in compact models.

1.5   How to read this thesis

As apparent from the outline above, this thesis is divided into two parts, namely Real Mirror Symmetry and The Real Topological String. Both parts can be read more or less independently. The first chapter of each part gives a general overview over the respective topic and aim and summarizes the results. Thus, the first chapter constitutes the most important chapter of each part and should be read first. The remaining chapters of each part are about more specific topics and calculations and, in principle, can be read independently (the chapters of part II are a bit more closely bound than the ones of part III).

This thesis is mainly written for experts in the field, nevertheless, where appropriate, some basic background material will be given, with depth varying from chapter to chapter. The reader not familiar with basics in topological field and/or string theory, might prefer to read first the introduction sections of chapter 9. If necessary, a more extensive and detailed presentation of background material can be found in [3].

Part II

Real Mirror Symmetry

Chapter 2

Overview and conclusion of part II

In this part of the thesis, we study real mirror symmetry for one-parameter Calabi-Yau hypersurfaces in weighted projective space. We identify mirror pairs of D-brane configurations (chapter 3), derive the corresponding inhomogeneous Picard-Fuchs equations (chapter 4), and solve for the domainwall tensions as analytic functions over moduli space (chapter 5). Our calculations exemplify several features that had not been seen in previous work on the quintic or local Calabi-Yau manifolds. The presentation mainly follows the author's publication [11].

2.1   Introduction

The Calabi-Yau hypersurfaces, X, in weighted projective space, with one-dimensional Kähler moduli space, i.e., $h_{11}(X) = 1 = h_{21}(Y)$, where Y is the mirror manifold of X, are characterized by the five positive integer weights $(\nu_1, \ldots, \nu_5)$, such that $k := \sum \nu_i$ is divisible by each of the ν_i (Gepner models), and all five mutually coprime. We will denote $k/\nu_i =: h_i$. There are three models of this type (excluding the quintic) and they were considered in the early days of mirror symmetry [19, 20, 21] as the simplest class of examples to which to extend the original computation of Candelas et al. [22] on the quintic.

The manifolds of the A-model, $X^{(k)}$, are hypersurfaces of degree k in weighted projective space $\mathbb{P}^4(\nu_1, \ldots, \nu_5)$:

$$
\begin{aligned}
X^{(6)} &\subset \mathbb{P}^4(1, 1, 1, 1, 2) \,, \\
X^{(8)} &\subset \mathbb{P}^4(1, 1, 1, 1, 4) \,, \\
X^{(10)} &\subset \mathbb{P}^4(1, 1, 1, 5, 2) \,.
\end{aligned}
\tag{2.1}
$$

The corresponding mirror manifolds, $Y^{(k)}$, are resolutions of quotients of specific one-parameter families of degree k hypersurfaces by the group $G = \hat{G}/\mathbb{Z}_k$, where

$$\hat{G} = \ker\left(\prod_i \mathbb{Z}_{h_i} \to \mathbb{Z}_k\right) , \tag{2.2}$$

is the Greene-Plesser orbifold group.

$$Y^{(6)} : \frac{1}{6}\left(x_1^6 + x_2^6 + x_3^6 + x_4^6 + 2x_5^3\right) - \psi x_1 x_2 x_3 x_4 x_5 = 0 ,$$

$$Y^{(8)} : \frac{1}{8}\left(x_1^8 + x_2^8 + x_3^8 + x_4^8 + 4x_5^2\right) - \psi x_1 x_2 x_3 x_4 x_5 = 0 , \tag{2.3}$$

$$Y^{(10)} : \frac{1}{10}\left(x_1^{10} + x_2^{10} + x_3^{10} + 2x_4^5 + 5x_5^2\right) - \psi x_1 x_2 x_3 x_4 x_5 = 0 .$$

For compact Calabi-Yau manifolds, the only systematic construction of D-branes of the A-model (Lagrangian submanifolds) is as the fixed point set of an anti-holomorphic involution for some choice of complex structure on $X^{(k)}$. The Fermat point $\sum x_i^{h_i} = 0$ in complex structure moduli space is the most convenient for comparison with boundary conformal field theory and derivation of the mirror configurations.

The Fermat polynomial defining the A-model

$$\sum_{i=1}^5 x_i^{h_i} = 0 , \tag{2.4}$$

where $h_i := k/\nu_i$, is invariant under anti-holomorphic involutions acting as

$$x_i \to \phi_i^{M_i} \bar{x}_i , \tag{2.5}$$

where $\phi_i = e^{\frac{2\pi i \nu_i}{k}}$ are phases with ν_i the weights of the ambient weighted $\mathbb{P}^4 \supset X^{(k)}$. The M_i are integer, but the sets (M_i) and $(M_i + \nu_i)$ define the same involution by projective identification. The fixed-point loci, $L_{[M]}^{(k)}$, of the involutions (2.5) are special Lagrangian submanifolds of $X^{(k)}$, and can be parameterized explicitly by $x_i = \phi_i^{M_i/2} y_i$, with y_i real. When h_i is odd, two involutions differing only in M_i are equivalent (though not identical) under the global symmetry group $\mathbb{Z}_{h_i}$, hence the corresponding $L_{[M]}^{(k)}$ are isomorphic. When h_i is even, we have to distinguish whether M_i is even or odd, which yields a sign in the equation determining the real locus,

$$\sum_{i=1}^5 (-1)^{M_i} y_i^{h_i} = 0 . \tag{2.6}$$

Again, for h_i odd, M_i is equivalent to $M_i + 1$ by changing $y_i \to -y_i$.

When at least one h_i is odd, say h_5, we can solve (2.6) uniquely over the reals for y_5, and identify

$$L_{[M]}^{(k)} \cong \{(y_1, \ldots, y_4) \neq (0,0,0,0)\}/\mathbb{R}^* \cong \mathbb{RP}^3 . \tag{2.7}$$

Thus,

$$L_{[M]}^{(6)} \cong \mathbb{RP}^3, \qquad L_{[M]}^{(10)} \cong \mathbb{RP}^3 . \tag{2.8}$$

for all M. The vacuum structure of a D-brane wrapped on $L_{[M]}^{(6)}$ or $L_{[M]}^{(10)}$ (think of a D6 or D4-brane in type IIA) is therefore very similar to the quintic [10]. In detail, since $H_1(\mathbb{RP}^3, \mathbb{Z}) = \mathbb{Z}_2$, there is a discrete choice of Wilson line on the D-brane wrapping the $\mathbb{RP}^3$ such that the worldvolume gauge theory will have two vacua, which we will parameterize by the discrete modulus $\sigma = \pm 1$. A BPS domainwall separating the two vacua can be obtained by wrapping a (D4 or D2-) brane on a holomorphic disk in $X^{(k)}$ with boundary on the non-trivial one-cycle in $\mathbb{RP}^3$ and with the remaining dimensions located in space-time [10]. The corresponding domainwall tension, which we will denote by $\mathcal{T}_A$, is the basic holomorphic observable associated with the D-brane configuration. At large volume, $\mathcal{T}_A$ clearly scales as $\mathcal{T}_A \sim t$, where t is the Kähler modulus. There are then quantum corrections to $\mathcal{T}_A$ due to worldsheet (disk) instantons. Monodromy considerations around $\text{Im}(t) \to +\infty$ identical to those on the quintic (which we will review momentarily) lead us to expect an expansion[1]

$$\mathcal{T}_A = \frac{t}{2} + \left(\frac{1}{4} + \frac{1}{2\pi^2} \sum_{d \text{ odd}} \tilde{n}_d q^{d/2} \right) , \tag{2.9}$$

where $q \equiv \exp(2\pi i t)$ and $\tilde{n}_d$ are the open Gromov-Witten invariants counting holomorphic maps from the disk to $X^{(k)}$ with boundary on $L_{[M]}^{(k)}$.

The reasoning that leads to the classical terms $t/2 + 1/4$ in (2.9) takes into account that the corresponding domainwall not only changes the vacuum on the brane ($\sigma = \pm 1$), but also the value of the Ramond-Ramond four and six form flux, N_4 and N_6, through the corresponding cycles of the Calabi-Yau manifold. We have [10]

$$\mathcal{T}_A = \mathcal{W}_{(N_4+1, N_6; +)} - \mathcal{W}_{(N_4, N_6; -)} = t - \left[\mathcal{W}_{(N_4, N_6; -)} - \mathcal{W}_{(N_4, N_6; +)} \right] , \tag{2.10}$$

where $\mathcal{W}$ denotes the space-time superpotential. The second equality follows from the fact that the domainwall mediating between N_4 and $N_4 + 1$ has tension equal to t. The large volume monodromy $t \to t + 1$ acts on the vacua as follows

$$
\begin{aligned}
(N_4, N_6; +) &\to (N_4, N_6 + N_4; -) , \\
(N_4, N_6; -) &\to (N_4 + 1, N_6 + N_4; +) .
\end{aligned} \tag{2.11}
$$

---

[1]The basic fact is the exact sequence $H_2(X; \mathbb{Z}) \to H_2(X, L; \mathbb{Z}) \to H_1(L; \mathbb{Z})$ in which the generator of $H_2(X, L; \mathbb{Z}) \cong \mathbb{Z}$ is mapped to the non-trivial class in $H_1(L; \mathbb{Z}) \cong H^2(L; \mathbb{Z}) \cong \mathbb{Z}_2$.

It is not hard to see that (2.9) is the only form consistent with these constraints. We emphasize that the monodromy (2.11) as well as the "one-loop" correction $\frac{1}{4}$ in (2.9) have not yet been derived from first principles, i.e. couplings of D-branes to Ramond-Ramond flux.

When all h_i are even, as happens in our examples for $X^{(8)}$, the topological type of $L_{[M]}^{(k)}$ cannot be determined straightforwardly by the previous argument, and in fact strongly depends on M. The problem was studied in a different context in [23]. It is not hard to see that in the present case we have the following types

$$
\begin{aligned}
L_{[0,0,0,0,0]} &= \{y_1^8 + y_2^8 + y_3^8 + y_4^8 + y_5^2 = 0\} \cong \emptyset \ , \\
L_{[0,0,0,0,1]} &= \{y_1^8 + y_2^8 + y_3^8 + y_4^8 - y_5^2 = 0\} \cong \mathbb{RP}^3 \cup \mathbb{RP}^3 \ , \\
L_{[0,0,0,1,0]} &= \{y_1^8 + y_2^8 + y_3^8 - y_4^8 + y_5^2 = 0\} \cong S^3 \ , \\
L_{[0,0,0,1,1]} &= \{y_1^8 + y_2^8 + y_3^8 - y_4^8 - y_5^2 = 0\} \cong (S^1 \times S^2)/\mathbb{Z}_2 \ , \\
L_{[0,0,1,1,0]} &= \{y_1^8 + y_2^8 - y_3^8 - y_4^8 + y_5^2 = 0\} \cong (S^1 \times S^2)/\mathbb{Z}_2' \ .
\end{aligned}
\tag{2.12}
$$

The distinction between the last two lines is in the action of $\mathbb{Z}_2$ on $S^1 \times S^2$. For $[M] = [0,0,0,1,1]$, it acts by an anti-podal map on S^2, and as inversion of S^1. The Lagrangian $L = L_{[0,0,0,1,1]}$ in this case can be thought of as an S^1 bundle over $\mathbb{RP}^2$, with $H_1(L;\mathbb{Z}) = \mathbb{Z} \times \mathbb{Z}_2$, and $H_2(X,L;\mathbb{Z}) = \mathbb{Z} \times \mathbb{Z}$. For $[M] = [0,0,1,1,0]$, the residual $\mathbb{Z}_2'$ acts by a half-shift on the S^1 and by inversion of the longitudinal direction on S^2. The Lagrangian in this case is an S^2 bundle over $\mathbb{RP}^1 \cong S^1$, with $H_1(L;\mathbb{Z}) = \mathbb{Z}$ and $H_2(X,L;\mathbb{Z}) = \mathbb{Z} \times \mathbb{Z}$.

In both cases, the Lagrangian contains a real one-cycle, namely the first Betti number $b_1(L) = 1$. As is well-known, this means that the $\mathcal{N} = 1$ worldvolume theory contains a chiral multiplet whose vev measures displacement of the Lagrangian away from its original position at the fixed point locus, as well as the continuous Wilson line around the corresponding one-cycle. As is equally well-known, this chiral multiplet is massless in the large volume limit, but can gain a mass by worldsheet disk instantons [24] (*i.e.*, it could be an obstructed deformation in the mathematical language, [25]) with boundary in the corresponding one-cycle. Using mirror symmetry, we can study the corresponding deformation problem using classical methods. Preliminary computations on the objects mirror to the above Lagrangians (see below) indicate that their modulus in fact remains massless even away from large volume [26]. It would be interesting to find evidence for this vanishing of worldsheet instanton contribution directly in the A-model.

Another interesting case is the second line in (2.12), $L_{[0,0,0,0,1]} \cong \mathbb{RP}^3 \cup \mathbb{RP}^3$. Here, $H_1(L;\mathbb{Z}) = \mathbb{Z}_2 \times \mathbb{Z}_2$, and $H_2(X,L;\mathbb{Z}) = \mathbb{Z} \times \mathbb{Z}_2$. Thus, the fixed point locus actually
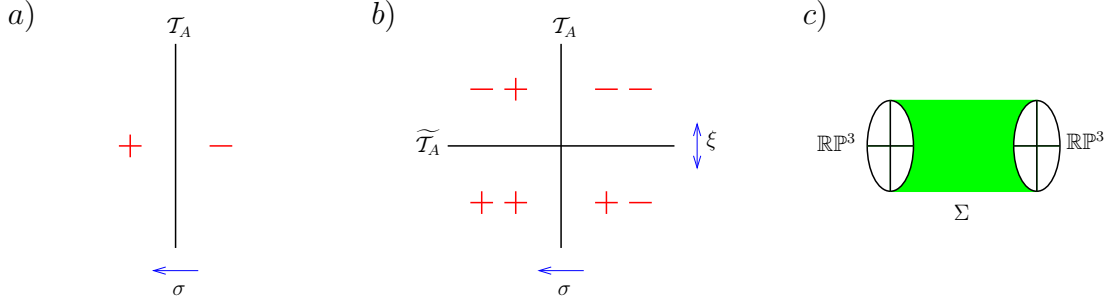
Figure 2.1: Illustration of the vacua of the worldvolume gauge theory of a D6-brane on a) $L^{(6)}_{[M]}$ and $L^{(10)}_{[M]}$, b) on $L^{(8)}_{[0,0,0,0,1]}$. c) Illustration of the 4-chain Σ separating the two $\mathbb{RP}^3$ components of $L^{(8)}_{[0,0,0,0,1]}$.

consists of two components that can be wrapped independently. As we will see below, the two components are actually homologous to each other, so that the worldvolume theory of a D-brane in this class has four vacua, labelled by the $\mathbb{RP}^3$ component it is wrapped on, and the choice of discrete Wilson line on the corresponding $\mathbb{RP}^3$. We will denote these moduli by (ξ, σ), with $\xi, \sigma = \pm 1$.

We illustrate the corresponding domainwalls in figure 2.1b. First, we have the domain-wall interpolating between the different Wilson lines on a fixed Lagrangian. For symmetry reasons, the tension does not depend which $\mathbb{RP}^3$ component we are talking about, and will be identical in structure to that on the quintic, $X^{(6)}$ and $X^{(10)}$, see (2.9). In addition, we have the possibility of interpolating between the two $\mathbb{RP}^3$'s. This is realized geometrically as a D-brane partially wrapped on an appropriate four-chain, as illustrated in figure 2.1c, with remaining directions extended in space-time. On dimensional grounds, the tension of this domainwall must scale as t^2 as $t \to i\infty$. In fact, one may see that by complex conjugation, we can complete the four-chain to a four-cycle, where a D6-brane wrapped on this four-cycle changes the two-form flux N_2 by one unit. The tension of this domainwall, Π_4, is nothing but the (quantum corrected) closed string period of the four-cycle. From closed string mirror symmetry [22, 20], we know that Π_4 has at large volume an expansion of the form

$$\Pi_4 = \partial_t \mathcal{F} = -\kappa \frac{t^2}{2} + at + b + \frac{1}{4\pi^2} \sum_d \tilde{N}_d q^d \,, \tag{2.13}$$

where $\mathcal{F}$ is the genus zero prepotential. Here $\tilde{N}_d$ are the closed string Gromov-Witten invariants, κ is the classical triple intersection, and b is related to the second Chern class of the Calabi-Yau. The number a is slightly ambiguous, but can be constrained by requiring

integrality of monodromy or by related considerations of D-brane charge quantization. For $X^{(8)}$, we use the values [20]

$$\kappa = 2, \qquad a = -3, \qquad b = \frac{11}{6}. \tag{2.14}$$

Thus, under large volume monodromy $t \to t + 1$,

$$\Pi_4 \to \Pi_4 + a't + b', \tag{2.15}$$

where $a' = -\kappa = -2$ and $b' = a - \frac{\kappa}{2} = -4$. We can now repeat the same steps that led to (2.9), taking into account also the 2-form flux. We find that the only way to obtain a consistent solution to the monodromy constraints is that $t \to t + 1$ acts on the vacua by

$$
\begin{aligned}
(N_2, N_4, N_6; -, +) &\to (N_2, N_4 + a'N_2, N_6 + N_4 + b'N_2; -, -), \\
(N_2, N_4, N_6; -, -) &\to (N_2, N_4 + a'N_2 + 1, N_6 + N_4 + b'N_2; -, +), \\
(N_2, N_4, N_6; +, +) &\to (N_2, N_4 + a'N_2 + \frac{a'}{2}, N_6 + N_4 + b'N_2 + \frac{b'}{2}; +, -), \\
(N_2, N_4, N_6; +, -) &\to (N_2, N_4 + a'N_2 + \frac{a'}{2} + 1, N_6 + N_4 + b'N_2 + \frac{b'}{2}; +, +),
\end{aligned}
\tag{2.16}
$$

and that with

$$
\begin{aligned}
\mathcal{T}_A &= \mathcal{W}_{(N_2,N_4+1,N_6;\xi,+)} - \mathcal{W}_{(N_2,N_4,N_6;\xi,-)} = t - \left(\mathcal{W}_{(N_2,N_4,N_6;\xi,-)} - \mathcal{W}_{(N_2,N_4,N_6;\xi,+)}\right), \\
\widetilde{\mathcal{T}_A} &= \mathcal{W}_{(N_2+1,N_4,N_6;-,\sigma)} - \mathcal{W}_{(N_2,N_4,N_6;+,\sigma)} = \Pi_4 - \left(\mathcal{W}_{(N_2,N_4,N_6;+,\sigma)} - \mathcal{W}_{(N_2,N_4,N_6;-,\sigma)}\right),
\end{aligned}
\tag{2.17}
$$

we must have an expansion of the form (2.9) for $\mathcal{T}_A$ and

$$\widetilde{\mathcal{T}_A} = \frac{\Pi_4}{2}, \tag{2.18}$$

with no further corrections. Note that the existence of a solution, and in particular the integrality of the monodromy of $\widetilde{\mathcal{T}_A}$ depends on the fact that a' and b' are even integers. In chapter 5, we will check that the monodromies around the other singular points in moduli space are also integral.

2.2 Outline

On the mirror side, the most convenient (and complete) description of B-type D-branes on $Y^{(k)}$ is as graded, $\hat{G}$-equivariant matrix factorizations of the hypersurface polynomial,

$W^{(k)}$, viewed as Landau-Ginzburg superpotential [27]. The basic algorithm for working out the configurations mirror to the real slices of $X^{(k)}$ is described in [28]. We will follow this procedure in chapter 3, however the full matching of the vacuum structure with that seen in the A-model is postponed to chapter 5.

In chapter 4 we then turn to the computation of more refined invariant information, namely the tension of BPS domainwalls, or superpotential differences, between the various brane vacua. As explained in [9], the appropriate mathematical concept is that of a Hodge theoretic normal function. In the B-model, it can be represented geometrically as an integral of the holomorphic three-form over a three-chain suspended between homologically equivalent holomorphic curves. The curves representing the brane vacua of our interest can be determined algorithmically from the matrix factorization Q via the algebraic second Chern class. In detail, the algebraic second Chern class of this matrix factorization can be represented by a homologically trivial codimension-2 algebraic cycle C (in other words, an integral linear combination of holomorphic curves)

$$c_2(Q) = [C] \in \mathrm{CH}^2_{\mathrm{hom}}(Y) , \tag{2.19}$$

which we will explicitly compute from the matrix factorization. There then exists a three-chain Γ of boundary C, well-defined up to closed three-cycle $\Gamma^c \in H_3(Y; \mathbb{Z})$. The domainwall tension is computed by the integral over Γ

$$\mathcal{T}_B(z) = \int_\Gamma \hat{\Omega}(z) , \tag{2.20}$$

where $\hat{\Omega}(z)$ is the appropriately normalized holomorphic three-form of the B-model geometry (see equation (4.2)).

Explicitly, we will have relations of the form

$$\mathcal{T}_B(z(t))/\varpi_0(z(t)) = \mathcal{T}_A(t) , \tag{2.21}$$

where the mirror map consists of the relation $z = z(t)$ between A- and B-model variables, and the normalization of the holomorphic three-form $\hat{\Omega}(z) \to \hat{\Omega}(z)/\varpi_0(z)$. As is well-known, this data can be obtained by solving the homogenous Picard-Fuchs equation satisfied by the B-model periods. The Picard-Fuchs operators of our three models are:

$$\begin{aligned}
\mathcal{L}^{(6)} &:= \theta^4 - 2^4 3^6 z(1/6 + \theta)(1/3 + \theta)(2/3 + \theta)(5/6 + \theta) , \\
\mathcal{L}^{(8)} &:= \theta^4 - 2^{16} z(1/8 + \theta)(3/8 + \theta)(5/8 + \theta)(7/8 + \theta) , \\
\mathcal{L}^{(10)} &:= \theta^4 - 5^5 2^8 z(1/10 + \theta)(3/10 + \theta)(7/10 + \theta)(9/10 + \theta) ,
\end{aligned} \tag{2.22}$$

with $\theta = z\Delta_z$, and $z \sim \psi^{-k}$. Namely, $\varpi_0(z)$ is the unique solution with power series behavior at $z = 0$, and if $\varpi_1(z) \sim \varpi_0(z)\log(z)$ is the solution with a single logarithm, we have

$$t(z) = \frac{\varpi_1(z)}{\varpi_0(z)} \ . \tag{2.23}$$

To calculate the chain integral in (2.20), we exploit that it satisfies an inhomogeneous version of the Picard-Fuchs equation (governing closed string mirror symmetry), with an inhomogeneous term that can be computed explicitly from the curve and the Griffiths-Dwork algorithm (we defer the actual computations to appendix A).

$$\mathcal{L}^{(k)}\mathcal{T}_B = \frac{c^{(k)}}{16}\sqrt{z} \ . \tag{2.24}$$

The central part of our computation is the determination of the parameters $c^{(k)}$ for each of our domainwalls.

Note that this Abel-Jacobi type method developed in [9] is similar in spirit to the computations in local geometries [5, 29, 6, 7].

With the inhomogeneous Picard-Fuchs equation in hand, we can then compute the fully quantum corrected domainwall tension over the entire closed string moduli space, see chapter 5. We will check integrality of all requisite monodromy matrices, as well as the spectrum of tensionless domainwalls, expected from the matrix factorization considerations.

2.3   Conclusion

Having obtained the correctly normalized domainwall tension, we can obtain numerical predictions for the number of disks ending on the Lagrangians of the A-model (which will turn out to be consistent with Ooguri-Vafa integrality [14]).

In detail, we can extract the Ooguri-Vafa invariants [14] from the Gromov-Witten expansion of the domainwall tension, (2.9). Recall that the familiar $1/l^3$-multicover formula is replaced in the open string context by $1/l^2$. In terms of the quantum part of the domainwall tension (2.9), the expansion takes the form

$$\frac{\pi^2}{4} \frac{\tau(z(q))}{\varpi_0(z(q))} = \sum_{l,d \text{ odd}} \frac{n_d^{(0,\text{real})}}{l^2} q^{dl/2} \ . \tag{2.25}$$

The resulting integers $n_d^{(0,\text{real})}$ (see table 2.1 for some examples) are BPS-invariants in the string/M-theory setup of [14]. Mathematically, they are predicted to be enumerative invariants counting real rational curves in $X^{(k)}$.

n_d	disk instanton numbers for $L_{[M]}^{(6)}$
1	24
3	5880
5	14328480
7	48938353176
9	204639347338560
11	965022386745454392

n_d	disk instanton numbers for $L_{[0,0,0,0,1]}^{(8)}$
1	48
3	65616
5	919252560
7	17535541876944
9	410874634758297216
11	10854343378339853472336

n_d	disk instanton numbers for $L_{[M]}^{(10)}$
1	128
3	2886528
5	465626856320
7	112339926393132928
9	33254907472965538667520
11	11110159357336987759939410816

Table 2.1: Low degree BPS invariants $n_d^{(0,\text{real})}$ for the three models $X^{(6)}$, $X^{(8)}$, and $X^{(10)}$.

It is interesting to note that Ooguri-Vafa integrality also holds for the second domainwall that appears for $X^{(8)}$, see (2.18). Since $\widetilde{\mathcal{T}}_A = \Pi_4/2$, where $\Pi_4 \sim \partial \mathcal{F}$, this integrality can be deduced from the integrality of ordinary closed string instanton numbers (obtained from prepotential $\mathcal{F}$ with $1/l^3$ multi-cover formula). Note however that this is not a totally trivial check because of the relative factors of 2 between open and closed string expansion.

In the absence of direct A-model computations of Gromov-Witten or Ooguri-Vafa invariants, further checks on the enumerative predictions of table 2.1 can be derived from the computation of loop amplitudes in the topological string.

As explained in [30, 17], the domainwall tensions that we obtained as solutions of the inhomogeneous Picard-Fuchs equation in the previous sections constitute tree-level data for the computation of topological string amplitudes on the appropriate Calabi-Yau orientifold models. Technically, we have an extension of ordinary special geometry to the open string sector, characterized infinitesimally by the two-point function on the disk, Δ. This is related to the tree-level domainwall $\mathcal{T}$ as $\Delta \sim D^2\mathcal{T} - CD\overline{\mathcal{T}}$, where C is the closed string Yukawa coupling (i.e., the infinitesimal invariant of the closed topological string), and D is the covariant derivative on moduli space. Under certain additional conditions

(no contribution from open string moduli, tadpole cancellation, further discussed in part III of this thesis (chapter 9)), the amplitudes for higher worldsheet topology are then recursively constrained by the extended holomorphic anomaly equation of [30], which is a generalization of the BCOV equations [31]. The main obstacle to carrying out this program is the holomorphic ambiguity, which at present is not very well understood in the open/unoriented sector (however, some progress on this will be made in chapter 9 of part III).

For the one-loop amplitudes however, we have a complete proposal [17], generalizing the result of [32]. We can therefore just plug in the tree-level data into this formula, and extract [14, 33, 17] one-loop BPS invariants for our three one-parameter hypersurfaces. One of the checks alluded to above is the following equality of tree-level and one-loop enumerative invariants on $X^{(6)}$:

$$k = 6: \qquad n_1^{(0,\mathrm{real})} = n_2^{(1,\mathrm{real})} = 24 \ . \tag{2.26}$$

We view this as the real version of the coincidence of the complex enumerative invariants (see, *e.g.*, [34])

$$k = 6: \qquad n_1^{(0)} = n_2^{(1)} = 7884 \ , \tag{2.27}$$

which arises from the relation between the corresponding intersection problems. The equality (2.26) gives evidence that this relation persists in the real version of the problem. Another check is the necessary equality of complex and real enumerative invariants modulo 2, *i.e.*,

$$k = 6, 8, 10: \qquad n_d^{(\hat{g},\mathrm{real})} = n_d^{(\hat{g})} \bmod 2 \ , \tag{2.28}$$

holds for all three models, all d, and $\hat{g} = 0, 1$.

Another interesting aspect of the loop computations derives from the disconnectedness of the real slice of $X^{(8)}$. As observed in [17], it appears that in order to obtain a satisfactory BPS interpretation for open topological string amplitudes on compact Calabi-Yau manifold, one has to consider an orientifold model and choose a D-brane configuration that cancels the tadpoles. In our models, we naturally choose the orientifold action that we used to define the D-branes, and put exactly one D-brane on top of the orientifold plane. For $k = 8$, however, the orientifold plane is disconnected, and there are more tadpole cancelling D-brane configurations (ten, using just the branes we discussed). In other words, the topological string amplitudes are a function of four discrete moduli $(\xi_1, \sigma_1, \xi_2, \sigma_2)$, in addition to the closed string modulus t. We have computed this function at one-loop and found an integral BPS expansion in all sectors. We will return to this elsewhere.

The integrality of the $n_d^{(0,\text{real})}$ from table 2.1 is a strong check that our overall picture is consistent. Note however that the overall normalization of these numbers is not fixed by integrality alone (in particular, all $n_d^{(0,\text{real})}$ are divisible by the first number, $n_1^{(0,\text{real})}$). Our confidence in the enumerative predictions therefore mainly rests on the agreement between the two different computations of this normalization constant, monodromy and Abel-Jacobi. As further comfort, we note that the corresponding predictions on the quintic [10] have been verified in [35] using the open Gromov-Witten theory of [36] and localization on the space of maps to the ambient $\mathbb{P}^4$. It would be interesting to verify our predictions in the weighted case by this or other methods.

In summary, we have accumulated evidence for a mirror symmetry identification between A-branes defined as the real slices of one-parameter hypersurfaces in weighted projective space and B-branes defined via certain matrix factorizations of the Landau-Ginzburg superpotential. We have made this identification at the level of the holomorphic data, namely the structure of $\mathcal{N} = 1$ supersymmetric vacua on the D-brane worldvolume and the tension of BPS domainwalls between them.

The basic structure is similar to the real quintic studied in [10, 9]. All models have in common that they possess real Lagrangians with $H_1(L, \mathbb{Z}) = \mathbb{Z}_2$. This discrete datum corresponds to a choice of discrete Wilson line. Using mirror symmetry, or just based on considerations of monodromy, one can show that the domainwall tension separating those vacua is captured by an inhomogeneous Picard-Fuchs equation with inhomogeneous term $\sim z^{1/2}$. It is tempting to speculate that this specific type of inhomogeneous extension will generally describe the domainwall separating the two possible vacua of a D-brane on Lagrangians with $H_1(L, \mathbb{Z}) = \mathbb{Z}_2$.

As a side remark, note that one might also ask if similar considerations could be applied as well to Lagrangians with more general torsion $H_1(L, \mathbb{Z}) = \mathbb{Z}_p$. A natural guess would be that the domainwalls separating these vacua are similarly captured on the B-side via an inhomogeneous extension of the ordinary Picard-Fuchs equations of the form $\sim z^{1/p}$. It would be interesting to find some explicit examples which support this proposal.

On a technical level, the key quantity to compute is the exact constant of proportionality of the inhomogeneous term in the Picard-Fuchs equation. We have determined these constants via two orthogonal approaches, namely consistency of monodromies (see chapter 5) and explicit computations of Abel-Jacobi type, resulting from the B-model matrix factorizations (see chapter 4).

The $k = 8$ hypersurface differs slightly from the other models by the fact that the real

Lagrangian of interest possesses two disconnected, but homologically equivalent components, and $H_1(L, \mathbb{Z}) = \mathbb{Z}_2 \times \mathbb{Z}_2$. Hence, this geometry has in addition a second discrete open string modulus corresponding to the component the D-brane is wrapped on, as well as a second domainwall, which is formed by a D-brane on the 4-chain separating the two components. The tension of this domainwall is simply a fractional (quantum corrected) closed string period. While this picture is suitable at the large volume point, we made the observation that continuation to the Gepner point induces a "mixing" of these (from a large volume point of view) different moduli. This is another manifestation of the break down of classical geometric concepts in the quantum regime, and perhaps the most interesting lesson of our computations.

Finally, note that for certain other choices of anti-holomorphic involution, also on $X^{(8)}$, the Lagrangian submanifold has a non-zero first Betti number, and hence a classical deformation space. It is of interest to ask whether this moduli space is lifted by quantum effects (worldsheet instantons). We cannot at the moment answer this question from A-model considerations. However, if our mirror proposal is correct, the B-model results indicate that this moduli space in fact persists at the quantum level, *i.e.*, no superpotential is generated for the corresponding chiral field.

Chapter 3

B-model matrix factorizations

In this chapter, we will present B-type D-branes in terms of matrix factorizations, which are expected to be mirror to A-type D-branes on the real loci we considered in section 2.1. For the reader's convenience, we will firstly recall some basics of the description of B-type D-branes in terms of matrix factorizations. For more details and references we refer to [8] and references therein.

3.1 Matrix factorizations

In order to introduce matrix factorizations, let us go back to $\mathcal{N} = (2,2)$ supersymmetric field theory in two dimensions, which is the starting point for perturbative string theory (especially for topological string theory, cf. section 9.1 of chapter 9).

The relevant two dimensional field theory is the bulk Landau-Ginzburg model, which can be most easily summarized in superspace notation as follows:

$$S_{LG} = \int d^2z d\theta^2 d\bar{\theta}^2 K(\Phi_i, \bar{\Phi}_i) + \int d^2z d^2\theta W(\Phi_i) + c.c.\,, \tag{3.1}$$

where Φ_i are n chiral superfields that satisfy $\bar{D}_\pm \Phi_i = 0$ with D the usual covariant derivative. Note that in the following we will denote the fields by ϕ_i if we consider them as complex variables rather than superfields. Further, K is the (non-holomorphic) Kähler potential (which however does not play any role in the infrared) and W is the (holomorphic) superpotential.

For a quasi-homogenous superpotential, *i.e.*, W satisfies $W(\lambda^{q_i}\phi_i) = \lambda W(\phi_i)$ with q_i the charge of the field ϕ_i, the theory flows in the infrared to a superconformal fixed-point theory that only depend on the singularity type of W. Especially, the hypersurface defined

by $W = 0$ describes a compact background, which corresponds for $n = 5$ and $\sum_i q_i = 1$ to a Calabi-Yau three-fold.

The theory can be twisted by adding a background charge such that the two supercharges turn into BRST operators (see also section 9.1). Upon such twisting, the theory becomes a topological field theory with a finite dimensional Hilbert space defined by the non-trivial cohomology of the BRST operators. In detail, here we will consider a B-type twist, such that the BRST operators are given by the supercharges $\bar{Q}_+$ and $\bar{Q}_-$.

We are interested in the open string version, namely, the Landau-Ginzburg model on a Riemannian surface with boundary, *i.e.*, on the disk D. The boundary ∂D breaks the supersymmetry of the bulk theory down to $\mathcal{N} = 2$ and we will choose B-type boundary conditions that are compatible with the B-type topological twist, that is, the surviving BRST operator is given by $Q_B = \bar{Q}_+ + \bar{Q}_-$.

However, since the Landau-Ginzburg Lagrangian (3.1) is invariant under supersymmetry only up to a total derivative, supersymmetry is broken for a non-trivial ∂D by a boundary term, in the present context the so-called Warner-term [37], which needs to be cancelled in order to restore supersymmetry:

$$S_{Warner} = \int_{\partial D} d\sigma d\theta W(\Phi|_{\partial D}) \,, \tag{3.2}$$

with σ and $\theta, \bar{\theta}$ coordinates of the corresponding superboundary.

One possibility to do so, is to introduce k boundary fermions π_a and $\bar{\pi}_a$ satisfying a Clifford algebra $\{\pi_a, \bar{\pi}_a\} = \delta_{ab}$. These fit into superfields $\Pi_a = \pi_a + \theta l_a$ with l_a auxiliary fields. However, the Π_a are not chiral but rather satisfy

$$\bar{D}\Pi_a = E_a(\Phi|_{\partial D}) \,, \tag{3.3}$$

where E_a are arbitrary polynomials in ϕ. Adding the boundary superpotential term

$$S_\partial = \int_{\partial D} d\sigma d\theta \sum_a \Pi_a J_a(\Phi|_{\partial D}) \,, \tag{3.4}$$

where again J_a are arbitrary polynomials in ϕ, one infers that its Q_B variation cancels the Warner-term, if

$$\sum_a J_a(\phi) E_a(\phi) = W(\phi) \,. \tag{3.5}$$

Rewriting the BRST operator associated with the boundary degrees of freedom as

$$Q(\phi) = \pi_a J_a(x) + \bar{\pi}_a E_a(\phi) = \begin{pmatrix} 0 & \mathcal{J}(\phi) \\ \mathcal{E}(\phi) & 0 \end{pmatrix} \,, \tag{3.6}$$

where we represented the boundary fermions by generalized $2^k \times 2^k$ dimensional Pauli matrices, the condition (3.5) turns into the matrix equation

$$Q^2 = \mathcal{J} \cdot \mathcal{E} = W \cdot \mathbf{1} \,. \tag{3.7}$$

This matrix equation essentially means that all supersymmetric B-type boundary conditions, hence B-type D-branes, compatible with the background described by $W = 0$ are identical to all the possible factorizations of W into matrices $\mathcal{J}$ and $\mathcal{E}$ with polynomial entries in ϕ. This statement is mathematically highly non-trivial since it associates the (usually complicated) category of coherent sheaves on the background with a category of (more or less simple) matrix factorizations (references for proofs can be found in [8]). Note that $\mathcal{J}$ and $\mathcal{E}$ may in general also depend on continuous geometrical data (moduli), which correspond to deformations of the D-brane background. This is one of the major advantages of the formulation of B-type D-branes via matrix factorizations, since it allows to derive the effective potential induced on them. A generic perturbation, *i.e.*, a generic perturbation of the bulk or D-brane setup, will lead away from a supersymmetric configuration (spoil a given matrix factorization) and induces an effective superpotential. In contrast, the true moduli of the system are those that preserve the factorization. They form a sub-locus of the combined open/closed deformation space which corresponds to the critical locus of the effective superpotential.

Finally, note that if we consider an orbifold of a Landau-Ginzburg action we need to supplement the matrix factorization by representations of the orbifold group such that Q is equivariant. Especially, this yields for a single matrix factorization of W a whole orbit of equivariant matrix factorizations.

3.2   Mirror B-model matrix factorizations

At the Fermat point $\psi = 0$, the polynomials in (2.3), viewed as Landau-Ginzburg potentials, $W = W^{(k)}$, admit the following set of matrix factorizations

$$Q = \sum_{i=1}^{5} \frac{1}{\sqrt{h_i}} \bigl(x_i^{l_i} \eta_i + x_i^{h_i - l_i} \bar{\eta}_i \bigr) \,, \tag{3.8}$$

where $\{\eta_i, \bar{\eta}_j\} = \delta_{ij}$ are matrices representing a Clifford algebra, and $0 < l_i < h_i$ are a set of integer parameters. Namely,

$$(Q)^2 = \sum x_i^{h_i} / h_i = W|_{\psi=0} \,. \tag{3.9}$$

The factorizations in (3.8) provide the Landau-Ginzburg description of the so-called Cardy or Recknagel-Schomerus boundary states [38] of the associated Gepner model. More precisely, we are interested in B-branes in the mirror model, which involves an orbifold of (2.3) by the Greene-Plesser orbifold group $\hat{G} = \ker\left(\prod \mathbb{Z}_{h_i} \to \mathbb{Z}_k\right)$. This means that we have to equip the linear space underlying Q with an action of $\hat{G}$ such that Q is equivariant with respect to the action of $\hat{G}$ on the x_i.

As shown in [28], the boundary states/matrix factorizations that provide the Landau-Ginzburg description of the real slices of the A-model hypersurfaces arise from the labels $l_i \approx h_i/2$ for $i = 1, \dots, 5$. We will momentarily describe this correspondence. But before that, we ought to note that the factorizations (3.8) in which $l_i = h_i/2$ for all i with odd ν_i ($\equiv k/h_i$) are reducible. This is because

$$A = \prod_{i, \nu_i \text{ odd}} (\eta_i - \bar{\eta}_i) , \tag{3.10}$$

is a non-trivial degree zero element of the cohomology of Q, of square $A^2 \sim$ id. As first discussed in the Gepner model context in [39, 40], we can then split Q into the eigenspaces of A, as in

$$Q^\pm = P^\pm Q P^\pm , \tag{3.11}$$

where $P^\pm \sim \frac{1 \pm A}{2}$. We will denote the elementary matrix factorization, equipped with the corresponding representation of $\hat{G}$, by

$$Q^\zeta_{[\mathbf{m}]} , \tag{3.12}$$

where $[\mathbf{m}] \in \left(\hat{G}\right)^* = \left(\prod \mathbb{Z}_{h_i}\right)/\mathbb{Z}_k$, and $\zeta = \pm 1$ is the eigenvalue of A.

The correspondence derived in [28] is that the real slice $L^{(k)}_{[M]}$ of an even-degree hypersurface with respect to the involution (2.5), is represented, at the level of topological charges, by the following linear combination of tensor product states:

$$[L_{[M]}] = \frac{1}{2}[Q_{[\mathbf{m}^+]}] - \frac{1}{2}[Q_{[\mathbf{m}^-]}] . \tag{3.13}$$

Here $\mathbf{m}^\pm = (m_1^\pm, \dots, m_5^\pm)$, and the $m_i^\pm$ are related to the M_i as follows: For M_i even, $m_i^+ = m_i^- = M_i/2$, and for M_i odd, $m_i^\pm = (m_i \pm 1)/2$. The l_i labels (cf. (3.8)) are determined as follows: For h_i even, $l_i = h_i/2$. For h_i odd, and M_i even, $l_i = (h_i - 1)/2$ in the first summand, and $l_i = (h_i + 1)/2$ in the second summand. For h_i odd, and M_i odd, $l_i = (h_i + 1)/2$ in the first summand, and $l_i = (h_i - 1)/2$ in the second summand.

The relation (3.13) was obtained in [28] by comparing, via the gauged linear sigma model, the topological charges of orientifold planes associated with A-type parity and complex conjugation (2.5) in large volume and in the Landau-Ginzburg phase. Our goal in this paper is however to obtain more refined information than just the topological charges, for which we need to lift (3.13) (at least) to the holomorphic sector. We have no principled way of doing this at the moment, however in certain cases we can make a plausible proposal based on the following set of observations. [1]

At large volume, the fixed point set of the anti-holomorphic involution is a special Lagrangian submanifold, *i.e.*, it is conformally invariant (in one-loop sigma-model expansion) and preserves space-time supersymmetry, in addition to preserving A-type worldsheet supersymmetry. An equivalent statement should hold at the Landau-Ginzburg point, since to get there we only need to vary the Kähler moduli. In general, the ($\mathcal{N} = 1$) spacetime supersymmetry preserved by an equivariant matrix factorization $Q_{[\mathbf{m}]}$ can be measured by the phase of the ($\mathcal{N} = 2$) central charge, which (for fixed l_i) varies $\propto \sum_{i=1}^{5} \frac{m_i}{h_i}$. It is not hard to see that in most cases, the two summands in (3.13) in general preserve different supersymmetry. This means that the supersymmetric D-brane corresponding to the real hypersurface must in general be some bound state of the above components.

Let us illustrate this for the real slices of $X^{(8)}$. Evaluating (3.13) (and taking into account that the irreducible factorizations from (3.12) have the same topological charges) gives (cf. (2.12)),

$$
\begin{array}{c|c|c}
\text{Langrangian} & \text{topology} & \text{matrix factorizations} \\
\hline
L_{[0,0,0,0,0]} & \emptyset & \left[Q^+_{[0,0,0,0,0]}\right] - \left[Q^+_{[0,0,0,0,0]}\right] = 0 \\
L_{[0,0,0,0,1]} & \mathbb{RP}^3 \cup \mathbb{RP}^3 & \left[Q_{[0,0,0,0,0]}\right] = \left[Q^+_{[0,0,0,0,0]}\right] + \left[Q^-_{[0,0,0,0,0]}\right] \\
L_{[0,0,0,1,0]} & S^3 & \left[Q^+_{[0,0,0,0,0]}\right] - \left[Q^+_{[0,1,0,0,0]}\right] \\
L_{[0,0,0,1,1]} & (S^1 \times S^2)/\mathbb{Z}_2 & \left[Q^+_{[0,0,0,0,0]}\right] + \left[Q^+_{[0,1,0,0,0]}\right] \\
L_{[0,0,1,1,0]} & (S^1 \times S^2)/\mathbb{Z}'_2 & \left[Q^+_{[0,0,0,0,0]}\right] - \left[Q^+_{[0,1,1,0,0]}\right]
\end{array}
\tag{3.14}
$$

The first two lines are very obvious cases: $L_{[0,0,0,0,0]}$ is empty, with vanishing boundary state. $L_{[0,0,0,0,1]}$ geometrically splits into two $\mathbb{RP}^3$ components, which we might tentatively identify with $Q^+_{[0,0,0,0,0]}$ and $Q^-_{[0,0,0,0,0]}$. (The correct dictionary must ultimately include the Wilson line degree of freedom, and is somewhat different, see eq. (5.32).) We propose that this identification holds at the holomorphic level, and probably also at the level of superconformal boundary states.

---

[1]For odd degree hypersurfaces, such as the quintic, we have only one term on the RHS of (3.13). The lift to the holomorphic sector is then more natural, and supported by a lot of evidence.

The situation for the other real slices (including those of $X^{(6)}$ and $X^{(10)}$) is less clear cut. As mentioned above, the Lagrangians can at best correspond to a bound state of the two components in (3.13), and at worst might not be continuously connected to the split form of (3.14). Nevertheless, our present observations and the calculations in the following sections suggest that the correspondence (3.14) can indeed be lifted to the holomorphic level.

To study this additional evidence, we need to present the deformation theory of the matrix factorizations Q of (3.8) with $l_i = [h_i/2]$ as we vary the complex structure parameter away from $\psi = 0$. This is a rather straightforward exercise.

For $Y^{(6)}$, we find that Q deforms in a unique way (up to gauge transformation), given explicitly by

$$Q(\psi) = \sum \frac{1}{\sqrt{6}} \left(x_i^3 \eta_i + x_i^3 \bar{\eta}_i \right) + \frac{1}{\sqrt{3}} \left(x_5 \eta_5 + x_5^2 \bar{\eta}_5 \right) - \sqrt{3} \psi x_1 x_2 x_3 x_4 \bar{\eta}_5 \ . \tag{3.15}$$

This deformation commutes with A from (3.10). Therefore, by splitting as in (3.12), we obtain two families $Q^\zeta(\psi)$ (with $\zeta = \pm 1$) of matrix factorizations. We expect that the $\mathbb{RP}^3$ special Lagrangians should correspond to an appropriate bound state of those with different $[\mathbf{m}]$ label, but identical ζ-label. The latter should correspond to the discrete Wilson line on $\mathbb{RP}^3$. Hence, we identify

$$\sigma = \zeta \ . \tag{3.16}$$

For $Y^{(8)}$, we find two inequivalent ways of deforming the factorization away from $\psi = 0$. We will denote those matrix factorizations as $Q(\psi, \mu)$, where the additional label $\mu = \pm 1$:

$$
\begin{aligned}
Q(\psi, +) &= \sum \frac{1}{\sqrt{8}} \left(x_i^4 \eta_i + x_i^4 \bar{\eta}_i \right) + \frac{1}{\sqrt{2}} \left((x_5 \eta_5 + x_5 \bar{\eta}_5) - \sqrt{2} \psi x_1 x_2 x_3 x_4 \eta_5 \right) , \\
Q(\psi, -) &= \sum \frac{1}{\sqrt{8}} \left(x_i^4 \eta_i + x_i^4 \bar{\eta}_i \right) + \frac{1}{\sqrt{2}} \left((x_5 \eta_5 + x_5 \bar{\eta}_5) - \sqrt{2} \psi x_1 x_2 x_3 x_4 \bar{\eta}_5 \right) .
\end{aligned}
\tag{3.17}
$$

Again, the deformation commutes with A. For $L_{[0,0,0,0,1]}$, this means that we obtain in total four families of matrix factorizations, naturally organized in two sets of two. Namely, we mind to the labels $\langle \mu, \zeta \rangle$, where ζ is the eigenvalue of A, and μ distinguishes the two lines in (3.17). We propose that those correspond to the four vacua that we identified in section 2.1 above. We emphasize at this stage that we still allow for a non-trivial transformation between the discrete A-model labels (ξ, σ) and the B-model labels $\langle \mu, \zeta \rangle$. We will determine this transformation after analytic continuation of domainwall tensions in chapter 5.

For $L_{[0,0,0,1,1]} \cong (S^1 \times S^2)/\mathbb{Z}_2$, we propose to identify the $\mu = \pm 1$ label from (3.17) with the two vacua associated with the discrete $\mathbb{Z}_2$ factor in $H_1(L_{[0,0,0,1,1]}) = \mathbb{Z} \times \mathbb{Z}_2$ (see paragraph below (2.12)). (The free factor in $H_1(L)$ (for $L = L_{[0,0,0,1,1]}$ and $L_{[0,0,1,1,0]}$) is associated at large volume with a continuous modulus, displacing the Lagrangian away from the fixed locus of the anti-holomorphic involution. As mentioned above, there are indications [26] that this open string modulus is in fact unobstructed, so should decouple from the superpotential computations.)

As on the quintic [10, 41], the two-fold way of deforming away from $\psi = 0$ is accompanied by the appearance, at $\psi = 0$, of an additional massless field in the open string spectrum. Also, the tension of the domainwall between the $\langle +, \zeta \rangle$ and the $\langle -, \zeta \rangle$ vacua should vanish at $\psi = 0$. This will be our way to complete the identification of the four vacua in A- and B-model.

Finally, for $Y^{(10)}$, the situation is somewhat in between that of $Y^{(6)}$ and that of $Y^{(8)}$. The main difference to $Y^{(6)}$ is that the tensor product factorization has an infinitesimal modulus (degree 1 cohomology element) Ψ, the main difference to $Y^{(8)}$ is that Ψ satisfies $\{A, \Psi\} = 0$ instead of $[A, \Psi] = 0$, where A is from (3.10). Without delving into details, the consequence is that the factorizations $Q^{\pm}$ from (3.12) deform in a unique way, which can be obtained by splitting the deformed factorization

$$Q(\psi) = \sum \frac{1}{\sqrt{10}} \left(x_i^5 \eta_i + x_i^5 \bar{\eta}_i \right) + \frac{1}{\sqrt{2}} \left(x_4 \eta_4 + x_4 \bar{\eta}_4 \right) + \frac{1}{\sqrt{5}} \left(x_5^2 \eta_5 + x_5^3 \bar{\eta}_5 \right)$$
$$- \frac{\psi}{\sqrt{2}} x_1 x_2 x_3 (\eta_4 + \bar{\eta}_4) x_5 - \frac{\psi^2}{2} \sqrt{5} x_1^2 x_2^2 x_3^2 \bar{\eta}_5 , \quad (3.18)$$

in eigenspaces of A. Again, we identify the eigenvalue of A with the discrete Wilson line on $\mathbb{RP}^3 \cong L_{[M]}^{(10)}$, as in (3.16)

Since the factorizations on $Y^{(6)}$ and $Y^{(10)}$ deform in a unique way, there is no additional massless open string, and we expect no tensionless domainwall at $\psi = 0$. We will confirm this in chapter 5.

Before closing this chapter, we note another property (valid for all three k's) of the factorizations around the Fermat point $\psi = 0$. This is a special point in moduli space in which the hypersurfaces $Y^{(k)}$ gain an additional $\mathbb{Z}_k$ automorphism multiplying one of the weight-one variables by a phase. Put differently, the monodromy around the Gepner point $\psi \to e^{2\pi i/k} \psi$ can be undone by rotating $x_1 \to e^{-2\pi i/k} x_1$. At the level of matrix factorizations, this monodromy has to be accompanied by conjugating Q with a representation of the $\mathbb{Z}_k$ symmetry group of the corresponding minimal model x_1^k. It is not hard to see

that the matrix A from (3.10) picks a sign under this symmetry. Thus, we conclude that monodromy around the Gepner point exchanges the vacua labelled by $\zeta = \pm 1$. [2] This is another clue that we will pick up in our monodromy discussion in chapter 5.

---

[2]To complete this, note that for $Y^{(8)}$, Gepner monodromy does not affect the μ-label, as can also be seen from (3.17).

Chapter 4

Inhomogeneous Picard-Fuchs equations

In this chapter, we will obtain the curves representing the algebraic second Chern classes from the matrix factorizations derived in the previous chapter. We then outline how to calculate from the curves the exact normalization factors $c^{(k)}$ of the inhomogeneous Picard-Fuchs equations governing the domainwall tensions (cf. (2.24)), via the method pioneered in [9] for the quintic. The actual computations can be found in appendix A.

4.1 From matrix factorizations to curves

Given the matrix factorizations, we obtain the curves representing the algebraic second Chern classes by the algorithm described in [9] for the quintic. This can be viewed as an application of the homological Calabi-Yau/Landau-Ginzburg correspondence [42, 43] together with elementary methods for the computation of Chern classes.

In the first step, one extracts geometric information, in terms of bundle data, out of a matrix factorization by making a detour through the linear sigma model following [43]. In detail, one first determines the R-charges R_n of the (equivariant) matrix factorization. In order to pass from the Landau-Ginzburg model to the Calabi-Yau, one has to pass through one of the "windows" between the singular points in moduli space using the "grade restriction rule" of [43]. This defines a set of consecutive integers $\Lambda = \{0, 1, 2, \ldots, d - 1\}$, with d the degree of the hypersurface. The linear sigma model charges $(\tilde{R}_n, q_n)$ can then be obtained from the relation $\tilde{R}_n = R_n + \frac{2q_n}{d}$ with $q_n \in \Lambda$. Knowing the charges, a set of infinite complexes can be constructed by placing $\mathcal{O}(q_n + dk)^{\oplus m}$, where m is the multiplicity of $\tilde{R}_n$

and k goes from 0 to ∞, at the position $\tilde{R}_n + 2k$ (the homological degree). From these complexes one can then extract the bundle data characterizing the brane (this involves an appropriate truncation of the infinite complexes to semi-infinite complexes). For our purposes, that is, obtaining the explicit curves representing the brane, only the 2-periodic complex, which is nothing than the original matrix factorization, is of relevance [9].

Thus, we can bypass the above sketched procedure of determining the bundle data and simply extract the relevant bundles E_ζ for $Y^{(6)}$ and $Y^{(10)}$, and respectively $E_{\zeta\mu}$ for $Y^{(8)}$, for which to compute the second Chern class, from $\mathrm{Ker}(\mathcal{E}^\zeta)$, respectively $\mathrm{Ker}(\mathcal{E}^{\zeta\mu})$, with $\mathcal{E}$ the component of Q as in (3.6) (see also the discussion in section 3.2). Note that since the second Chern class does not depend on the representation of $\hat{G}$, we have omitted the [**m**] label.

In the second step, one then calculates $c_2(E_\zeta)$, respectively, $c_2(E_{\zeta\mu})$. For that, note that for a bundle of rank r with sufficiently many sections, one can determine the second Chern class by choosing $r-1$ generic sections and finding the codimension-2 locus where those sections fail to be linearly independent. For a detailed explanation, we refer to [44]. Out of this calculation one can then extract pairs, respectively two pairs, of algebraic curves C_ζ, respectively $C_{\langle\mu,\zeta\rangle}$, such that differences of the curves are homologically trivial and hence define a normal function.

Note that in the following, the only point on which we will be slightly less rigorous than in [9] is that we will perform our computation as if we were pretending to be working on the hypersurfaces (2.3) in weighted projective space, without orbifold. In actuality, however, everything is taking place on the B-model side, *i.e.*, the underlying manifolds are indeed $Y^{(k)}$, after quotienting by $G = \hat{G}/\mathbb{Z}_k$.

Following the procedure sketched above, we find that the relevant part of the second Chern classes of the matrix factorizations from eqs. (3.15), (3.17), (3.18) can be represented with the following set of curves.

$$k = 6 : C_\zeta^{(6)} = \{x_1 + (\alpha^{(6)})^\zeta x_2 = 0, x_3 + \alpha^{(6)} x_4 = 0, x_5^2 - 3\psi x_1 x_2 x_3 x_4 = 0\}$$

$$k = 8 : C_{\langle\mu,\zeta\rangle}^{(8)} = \begin{cases} \{x_1 + (\alpha^{(8)})^\zeta x_2 = 0, x_3 + \alpha^{(8)} x_4 = 0, x_5 = 0\} & \mu = +1 \\ \{x_1 + (\alpha^{(8)})^\zeta x_2 = 0, x_3 + \alpha^{(8)} x_4 = 0, x_5 - 2\psi x_1 x_2 x_3 x_4 = 0\} & \mu = -1 \end{cases}$$

$$k = 10 : C_\zeta^{(10)} = \{x_1 + (\alpha^{(10)})^\zeta x_2 = 0, x_3^5 + (\alpha^{(10)})^5 \sqrt{5}(x_5 - \psi x_1 x_2 x_3 x_4) = 0,$$
$$2x_4^3 - 5\psi^2 x_1^2 x_2^2 x_3^2 = 0\} \ .$$
$$(4.1)$$

Let us explain our notation and the precise meaning of those equations. First of all,

k	G_{fix}	generator
6	$\mathbb{Z}_6$	$(\gamma, \gamma, \gamma^{-1}, \gamma^{-1}, 1)$
8	$\mathbb{Z}_4$	$(\gamma, \gamma, \gamma^{-1}, \gamma^{-1}, 1)$
10	$\mathbb{Z}_{10}$	$(\gamma, \gamma, \gamma^8, 1, 1)$

Table 4.1: The curves from (4.1) are invariant under certain subgroup of the orbifold group G. For each k, $\gamma = \gamma_k = \exp(2\pi i/k)$.

$\alpha^{(k)}$ are phases which fulfill $(\alpha^{(k)})^k = -1$. One then easily checks that the curves actually lie on the corresponding hypersurface, *i.e.*, $W^{(k)} = 0$ identically whenever a group of three equations from (4.1) are satisfied. The subscript ζ comes from the eigenvalue of A used to split the reducible Q from (3.8) in two components (for the geometric meaning of ζ, see two paragraphs below).

Next, we notice that the curves in (4.1) are not invariant under the orbifold group G. Instead, G maps each curve to a similar one with different choices of k-th roots of -1 in the corresponding equation, and the second Chern class should be thought of as this orbit of curves in $Y^{(k)}$. However, note that in each case, a certain subgroup $G_{\text{fix}} \subset G$ does leave the curve invariant. This will lead to an additional normalization factor in our calculations in the next subsection. We identify the respective subgroups in table 4.1.

To explain the geometric role of the parameter $\zeta = \pm 1$ in (4.1), we consider the case $k = 6$ (the discussion on the other two models is the same). The set of curves $\{x_1 + \alpha x_2 = 0, x_3 + \beta x_4 = 0, x_5^2 - 3\psi x_1 x_2 x_3 x_4 = 0\}$, where α and β are arbitrary 6-th roots of -1 all lie on $X^{(6)}$. Those curves organize into two distinct orbits under the action of $G^{(k)}$, precisely distinguished by $\zeta = \pm 1$. It is clear that the Gepner monodromy $\psi \to e^{2\pi i/k}\psi$, $x_1 \to e^{-2\pi i/k}x_1$ exchanges those two orbits, $\zeta \to -\zeta$, just as we had noted it at the end of the previous section.

4.2   From curves to Picard-Fuchs

We derive the inhomogeneous Picard-Fuchs equation, *i.e.*, the constants $c^{(k)}$ in (2.24) by using the Griffiths-Dwork method. We give the details of the computation in appendix A, and only summarize the salient steps here.

The normalization of the holomorphic three-form for which we will quote the $c^{(k)}$ is

k	$\Upsilon^{(k)}$	$\mathrm{Ord}(G^{(k)})$	$\sqrt{z}$	$\rho^{(k)}$
6	$6^{-4}\psi^{-3}$	$3 \cdot 6^2$	$2 \cdot 6^{-3}\psi^{-3}$	$3^2\pi^{-4}$
8	$2^{-12}\psi^{-6}$	$2 \cdot 8^2$	2^{-8}	$2^3\pi^{-4}\psi^{-2}$
10	$10^{-4}\psi^{-8}$	10^2	$2^{-4}5^{-5/2}\psi^{-5}$	$4 \cdot 5^{1/2}\pi^{-4}\psi^{-3}$

Table 4.2: Parameters used in the main text for the hypersurfaces under consideration.

given by

$$\hat{\Omega} = \frac{\mathrm{Ord}(G^{(k)})}{(2\pi i)^3}\psi\Omega \ , \tag{4.2}$$

where Ω is the standard residue from projective space (see below (A.2)) and the $\mathrm{Ord}(G^{(k)})$ are the orders of the groups yielding the mirror manifold. We list those together with some other normalization data in table 4.2. The choice (4.2) is the normalization in which the regular integral period $\varpi_0(z)$ has a unit constant term, $\varpi_0(z) = 1 + \mathcal{O}(z)$.

The implementation of the Griffiths-Dwork algorithm however is easier in a slightly different normalization of the holomorphic three-form, in which the homogeneous Picard-Fuchs operator takes the form $\tilde{\mathcal{L}}^{(k)}$ given in equations (A.7), (A.30) and (A.49). They are related to the Picard-Fuchs operators $\mathcal{L}^{(k)}$ given in equation (2.22) by the relation

$$\mathcal{L}^{(k)} = -\Upsilon^{(k)}\tilde{\mathcal{L}}^{(k)}\frac{1}{\psi} \ , \tag{4.3}$$

where the $\Upsilon^{(k)}$ are given in table 4.2.

Putting the normalization together, the statement that $\mathcal{T}_B$ given in (2.20) (for a certain choice of curves and three-chain, explained momentarily) satisfies the inhomogeneous Picard-Fuchs equation given in (2.24) translates to the identity

$$\tilde{\mathcal{L}}^{(k)}\int_{T_\epsilon(\Gamma)}\tilde{\Omega} = -\frac{(2\pi i)^4}{\Upsilon^{(k)}\,\mathrm{Ord}(G^{(k)})}c^{(k)}\sqrt{z} \ , \tag{4.4}$$

where $\tilde{\Omega}$ is defined in (A.2) and where we have used (A.4). If the functional form $\propto \sqrt{z}$ is correct, the $c^{(k)}$ are the only unknown parameters, and the claim reduces to determine the constants $c^{(k)}$ in (4.4). That is, we can solve for $c^{(k)}$:

$$c^{(k)} = -\rho^{(k)}\tilde{\mathcal{L}}^{(k)}\int_{T_\epsilon(\Gamma)}\tilde{\Omega} \ , \tag{4.5}$$

where the $\rho^{(k)}$ are given in table 4.2.

In (4.4), $T_\epsilon(\Gamma)$ is a small tube around a three-chain suspended between the appropriate combination of curves. We are interested in the following B-model integrals (the curves are defined in (4.1)):

k	domainwall tension	curve combination
6	$\mathcal{T}_B$	$C_+^{(6)} - C_-^{(6)}$
8	$\mathcal{T}_B$	$C_{\langle +,+\rangle}^{(8)} - C_{\langle -,+\rangle}^{(8)}$
8	$\widetilde{\mathcal{T}_B}$	$C_{\langle +,+\rangle}^{(8)} - C_{\langle -,-\rangle}^{(8)}$
10	$\mathcal{T}_B$	$C_+^{(10)} - C_-^{(10)}$

$$(4.6)$$

For $k = 8$, we make the choice to denote by $\mathcal{T}_B$ the domainwall tension that vanishes at $\psi = 0$, which completely specifies the 3-chain between the respective curves. All other domainwall tensions are only define modulo integral periods for the moment.

There are in principle two types of contributions to $\tilde{\mathcal{L}}^{(k)} \int_{T_\epsilon(\Gamma)} \tilde{\Omega}$, depending on whether $\tilde{\mathcal{L}}^{(k)}$ acts on the holomorphic three-form, or on the (tube over the) three-chain. As on the quintic, it turns out that the latter contribution always vanishes (see appendix A). Thus, we just need to evaluate

$$\int_{T_\epsilon(\Gamma)} \tilde{\mathcal{L}}^{(k)}\tilde{\Omega} = \int_{T_\epsilon(\Delta\Gamma)} \tilde{\beta}^{(k)} \ , \tag{4.7}$$

where $\tilde{\beta}^{(k)}$ are the exact parts of the inhomogeneous Picard-Fuchs equations given in equations (A.8), (A.31) and (A.50). Thus the crucial integrals are those of $\tilde{\beta}^{(k)}$ over the tubes around the curves $C_\zeta^{(k)}$ for $k \in \{6, 10\}$ and $C_{\zeta\mu}^{(k)}$ for $k = 8$.

The main property of the curves that allows the evaluation of these integrals is their planarity. Namely, as on the quintic, the curves $C_\zeta^{(k)}$ and $C_{\zeta\mu}^{(8)}$ are components of the intersection of the hypersurface with an appropriately chosen plane $P^{(k)}$. Except for a small neighborhood of the intersection of the components of $P^{(k)} \cap Y^{(k)}$, the tube around the curves can be laid into the plane, where the meromorphic three-form $\tilde{\beta}^{(k)}$ vanishes trivially. We give the remaining details of this calculation in the appendix. The results are the following:

$$k = 6: \qquad \int_{T_\epsilon(C_\zeta^{(6)})} \tilde{\beta}^{(6)} = \zeta \, \frac{4}{3}\pi^2 \ ,$$

$$k = 8: \qquad \int_{T_\epsilon(C_{\zeta\mu}^{(8)})} \tilde{\beta}^{(8)} = \zeta\mu \, 3\pi^2\psi^2 \ , \tag{4.8}$$

$$k = 10: \qquad \int_{T_\epsilon(C_\zeta^{(10)})} \tilde{\beta}^{(10)} = \zeta \, \frac{16}{5}\sqrt{5}\pi^2\psi^3 \ .$$

Referring to (4.5) and (4.6), this translates to the following values for the constants $c^{(k)}$ for each of our domainwalls:

k	domainwall	$c^{(k)}$
6	$\mathcal{T}_B$	$\frac{24}{\pi^2}$
8	$\mathcal{T}_B$	$\frac{48}{\pi^2}$
8	$\widetilde{\mathcal{T}_B}$	0
10	$\mathcal{T}_B$	$\frac{128}{\pi^2}$

(4.9)

We now proceed to the explicit solution of the inhomogeneous Picard-Fuchs equation (2.24).

Chapter 5

Monodromy considerations

As on the quintic [10], it turns out that the constant $c^{(k)}$ that we computed in the previous chapter can almost uniquely be recovered by assuming an inhomogeneous term $\sim \sqrt{z}$ and requiring integrality of monodromy around the various special points in moduli space. In this chapter, we will follow this route (sections 5.1 and 5.2) and connect to the previous discussions at the end (section 5.3).

5.1   Analytic continuation of solutions

Let us fix some notations. We denote by $\tau^{(k)}(z)$ the solution of the corresponding fifth order operator $(2\theta - 1)\mathcal{L}^{(k)}$ with squareroot behaviour at $z = 0$. The Picard-Fuchs operators $\mathcal{L}^{(k)}$ are listed in equation (2.22) of chapter 2. Note that for simplicity, we will sometimes drop the $^{(k)}$ indices in the following, which quantity carries a $^{(k)}$ index should be clear from the context.

The solutions of the Picard-Fuchs equations of our hypersurfaces around $z = 0$ can by obtained by the Frobenius method from the following hypergeometric generating function

$$\Pi^{(k)}(z; H) = \sum_{m=0}^{\infty} z^{m+H} \frac{\Gamma\big(k(m + H) + 1\big)}{\prod_{i=1}^{5} \Gamma\big(\nu_i(m + H) + 1\big)} \ . \tag{5.1}$$

Namely, one checks that by expanding (5.1) in powers of H,

$$\Pi^{(k)}(z; H) = \sum_{j=0}^{3} H^j \Pi_{2j}^{(k)}(z) \bmod H^4 \ , \tag{5.2}$$

the $\Pi_{2j}^{(k)}(z)$ satisfy $\mathcal{L}^{(k)}\Pi_{2j}^{(k)}(z) = 0$. Quite remarkably, the additional solution of our inhomogeneous equation can be obtained by setting $H = 1/2$ in (5.1)

$$\tau^{(k)}(z) = \Pi^{(k)}(z; 1/2) . \tag{5.3}$$

It satisfies

$$\mathcal{L}^{(k)}\tau^{(k)}(z) = \frac{\tilde{c}^{(k)}}{16}\sqrt{z} , \tag{5.4}$$

where

$$\tilde{c}^{(k)} = \frac{\Gamma(k/2+1)}{\prod \Gamma(\nu_i/2+1)} . \tag{5.5}$$

The radius of convergence of the series (5.3) is, as for the closed string periods, given by $|z| < R_* \equiv \prod \nu_i^{\nu_i}/k^k$. To analytically continue $\tau^{(k)}(z)$ to the rest of the moduli space, in particular the Gepner point $1/z = 0$, we utilize the familiar integral representation

$$\tau^{(k)}(z) = \frac{1}{2\pi i} \int \frac{\Gamma\left(\frac{1}{2}-s\right)\Gamma\left(\frac{1}{2}+s\right)\Gamma\left(ks+1\right)}{\prod \Gamma\left(\nu_i s+1\right)} e^{i\pi(s-\frac{1}{2})} z^s , \tag{5.6}$$

where the integration contour runs straight up the imaginary axis. For $|z| < R_*$, we close the contour on the positive real axis, pick up the poles at $s = m + \frac{1}{2}$ for $m = 0, 1, \ldots$, and recover (5.3). For $|z| > R^*$, we close on the negative real axis, where we find poles of Γ-functions in the numerator at $s = -m - \frac{1}{2}$ and at $s = -\frac{m}{k}$ for $m = 1, 2, \ldots$. When k is even, the second actually encompass the former. In that case, however, we also have exactly one even weight (ν_5 in our notation) so that there is also a pole in the denominator, and the total pole at $s = -m - \frac{1}{2}$ is first order. To make progress, we separate the terms with half-integer power of z from the terms with powers on the list of exponents of the homogeneous equation,

$$\tau^{(k)}(z) = \tau_1^{(k)}(z) + \tau_2^{(k)}(z) , \tag{5.7}$$

where

$$\begin{aligned}
\tau_1^{(k)}(z) &= \sum_{m=0}^{\infty} \frac{\nu_5}{k}(-1)^{\frac{k}{2}+\frac{\nu_5}{2}+1} \frac{\Gamma\left(\nu_5 m + \frac{\nu_5}{2}\right)}{\Gamma\left(km+\frac{k}{2}\right) \prod_{i,\nu_i \text{ odd}} \Gamma\left(1-\nu_i(m+\frac{1}{2})\right)} z^{-m-\frac{1}{2}} , \\
\tau_2^{(k)}(z) &= -\frac{\pi}{k} \sum_{m=1}^{\infty} \frac{e^{i\pi\left(m-\frac{m}{k}-\frac{1}{2}\right)}}{\cos \pi \frac{m}{k}} \frac{1}{\Gamma(m) \prod \Gamma\left(1-\frac{\nu_i}{k}m\right)} z^{-m/k} .
\end{aligned} \tag{5.8}$$

In the sum for $\tau_2^{(k)}$, we have to exclude those m for which m/k is a half integer, since we have already attributed these terms to $\tau_1^{(k)}$. On the other hand, all other terms for which $\nu_i m/k$ is integer can be trivially included.

Our next task is to express $\tau_2^{(k)}$ in terms of the solutions of the homogeneous equation. We use the set of solutions of [20],

$$\varpi_j^{(k)}(z) = -\frac{\pi}{k} \sum_{m=1}^{\infty} \frac{e^{i\pi(m-\frac{m}{k})} e^{2\pi ijm/k}}{\sin \pi\frac{m}{k}} \frac{1}{\Gamma(m) \prod \Gamma\left(1 - \frac{\nu_i}{k}m\right)} z^{-m/k} , \tag{5.9}$$

for $j = 0, \ldots, k-1$. Comparing (5.8) with (5.9), we find that

$$\tau_2^{(k)}(z) = \sum a_j \varpi_j(z) , \tag{5.10}$$

provided the a_j satisfy the equations

$$- i \, \tan \pi\frac{m}{k} = \sum_{j=0}^{k-1} a_j e^{2\pi ijm/k} , \tag{5.11}$$

for $m - 0, 1, \ldots, k-1$, and where the LHS is set to 0 for $m = k/2$. Of course, the a_j are not uniquely determined by (5.10), because the $\varpi_j(z)$ satisfy some linear relations owing to the poles in the denominator of (5.9). Following [22, 20], we will use the "period vector at the Gepner point"

$$\varpi^{(k)} = \left(\varpi_2, \varpi_1, \varpi_0, \varpi_{k-1}\right) , \tag{5.12}$$

and write

$$\tau_2^{(k)} = \tilde{a}^{(k)} \cdot \varpi^{(k)} . \tag{5.13}$$

We have the following results for the vectors $a^{(k)}$ and $\tilde{a}^{(k)}$.

k	$a^{(k)}$	$\tilde{a}^{(k)}$
6	$\frac{1}{3}(0, -2, 1, 0, -1, 2)$	$\frac{1}{3}(2, -2, 1, 2)$
8	$\frac{1}{4}(0, -3, 2, -1, 0, 1, -2, 3)$	$(1, -1, 0, 1)$
10	$\frac{1}{5}(0, -4, 3, -2, 1, 0, -1, 2, -3, 4)$	$\frac{1}{5}(2, -4, 1, 2)$

$$\tag{5.14}$$

Also from [20], we extract the analytic continuation matrices between the Gepner basis $\varpi^{(k)}$ and the large volume basis $\Pi^{(k)} = (\Pi_6, \Pi_4, \Pi_2, \Pi_0)$. (This basis is almost the one from (5.2). See [20] for precise definitions.) Namely,

$$\Pi^{(k)} = M^{(k)} \varpi^{(k)} , \tag{5.15}$$

with

$$
M^{(6)} = \begin{pmatrix} 0 & -1 & 1 & 0 \\ -1 & 0 & 3 & 2 \\ \frac{1}{3} & \frac{1}{3} & -\frac{1}{3} & -\frac{1}{3} \\ 0 & 0 & 1 & 0 \end{pmatrix}, \qquad
M^{(8)} = \begin{pmatrix} 0 & -1 & 1 & 0 \\ -1 & 0 & 3 & 2 \\ \frac{1}{2} & \frac{1}{2} & -\frac{1}{2} & -\frac{1}{2} \\ 0 & 0 & 1 & 0 \end{pmatrix},
$$

$$
M^{(10)} = \begin{pmatrix} 0 & -1 & 1 & 0 \\ 0 & 1 & 1 & 1 \\ 1 & 0 & 0 & -1 \\ 0 & 0 & 1 & 0 \end{pmatrix} .
\tag{5.16}
$$

Finally, we record the action of the Gepner monodromy

$$
z^{-\frac{1}{k}} \rightarrow e^{\frac{2\pi i}{k}} z^{-\frac{1}{k}} ,
\tag{5.17}
$$

on the basis $\Pi^{(k)}$ (along the path leading to the above basis transformation). We have $\Pi^{(k)} \rightarrow A^{(k)} \Pi^{(k)}$ with

$$
A^{(6)} = \begin{pmatrix} -3 & -1 & -6 & 4 \\ -3 & 1 & 3 & 3 \\ 1 & 0 & 1 & -1 \\ -1 & 0 & 0 & 1 \end{pmatrix}, \qquad
A^{(8)} = \begin{pmatrix} -3 & -1 & -4 & 4 \\ -2 & 1 & 2 & 2 \\ 1 & 0 & 1 & -1 \\ -1 & 0 & 0 & 1 \end{pmatrix},
$$

$$
A^{(10)} = \begin{pmatrix} -2 & -1 & -1 & 3 \\ 0 & 1 & 1 & 0 \\ 1 & 0 & 1 & -1 \\ -1 & 0 & 0 & 1 \end{pmatrix},
\tag{5.18}
$$

5.2   Open string period monodromy

We now have all expressions at our disposal to discuss the analytic continuation and monodromy properties of the open string periods. After the mirror map, our current ansatz for the B-model version of the domainwall tension with large volume expansion (2.9) is [1]

$$
\mathcal{T}_A^{(k)} = \frac{\Pi_2^{(k)}}{2} + \frac{\Pi_0^{(k)}}{4} + d\tau^{(k)} ,
\tag{5.19}
$$

---

[1]We use A/B subscript to distinguish the large/small volume basis, and leave the mirror map (2.21) implicit.

where d is a constant. For $k = 8$, the additional domainwall interpolating between the two $\mathbb{RP}^3$ components of $L^{(8)}_{[0,0,0,0,1]}$ has tension

$$\widetilde{\mathcal{T}_A} = \frac{\Pi^{(8)}_4}{2} \ . \tag{5.20}$$

By construction, $\mathcal{T}_A$ and $\widetilde{\mathcal{T}_A}$ have integral large volume monodromy as $t \to t + 1$. Namely,

$$t \to t+1: \qquad \begin{array}{l} \mathcal{T}_A \ \to \Pi_2 - \mathcal{T}_A \\ \widetilde{\mathcal{T}_A} \ \to \widetilde{\mathcal{T}_A} - \Pi_2 - 2\Pi_0 \ . \end{array} \tag{5.21}$$

Consider now the Gepner monodromy, using (5.16) and (5.18). From the splitting (5.7), we see that $\tau^{(k)}_1$ changes sign as we circle $1/z = 0$ once. Since the squareroot is the hallmark of the inhomogeneity, we see that $\mathcal{T}_A$ must come back to minus itself, up to a solution of the homogeneous equation. To ensure that this solution is an integral period, we consider the behaviour of $\tau^{(k)}_2$. Combining (5.13) and (5.18), we find

$$\tau^{(k)}_2 \to -\tau^{(k)}_2 + \Pi^{(k)}_6 \ . \tag{5.22}$$

Since for each $k = 6, 8, 10$, the classical part of the domainwall tension transforms as

$$\mathcal{T}_{A,cl} = \frac{\Pi_2}{2} + \frac{\Pi_0}{4} \to \frac{\Pi_6}{4} + \Pi_2 - \mathcal{T}_{A,cl} \ , \tag{5.23}$$

we see that the minimal value of d that guarantees integrality is

$$d = -\frac{1}{4} \ . \tag{5.24}$$

The Gepner monodromy then acts as

$$z^{-1/k} \to e^{2\pi i/k} z^{-1/k}: \qquad \begin{array}{l} \mathcal{T}_A \ \to \Pi_2 - \mathcal{T}_A \\ \widetilde{\mathcal{T}_A} \ \to \widetilde{\mathcal{T}_A} - \Pi_6 + \Pi_2 + \Pi_0 \ . \end{array} \tag{5.25}$$

Integrality in the last line is ensured by the evenness of the appropriate entries in (5.18). A noteworthy consequence is the invariance of $\mathcal{T}_A$ under the conifold monodromy, resulting from combination of (5.21) and (5.25).

5.3 Domainwall spectrum and final matching of vacua

The domainwall tensions (5.19), (5.20) satisfy the same inhomogeneous Picard-Fuchs equation that we had obtained in chapter 4. Namely, with $\tilde{c}^{(k)}$ from (5.5) and $d = -1/4$ from (5.24), we find

$$\frac{1}{4}\tilde{c}^{(k)} = c^{(k)} \ , \tag{5.26}$$

where $c^{(k)}$ are the non-zero entries in (4.9). And $\widetilde{\mathcal{T}_A}$ satisfies the homogeneous equation by construction.

The fact that $\mathcal{T}_A^{(k)}$ comes back to minus itself (up to an integral period) in (5.25) means that the corresponding brane vacua are exchanged under Gepner monodromy. This is precisely what we had noted in section 2.1.

Finally, we test for tensionless domainwalls at the Gepner point. Using (5.13), we find that the leading behaviour of $\mathcal{T}_A$ around $1/z \to 0$ is given by

$$\mathcal{T}_A \sim \sqrt{z} + \tilde{b}^{(k)} \cdot \mathrm{II}^{(k)} \ , \tag{5.27}$$

where $\tilde{b}^{(k)} = -\frac{1}{4}(M^{(k)})^{-T}\tilde{a}^{(k)} + (0, 0, \frac{1}{2}, \frac{1}{4})$, explicitly,

k	$\tilde{b}^{(k)}$
6	$\frac{1}{3}(-2, -1, -3, 4)$
8	$(-1, -\frac{1}{2}, -1, 2)$
10	$\frac{1}{5}(-2, -1, 2, 4)$

$$\tag{5.28}$$

Thus, for $k = 6, 10$, the leading behaviour at $1/z = 0$ is always dominated by a non-vanishing closed string period, and we have no tensionless domainwall.[2] This is exactly what we predicted in section 2.1 under the identification (3.16), and concludes our discussion for those two models.

We continue with $k = 8$. First of all, we see from (5.28) that by combining $\mathcal{T}_A$ with $\widetilde{\mathcal{T}_A}$, we obtain a tensionless domainwall[3] at the Gepner point, which is again precisely as predicted! In chapter 4, we had denoted this vaninishing domainwall by $\mathcal{T}_B$, so we identify

$$\mathcal{T}_B = \mathcal{T}_A + \widetilde{\mathcal{T}_A} \ . \tag{5.29}$$

The other open string period from section 4 satisfies the homogeneous equation, so we have

$$\widetilde{\mathcal{T}_B} = \widetilde{\mathcal{T}_A} \ . \tag{5.30}$$

Now recalling the definitions (2.17) and (4.6) (and ignoring RR-flux, as we said),

$$\begin{aligned}
\mathcal{T}_A &= \mathcal{W}_{(\xi,+)} - \mathcal{W}_{(\xi,-)} \ , & \widetilde{\mathcal{T}_A} &= \mathcal{W}_{(\xi,\sigma)} - \mathcal{W}_{(-\xi,\sigma)} \ , \\
\mathcal{T}_B &= \mathcal{W}_{\langle +,+\rangle} - \mathcal{W}_{\langle -,+\rangle} \ , & \widetilde{\mathcal{T}_B} &= \mathcal{W}_{\langle \mu,\zeta\rangle} - \mathcal{W}_{\langle -\mu,-\zeta\rangle} \ ,
\end{aligned} \tag{5.31}$$

---

[2]This does not exclude the interesting possibility that there are tensionless domainwalls somewhere else in the moduli space.

[3]This, as well as all remaining statements in this section, are understood modulo integral periods. Those correspond to changing Ramond-Ramond flux, which is invisible on the brane. We also leave the mirror map implicit.
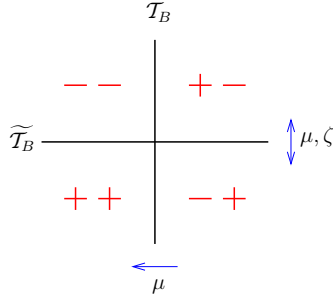
Figure 5.1: Set of vacua and basis of domainwalls at the Gepner point of $X^{(8)}$.

we obtain an exact match of domainwall spectrum if we identify the large volume brane vacua (ξ, σ) with those at the Gepner point $\langle \mu, \zeta \rangle$ according to

$$\mu = \xi \ , \ \zeta = \xi \sigma \ . \tag{5.32}$$

More pictorially, one may compare figure 2.1 with figure 5.1. The former shows the collection of vacua and interpolating domainwalls at the large volume point in the A-model, while the second illustrates the domainwall spectrum obtained in the B-model at the Gepner point.

Part III

The Real Topological String

Chapter 6

Overview and conclusion of part III

This part of the thesis is based on the author's publication [18]. The presentation differs from the original publication mainly by the inclusion of some necessary background material, making this write-up more easily accessible than the original work. The main outcome is the explicit calculation of real Gopakumar-Vafa invariants for local $\mathbb{P}^2$ via three complementary schemes. The results are listed in appendix C.

6.1 Introduction

The target space that we shall study is the local Calabi-Yau $X = \mathcal{O}_{\mathbb{P}^2}(-3)$. The involution I defining the orientifold projection is simply complex conjugation. The fixed point locus, L, on which we shall wrap one D-brane, is the real version of the canonical bundle, and can be thought of as the real line bundle defined by the orientation bundle over $\mathbb{RP}^2$. (Note that, as special Lagrangian, L, itself, is oriented.)

The central object to compute is the total, or combined open-closed-unoriented topological string free energy (the reader unfamiliar with basic terms of topological string theory, might prefer to read first the introduction sections of chapter 9), which in a perturbative expansion can be written as [1]

$$ \mathcal{G} = \sum_{\chi=-2}^{\infty} \mathcal{G}^{(\chi)} \lambda^{\chi} \, . \tag{6.1} $$

Here $\mathcal{G}^{(\chi)}$ is the contribution at order χ, and λ is the string coupling. In general, the $\mathcal{G}$

---

[1]To emphasize one point again: When the tadpole canceling D-branes are put right on top of the orientifold plane, we refer to the theory as "real". Certain of the present definitions are good somewhat more generally.

and $\mathcal{G}^{(\chi)}$ depend on closed and open string moduli, which in the A-model consist of Kähler moduli of X and complexified Wilson lines on the D-branes. In the example of interest, we have $H_2(X;\mathbb{Z}) = \mathbb{Z}$, and $H_1(L;\mathbb{Z}) = \mathbb{Z}_2$, so we have one continuous closed string modulus, denoted by $t \equiv \log q$, and one discrete open string modulus, $\epsilon = \pm 1$. Thus,

$$\mathcal{G}^{(\chi)} = \mathcal{G}^{(\chi)}(t, \epsilon) \,. \tag{6.2}$$

On general grounds, one expects to be able to compute $\mathcal{G}^{(\chi)}$ by summing contributions from individual world-sheet topologies, [2]

$$\mathcal{G}^{(\chi)} = \sum_{2g+h-2=\chi} \mathcal{F}^{(g,h)} + \sum_{2g+h-1=\chi} \mathcal{R}^{(g,h)} + \sum_{2g+h-2=\chi} \mathcal{K}^{(g,h)} \,. \tag{6.3}$$

Namely, $\mathcal{F}^{(g,h)}$ (with $\mathcal{F}^{(g)} \equiv \mathcal{F}^{(g,0)}$) is the contribution of oriented genus g surfaces with h boundaries, $\mathcal{R}^{(g,h)}$ is the contribution of unoriented genus g surfaces with h boundaries and an odd number of cross-caps (note that one can trade three cross-caps for a handle plus a cross-cap) and $\mathcal{K}^{(g,h)}$ comes from unoriented genus g surfaces with h boundaries and an even number of cross-caps. (Note that one can trade two cross-caps for a Klein handle, that is a handle with orientation reversal. The genus g in $\mathcal{K}^{(g,h)}$ refers to the number of handles plus the number of Klein handles, with at least one Klein handle.)

Moreover, each of those contributions in (6.3) should be computable by counting the number of maps from the appropriate surfaces into the background, similar to the expansion of the closed string free energy

$$\mathcal{F} = \sum_{g=0}^{\infty} \mathcal{F}^{(g)} \lambda^{2g-2} \,, \tag{6.4}$$

with (ignoring constant map contributions polynomial in $t = \log q$)

$$\mathcal{F}^{(g)} = \sum_d \tilde{n}_d^{(g)} q^d \,, \tag{6.5}$$

where the sum is over (positive) $d \in H_2(X;\mathbb{Z})$, and $\tilde{n}_d^{(g)}$ are the rational Gromov-Witten invariants. For future reference, we note the following expansion of $\mathcal{F}$ in terms of integer BPS degeneracies, $i.e.$, Gopakumar-Vafa invariants $N_d^{(g)}$ [12, 13] (details on the physical definition of these invariants are postponed to section 9.3),

$$\mathcal{F} = \sum_{g,d,k} N_d^{(g)} \frac{1}{k} \left(2\sinh\frac{\lambda k}{2} \right)^{2g-2} q^{kd} \,. \tag{6.6}$$

---

[2]In contrast to the physically motivated normalization of $\mathcal{G}^{(\chi)}$ used in [17], we chose here a different normalization which is more convenient for practical computations.

In hindsight (say if one is given the answer by some other means) it is not necessarily clear how to disentangle the individual contributions in (6.3). Cancellation of the O-plane tadpole allows wrapping only a single D-brane on L, so we only have one discrete open string modulus ϵ at our disposal. This only allows distinguishing whether h is even or odd. In some of our computations, however, there are ways to effectively introduce arbitrary numbers of brane-antibrane pairs, each with their discrete Wilson line degree of freedom. This allows keeping track of individual world-sheet topologies. Then we may write for $h > 0$:

$$
\begin{aligned}
\mathcal{F}^{(g,h)} &= \sum_{d \equiv h \bmod 2} \tilde{n}_d^{(g,h)} q^{d/2} \epsilon^h \,, \\
\mathcal{K}^{(g,h)} &= \sum_{d \equiv h \bmod 2} \tilde{n}_d^{(g,h)_k} q^{d/2} \epsilon^h \,,
\end{aligned}
\tag{6.7}
$$

where the $\tilde{n}_d^{(g,h)}$ and $\tilde{n}_d^{(g,h)_k}$ are appropriate open and unoriented Gromov-Witten invariants. In these expressions, d refers to the relative homology class in $H_2(X, L)$, or in the case of unoriented surfaces, the homology class of the covering map.

More precisely, to write (6.7), one has to assume a certain prescription to deal with homologically trivial boundaries, which we will recall below. This prescription, together with the map $H_2(X, L) \to H_1(L)$ also explains the restriction to $d \equiv h \bmod 2$, and entails the vanishing of the $\mathcal{R}^{(g,h)}$ in our model.

Independently of such assumptions, we can isolate the contribution from purely oriented closed strings (because that is known from before the orientifold projection!). Thus we define the amplitude $\mathcal{G}'^{(\chi)}$

$$
\mathcal{G}'^{(\chi)} = \mathcal{G}^{(\chi)} - \begin{cases} \mathcal{F}^{(\frac{\chi}{2}+1,0)} & \text{for } \chi \text{ even} \\ 0 & \text{for } \chi \text{ odd} \end{cases} \,,
\tag{6.8}
$$

which can be seen to have an expansion of the form

$$
\mathcal{G}'^{(\chi)} = \sum_{d \equiv \chi \bmod 2} n_d'^{(\chi)} q^{d/2} \epsilon^\chi \,,
\tag{6.9}
$$

in terms of rational numbers $n_d'^{(\chi)}$, which one might call real Gromov-Witten invariants. As found in [17], the combined open-closed-unoriented topological string free energy without oriented closed string contribution,

$$
\mathcal{G}' = \sum_\chi \mathcal{G}'^{(\chi)} \lambda^\chi \,,
\tag{6.10}
$$

possesses an expansion with integer coefficients $N_d'^{(\chi)}$, similar to that of the $\mathcal{F}^{(g)}$ in eq. (6.6)

$$\frac{1}{2}\mathcal{G}' = \sum_{\substack{d \equiv \chi \bmod 2 \\ k \text{ odd}}} N_d'^{(\chi)} \frac{1}{k} \left(2 \sinh \frac{\lambda k}{2}\right)^{\chi} q^{kd/2} \, \epsilon^{\chi} \,. \tag{6.11}$$

The $N_d'^{(\chi)}$ should be seen as a real version of Gopakumar-Vafa invariants, counting real degree d curves. Physically, they also count dimensions of Hilbert spaces of appropriate BPS objects [14].

6.2 Outline

For the model at hand, the individual contributions in (6.7) can be explicitly calculated via localization on the moduli space of stable maps, as performed by Kontsevich to calculate $\tilde{n}_d^{(0)}$ [45], generalized by several authors to the open string case [46, 47] and recently completed by the inclusion of unoriented strings [17]. Especially, localization was used to compute various oriented amplitudes for our model of interest, *i.e.*, local $\mathbb{P}^2$, in [48, 49]. The essential point that allows the extension to the real case, in this and other models, is that although the real brane is usually non-toric, it is often left invariant by the action of at least a one-dimensional torus. This is enough for localization to apply. (A toric brane in the usual sense is by definition always invariant under a two-dimensional torus.) We will review and apply this approach in chapter 7 to calculate the individual contributions to the topological amplitudes of local $\mathbb{P}^2$ for some higher χ and d. The explicit results in terms of real Gromov-Witten invariants are listed in appendix B. The localization computations quickly become rather complicated with increasing genus and degree. There are two sources of complexity. First, one has to generate the decorated graphs and correctly determine their automorphism groups. This can be tricky especially in the real case (cf. section 7.2). Second, one has to evaluate the graphs, and in particular to compute the Hodge integrals. The best available general algorithm for this still is Faber's. On the other hand, note that the computation of the Hodge integral is a local problem, attached to the fixed points of the torus action. Some years ago, it has been realized that there is in fact a closed formula that resums the requisite Hodge integrals to all orders in the genus expansion, and that incidentally also solves the first-mentioned graph combinatorial problem in a very efficient way. This is the topological vertex [50]. We will discuss this approach in chapter 8. Especially, we will derive the total topological string amplitudes via a real version of the topological vertex. Recall that the standard topological vertex solves the closed

topological string (with background toric branes) on local toric Calabi-Yau threefolds by evaluating a certain cubic field theory on the toric diagram of the Calabi-Yau viewed as a Feynman diagram [50]. Applications of the topological vertex to orientifolds have been considered before, such as in [51, 52]. In these works, the involution defining the orientifold was taken to be freely acting. The main new feature in our study is that we deal with a non-empty orientifold plane. This also requires the introduction of a specific D-brane into the background on top of the O-plane. An orientifold model that can be solved with these techniques of either localization or the topological vertex has the property that the toric diagram has an involutive symmetry to define the orientifold projection. (Toric Calabi-Yaus, which are rigid, are always invariant under complex conjugation, but unless this can be dressed with a symmetry of the toric diagram, no toric symmetry will be preserved.) There are then several possible cases for the fixed point locus. A new feature arises when there are vertices fixed under the involution of the toric diagram, and one then has to distinguish whether the fixed leg (of which there is necessarily exactly one) ending on the fixed vertex is "external" to the toric diagram or not. We will call the requisite transition amplitude the "real topological vertex". By studying real local $\mathbb{P}^2$, we will be able to deduce the real vertex in which the fixed leg is external. Since our main aim here is a proof of principle, we will not try to go beyond that. It is conceivable that a more complete theory exists. Both localization and the topological vertex fail in general for compact models. The only tool available which works also in the compact setup, is mirror symmetry together with the (extended) holomorphic anomaly equations of [31, 30], to be discussed in chapter 9.

Note that while we introduced the A-model topological string free energies $\mathcal{F}(t), \mathcal{K}(t)$ and $\mathcal{G}(t)$ in a rather geometric way as a count of holomorphic maps from world-sheets with specific topology into a Calabi-Yau manifold with Kähler parameter t, it is important to note that this interpretation only holds at large volume. Away from this point in moduli space, classical notions of geometry break down and so does the original interpretation of the free energies. On the other hand, the proper definition of the perturbative amplitudes is really in terms of the topologically twisted 2d world-sheet theory, which is well-defined over the entire stringy Kähler moduli space. Here it is where mirror symmetry comes to rescue, since the A-twisted world-sheet theory on X is equivalent to a B-twisted theory on a mirror Calabi-Yau geometry Y, with Kähler parameter traded for complex structure, such that the B-model captures the quantum regime of the A-model. In particular, the corresponding B-model amplitudes $\mathcal{F}(z, \bar{z}), \mathcal{K}(z, \bar{z})$ and $\mathcal{G}(z, \bar{z})$ are now functions over the complex structure moduli space of Y, which we will denote as $\mathcal{M}_Y$.

A key point that allows to efficiently solve for the amplitudes in the B-model is that their anti-holomorphic derivatives over $\mathcal{M}_Y$ do not vanish [31], as we have indicated in the notation. The so-called holomorphic anomaly equations [31, 30, 17], completely determine the anti-holomorphic dependence of the amplitudes, and reduce the problem to the fixing of the holomorphic part. Constraints of modular invariance and a priori knowledge about the compactification of the moduli space make this a finite-dimensional problem. Its general solution is still rather elusive, but important progress has been made in recent years.

To emphasize this important point, the notorious problem of the B-model approach is that one has to fix the holomorphic ambiguity (boundary conditions on moduli space) at each order in perturbation theory. In the closed topological string it has been shown [53, 34] that detailed information about the singularity structure at the conifold locus can be carried over to compact models and leads to a very efficient solution scheme up to very high genus. For non-compact models, the same structure leads to complete integrability (for an explicit example, see [54]). It is natural to look for a similar structure also in the real topological string, and indeed we will make a find, see section 9.7.

An additional bonus of the B-model is the possibility to analyze the structure of the amplitudes at special points in moduli space other than large volume.

Mirror symmetry and the holomorphic anomaly have the advantage that they give an answer to all orders in the instanton expansion, but the disadvantage that they are limited to an order-by-order calculation in the string coupling expansion. On the other hand, the topological vertex gives an all-order result in the string coupling, but in practical computations is limited to the first few orders in the instanton expansion. Finally, localization is an order-by-order computation in both directions, and also computationally rather challenging. What it has going for it is that of the three techniques we study, it is the one that is likely easiest to put on a rigorous mathematical foundation. Finally, the results for the real Gopakumar-Vafa invariants $N_d'^{(\chi)}$ of local $\mathbb{P}^2$ are collected in appendix C.

6.3   Conclusion

In this part of the thesis, we have initiated a detailed study of the real topological string on local Calabi-Yau threefolds. Whereas the topological string on local (toric) Calabi-Yaus (with toric branes) is essentially solved, and understood from a variety of different perspectives, and we have made significant progress on the systematics of the real topological string, much remains to be understood (both in the local and the compact situation). We

see possibilities for further work in several directions.

The most interesting question to us is whether it is possible to achieve full integrability in the B-model, as is the case for the local closed topological string. As discussed in section 9.7, the behavior of the real amplitudes at the conifold point in moduli space does not yield enough constraints to fully fix the holomorphic ambiguities. Therefore, it would be very desirable to find additional systematic constraints in order to completely fix those ambiguities. A related question is the interpretation of the leading singularity of the Klein bottle amplitudes (without boundaries) at the conifold point. One expects to be able to find a closed expression for the leading coefficient and thereby obtain an additional constraint which aids in fixing the ambiguities.

Another possible line to follow would be to generalize the real topological vertex presented in chapter 8 to arbitrary local toric Calabi-Yau 3-folds. This would put the real topological string on equal footing with the closed topological string (for local geometries) and would open up the arena for various case studies and further investigations. One might also try to generalize the recent progress on spectral curve methods (see [55] for a review and references) as a B-model version of the topological vertex, to the real topological string. The explicit data obtained in this work should be helpful as guideline to find the right formulation.

Finally, from a mathematical point of view, the localization technique originally sketched in [10, 17], and reviewed and applied in chapter 7, needs to be formulated in a more rigorous way (especially the tadpole cancellation). Also, in order to put the enumerative aspects of the real topological string on a firmer mathematical ground, one should seek a proper definition of real Gopakumar-Vafa invariants.

We believe that with the present work in hand, the real topological string can indeed be put on equal footing with the topological string on local geometries in the near future. The compact case on the other hand might remain as a challenge for some time to come. The localization and topological vertex techniques are not applicable in the compact setting at higher genus. On the other hand, it is reasonable to expect that the gap structure that we found at the conifold will persist in compact models. This should allow for their solution to much higher level than before. Ultimately, progress on the open sector should also feed back to the closed topological string. So perhaps in combination, one can learn enough to solve both simultaneously. We look forward to further research on these matters.

Chapter 7

The A-model

In this chapter, we explain the computation of open and unoriented Gromov-Witten invariants of the real topological string on local $\mathbb{P}^2$ using localization on the space of maps. For the reader's convenience, we firstly recall some basics about the localization calculation for pure closed string world-sheets. A more detailed exposition can be found in standard textbooks on mirror symmetry, for example [56, 3], or in the original works [45, 57]. We then discuss the extension to open and unoriented world-sheets developed in [17]. Especially, we will work out in more detail some technical issues which are important at higher degree and genus. One should note that performing the computations (that is, developing a working and sufficiently fast computer implementation of the scheme sketched below) is highly non-trivial and therefore forms one of the major achievements of this thesis. The actual results of our calculations are listed in appendices B and C.

7.1 Localization

We first briefly recall the basics of how to calculate the pure oriented closed string contribution $\tilde{n}_d^{(g,0)}$ for local $\mathbb{P}^2$ via localization.

Define $\overline{\mathcal{M}}_d^{\hat{\Sigma}} \equiv \overline{\mathcal{M}}_{\hat{g},0}(d, \mathbb{P}^2)$ as the moduli space of stable maps $\hat{f} : \hat{\Sigma} \to \mathbb{P}^2$ from genus $\hat{g}$ curves into $\mathbb{P}^2$ with image of degree $d \in H_2(\mathbb{P}^2, \mathbb{Z})$. Let $\mathbf{e}(\mathcal{E}_d)$ be the Euler class of the bundle $\mathcal{E}_d = H^1(\Sigma^g, f^*\mathcal{O}(-3))$ over $\overline{\mathcal{M}}_d^{\hat{\Sigma}}$. Then, the Gromov-Witten invariants $\tilde{n}_d^{\hat{\Sigma}} \equiv \tilde{n}_d^{(\hat{g},0)}$ are given by

$$\tilde{n}_d^{\hat{\Sigma}} = \int_{\overline{\mathcal{M}}_d^{\hat{\Sigma}}} \mathbf{e}(\mathcal{E}_d). \tag{7.1}$$

These integrals can be evaluated by the Atiyah-Bott localization formula.

To this end, consider the $\hat{\mathbb{T}} = (\mathbb{C}^*)^3$ group action on $\mathbb{P}^2$. The fixed points of $\hat{\mathbb{T}}$ on $\mathbb{P}^2$ are the three points p_i given by the projectivization of the i-th coordinate line of $\mathbb{C}^3$. The only curves invariant under $\hat{\mathbb{T}}$ are the three lines l_{ij} joining the p_i. The $\hat{\mathbb{T}}$ action can be pulled back to an action on $\overline{\mathcal{M}}_d^{\hat{\Sigma}}$. We will denote the $\hat{\mathbb{T}}$-invariant subspace of $\overline{\mathcal{M}}_d^{\hat{\Sigma}}$ as $\hat{\mathbb{T}}\overline{\mathcal{M}}_d^{\hat{\Sigma}}$. Since a point in $\hat{\mathbb{T}}\overline{\mathcal{M}}_d^{\hat{\Sigma}}$ is a map of a genus $\hat{g}$ curve $\hat{\Sigma}$ to the $\hat{\mathbb{T}}$-invariant locus in $\mathbb{P}^2$, we immediately deduce that $\hat{\Sigma}$ can only consist of the union of a certain number of n_v-pointed irreducible genus g_v curves $C_{v,n_v}^{(g_v)}$ joined together by 2-pointed spheres. The $C_{v,n_v}^{(g_v)}$ are contracted to one of the three points p_i, while the spheres are mapped to the l_{ij}. It follows that each map $\hat{f}$ can be represented combinatorially as a connected graph, *i.e.*, to each map $\hat{f}$ we associate a graph $\hat{\Gamma}$ by identifying each contracted component of $\hat{\Sigma}$ with a decorated vertex, where the decoration is given by the genus of the component and the point p_i it maps to in target space. The spheres joining the contracted components are then identified with edges joining the corresponding vertices, where each edge is decorated with the degree (*i.e.*, the multi-cover) of the map which sends the corresponding sphere to l_{ij}.

Thus, we have a map which associates to each point in $\hat{\mathbb{T}}\overline{\mathcal{M}}_d^{\hat{\Sigma}}$ a decorated graph. Note that the map is not one-to-one, but rather each graph $\hat{\Gamma}$ corresponds to a subspace $\hat{M}_d^{\hat{\Gamma}} \subset {}^{\hat{\mathbb{T}}}\overline{\mathcal{M}}_d^{\hat{\Sigma}}$.

In order to see this, observe that each vertex of the graph $\hat{\Gamma}$ comes with the moduli space of an n_v-pointed genus g_v curve, usually denoted as $\overline{\mathcal{M}}_{g_v,n_v}$. Hence, each graph corresponds to the moduli space $\overline{\mathcal{M}}_{\hat{\Gamma}}$ given by

$$\overline{\mathcal{M}}_{\hat{\Gamma}} = \prod_v \overline{\mathcal{M}}_{g_v,val(v)} \ . \tag{7.2}$$

Obviously, there exists a map $\gamma_{\hat{\Gamma}} : \overline{\mathcal{M}}_{\hat{\Gamma}} \rightarrow \hat{M}_d^{\hat{\Gamma}}$, which is however not an isomorphism. In order to obtain an isomorphism, we need to quotient by the automorphism group of $\overline{\mathcal{M}}_{\hat{\Gamma}}$ given by $\mathbb{A}_{\hat{\Gamma}} = \mathrm{Aut}(\hat{\Gamma}) \ltimes \prod_e \mathbb{Z}_{d_e}$, where $\mathrm{Aut}(\hat{\Gamma})$ is the automorphism group of $\hat{\Gamma}$ as a decorated graph.

Thus, we have

$$\hat{\mathbb{T}}\overline{\mathcal{M}}_d^{\hat{\Sigma}} \cong \bigcup_{\hat{\Gamma}} \left(\overline{\mathcal{M}}_{\hat{\Gamma}} / \mathbb{A}_{\hat{\Gamma}} \right) \ , \tag{7.3}$$

where the union is over the set of all non-isomorphic graphs $\hat{\Gamma}$ whose topology and decoration fulfill the following criteria:

- $\sum_e d_e = d$.

- $1 - |v| + |e| + \sum_v g_v = \hat{g}$, where $|v|$ and $|e|$ is the number of vertices and edges, respectively.

- $i(v_a) \neq i(v_b)$, for v_a connected to v_b, where $i(v_j)$ encodes the point in target space the corresponding component maps to.

Applying the Atiyah-Bott localization formula then tells us that we can evaluate (7.1) via a sum over graphs:

$$\tilde{n}_d^{\hat{\Sigma}} = \sum_{\hat{\Gamma}} \frac{1}{|\mathbb{A}_{\hat{\Gamma}}|} \int_{\overline{\mathcal{M}}_{\hat{\Gamma}}} \frac{\mathbf{e}(i^* \mathcal{E}_d)}{\mathbf{e}(\mathcal{N}_{\hat{\Gamma}}^{vir})} \ , \tag{7.4}$$

where $|\mathbb{A}_{\hat{\Gamma}}|$ is the order of the group $\mathbb{A}_{\hat{\Gamma}}$.

Explicit expressions for $\mathbf{e}(i^* \mathcal{E}_d)$ and $\mathbf{e}(\mathcal{N}_{\hat{\Gamma}}^{vir})$ in equivariant cohomology have been derived in [57]. We restate them here for convenience:

$$\mathbf{e}(i^* \mathcal{E}_d) = \prod_v \lambda_{i(v)}^{val(v)-1} P_{g(v)}(\Lambda_{i(v)}) \prod_e \prod_{m=1}^{3d_e-1} \left[\Lambda_{i(e)} + \frac{m}{d_e}(\lambda_{i(e)} - \lambda_{j(e)}) \right] \ , \tag{7.5}$$

$$\frac{1}{\mathbf{e}(\mathcal{N}_{\Gamma}^{vir})} = \prod_e \frac{(-1)^{d_e} d_e^{2d_e}}{(d_e!)^2 (\lambda_{i(e)} - \lambda_{j(e)})^{2d_e}} \prod_{\substack{k \neq i(e), j(e) \\ a=0}}^{d_e} \frac{1}{\frac{a}{d_e}\lambda_{i(e)} + \frac{d_e-a}{d_e}\lambda_{j(e)} - \lambda_k}$$

$$\times \prod_v \prod_{j \neq i(v)} (\lambda_{i(v)} - \lambda_j)^{val(v)-1} \tag{7.6}$$

$$\times \begin{cases} \prod_v \left[\left(\sum_F w_F^{-1}\right)^{val(v)-3} \prod_{F \ni v} w_F^{-1} \right] & \text{for } g(v) = 0 \\ \prod_v \prod_{j \neq i(v)} P_{g(v)}(\lambda_{i(v)} - \lambda_j) \prod_{F \ni v} \frac{1}{w_F - \kappa_F} & \text{for } g(v) \geq 1 \end{cases} \ ,$$

with

$$w_F = (\lambda_{i(F)} - \lambda_{j(F)})/d_e \ ,$$
$$\Lambda_i = \lambda_1 + \lambda_2 + \lambda_3 - 3\lambda_i \ ,$$
$$P_g(x) = \sum_{r=0}^{g} c_{g-r}(E^*) x^r \ , \tag{7.7}$$

where $i(e)$ and $j(e)$ refer to the target space points the vertices attached to the edge e map to, F runs over the set of flags of a vertex, that is, all pairs (v, e) for a fixed vertex v with e ending on v. For a flag, we have $i(F) = i(v)$ and $j(F)$ refers to the other end point of e. Finally, E is the Hodge bundle, κ_F is a gravitational descendant and λ_i are the torus weights.

Thus, the integration in equation (7.4) boils down to the evaluation of Hodge integrals, for which one can use Faber's algorithm [58].
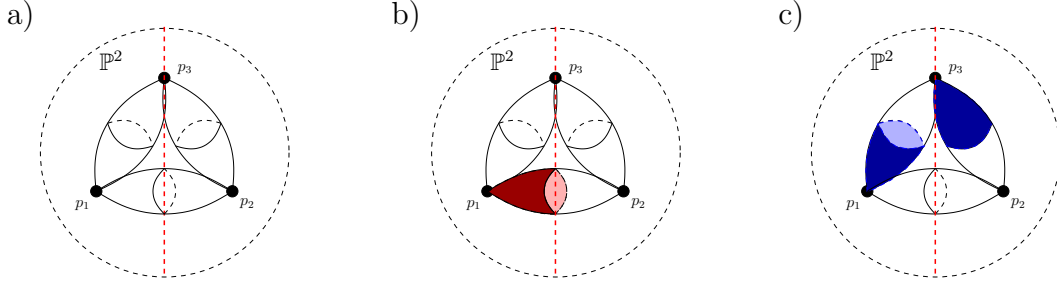
Figure 7.1: a) The orientifold is chosen to act on $\mathbb{P}^2$ such that the $\hat{\mathbb{T}}$ fixed points p_1 and p_2 are identified, while p_3 is mapped to itself. The sketched (football-shaped) spheres correspond to the lines l_{ij}. b) The line l_{12} can be mapped to from either a disk or a cross-cap. c) The line l_{13} corresponds in the quotient either to a 2-sphere by gluing disks of different color or to a Klein handle by gluing two disks of the same color.

7.2   Orientifolded localization

In order to calculate the remaining contributions to $\mathcal{G}^{(\chi)}$ via localization, one would like to replace $\overline{\mathcal{M}}_d^{\hat{\Sigma}}$ by something like the moduli space $\overline{\mathcal{M}}_d^{\Sigma}$ of stable maps $f : \Sigma \to C$ from curves Σ of Euler characteristic χ (with boundaries and cross-caps) into $\mathbb{P}^2$ with image d in the relative homology group $d \in H_2(\mathbb{P}^2, L; \mathbb{Z})$.

The proper mathematical definitions related to $\overline{\mathcal{M}}_d^{\Sigma}$ have so far not been given, except when Σ is the disk [35]. Nevertheless, and following [17], we can give a computational scheme that allows the evaluation of a putative virtual fundamental class of $\overline{\mathcal{M}}_d^{\Sigma}$, after localization. The main reason for this simplification is that after implementing the tadpole cancellation condition of [17], we effectively only need to count maps that send any boundary to a non-trivial one-cycle on L, and that do not contract any cross-caps. As a result, we have to deal only with moduli spaces of n-pointed genus g curves, as without orientifold projection, and also avoid potentially dangerous regions in moduli space where a node lies right on top of the orientifold-plane.

To begin, we choose the involution I such that it is maximally compatible with the covering space action $\hat{\mathbb{T}}$. This means that the projection leaves a subtorus $\mathbb{T} \cong \mathbb{C}^* \subset \hat{\mathbb{T}}$ intact. Such an I identifies two of the three covering space fixed-points p_i and as well two of the fixed-lines l_{ij}. We arrange it such that p_1 is identified with p_2. The corresponding action I is sketched in figure 7.1a. We infer that l_{12} is mapped to itself and can receive a disk or a cross-cap, as sketched in figure 7.1b. Note that one can glue two of these

disks or two cross-caps to obtain a 2-sphere or a Klein handle, respectively. The line l_{13} can correspond to either a 2-sphere or a Klein handle. How that Klein handle occurs is sketched in figure 7.1c. In detail, one half of the line can be thought to correspond to the line l_{13} while the other half comes from the mirror line l_{23}.

As in the case without orientifold projection, we can pull back the $\mathbb{T}$ action to an action on $\overline{\mathcal{M}}_d^\Sigma$. We will denote the $\mathbb{T}$ invariant subspace as $^{\mathbb{T}}\overline{\mathcal{M}}_d^\Sigma$. Due to our restriction to homologically non-trivial boundaries, we have that Σ can only be the union of n-pointed irreducible genus g curves mapping under f to one of the two non-invariant torus fixed points p_1, p_2, and joined together by either 2-spheres or Klein handles. Furthermore, irreducible disk or cross-cap components can be attached to a contracted component. As before, it follows that each map f can be represented combinatorially as a connected graph Γ, with a bit of additional decoration.

The contracted component curves correspond again to vertices decorated with the genus of each component, as well as by the point it maps to in target space. As before, the 2-spheres joining the contracted components are mapped to edges connecting the corresponding vertices. As a novelty, the Klein handles joining contracted components are identified with Klein edges, which we may draw as an edge with a cross on top. Note that a Klein edge can be attached to a single vertex, *i.e.*, it may form a loop (in distinction to an ordinary edge). We will refer to these Klein edges also as external Klein edges, while the Klein edges connecting two distinct vertices will be refered to as internal Klein edges. The disks and the cross-caps map to half-edges (also known as legs), or cross-edges attached to the vertices corresponding to the contracted component to which the disk or cross-cap are attached to, respectively. We will draw these simply as half-edges or half-edges with an arrow, attached to vertices (with $i(v) = 1$ or 2 decoration). Note that there is a non-trivial restriction on graphs with Klein edges. Namely, since a Klein edge represents a handle (with orientation reversal), a proper graph should not split into disconnected components after removal of a Klein edge.

As in the unorientifolded theory, each vertex can be associated to an ordinary moduli space $\overline{\mathcal{M}}_{g_v, val(v)}$, such that the full graph corresponds to the moduli space

$$\overline{\mathcal{M}}_\Gamma = \prod_v \overline{\mathcal{M}}_{g_v, val(v)} \ . \tag{7.8}$$

Again, there is a morphism $\gamma_\Gamma : \overline{\mathcal{M}}_\Gamma \to M_d^\Gamma \subset {}^{\mathbb{T}}\overline{\mathcal{M}}_d^\Sigma$, which becomes an isomorphism if

we quotient by $\mathbb{A}_\Gamma$, the automorphism group of $\overline{\mathcal{M}}_\Gamma$. Thus,

$$\mathbb{T}\overline{\mathcal{M}}_d^\Sigma \cong \bigcup_\Gamma \left(\overline{\mathcal{M}}_\Gamma / \mathbb{A}_\Gamma\right) \ . \tag{7.9}$$

However, one has to be extra careful with $\mathbb{A}_\Gamma$. In order to illustrate why, let us slightly change our point of view.

To each curve Σ we can associate a corresponding covering curve $\hat{\Sigma}$ with $\Sigma = \hat{\Sigma}/\sigma$. The covering space curve $\hat{\Sigma}$ has genus $\hat{g} = \chi + 1$. Moreover each map f can be lifted to a covering space map $\hat{f}$ which is equivariant:

$$\hat{f} = I \circ \hat{f} \circ \sigma^{-1} \ . \tag{7.10}$$

That is, the following diagram commutes:

$$\begin{array}{ccc}
\hat{\Sigma} & \xrightarrow{\ \hat{f}\ } & X \\
{\scriptstyle\sigma}\downarrow & & \downarrow{\scriptstyle I} \\
\hat{\Sigma} & \xrightarrow{\ \hat{f}\ } & X
\end{array} \tag{7.11}$$

Thus, $\overline{\mathcal{M}}_d^\Sigma$ can as well be defined as the fixed locus of the moduli space $\overline{\mathcal{M}}_d^{\hat{\Sigma}}$ of the corresponding doubled curve, *i.e.*, $\overline{\mathcal{M}}_d^\Sigma = {}^{\omega^*}\overline{\mathcal{M}}_d^{\hat{\Sigma}}$, with ω^* the map obtained by conjugating with I and σ, as in (7.10). In particular,

$$\mathbb{T}\overline{\mathcal{M}}_d^\Sigma = {}^{\omega^*}\hat{\mathbb{T}}\overline{\mathcal{M}}_d^{\hat{\Sigma}} \ . \tag{7.12}$$

Recall that to each $\hat{f} \in \hat{\mathbb{T}}\overline{\mathcal{M}}_d^{\hat{\Sigma}}$ and $f \in \mathbb{T}\overline{\mathcal{M}}_d^\Sigma$ we have associated a corresponding graph $\hat{\Gamma}$, or Γ, respectively. In thinking about these various identifications, and their automorphism groups, one's first naive expectation is that

$$\Gamma = \hat{\Gamma}/\omega^* \ , \tag{7.13}$$

holds, with

$$|\mathrm{Aut}(\Gamma)| = |\mathrm{Aut}(\hat{\Gamma})^*| \ , \tag{7.14}$$

where $\mathrm{Aut}(\hat{\Gamma})^*$ is the subgroup of $\mathrm{Aut}(\hat{\Gamma})$ that commutes with ω^*. Note that ω^* acting on Γ leaves no vertices fixed, due to our restriction to non-trivial boundaries and cross-caps.

To see that the relation is more subtle than described in (7.13) and (7.14), note first that the inverse of relation (7.13) is always true. Namely, to a given graph Γ we can associate a corresponding covering space graph $\hat{\Gamma}$ via the following "doubling" procedure: For each
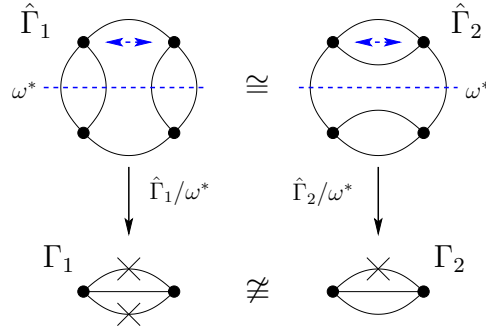
Figure 7.2: The two graphs $\Gamma_1 \not\cong \Gamma_2$ can potentially contribute to $\tilde{n}_6^{(2,0)_k}$. However, we have that $\hat{\Gamma}_1 \cong \hat{\Gamma}_2$, with $\Gamma_1 = \hat{\Gamma}_1/\omega^*$ and $\Gamma_2 = \hat{\Gamma}_2/\omega^*$, hence only one should contribute to $\tilde{n}_6^{(2,0)_k}$.

vertex v draw a corresponding mirror vertex v' with same $v(g)$ but mirror $i(v)$ decoration and for each edge draw a corresponding mirror edge. Then, for each disk and cross-cap connected to a vertex, draw an edge connecting the vertex with its mirror. Further, for each external Klein edge draw two edges connecting the vertex and its mirror, while for each internal Klein edge connecting the vertices v_1 and v_2 draw an edge connecting v_1 to v_2' and one connecting v_2 to v_1', where v_i' are the mirror vertices.

However, while this doubling procedure gives a well-defined map $\Gamma \mapsto \hat{\Gamma}$, there is generally no good inverse, *i.e.*, relation (7.13) does not hold in general. For example, consider the graphs $\hat{\Gamma}_1$ and $\hat{\Gamma}_2$ shown in figure 7.2. Both belong to the same equivalence class $[\hat{\Gamma}]$, *i.e.*, there exists an isomorphism $a : \hat{\Gamma}_1 \to \hat{\Gamma}_2$, equivariant with respect to ω^*. However, the corresponding quotient graphs under ω^* are not isomorphic. This is because in general the quotient graph $[\hat{\Gamma}]/\omega^*$ depends on the choice of representative of $[\hat{\Gamma}]$, *i.e.*, we have that

$$[\hat{\Gamma}]/\omega^* = \bigcup_i [\Gamma_i], \tag{7.15}$$

where $[\Gamma_i]$ are equivalence classes of non-isomorphic quotient graphs Γ_i. Nevertheless, the equivariance condition for $\hat{f}$ implies that we should include only one graph $\Gamma \in \{\Gamma_i\}$, since $\hat{f}$ should descend to a unique f.

Hence, the relations $M_d^\Gamma = {}^{\omega^*}M_d^{\hat{\Gamma}} \subset {}^{\mathbb{T}}\overline{\mathcal{M}}_d^\Sigma$, and (7.13), should be understood in the sense that they may include a choice of representative of $[\hat{\Gamma}]$. However, note that independent of a choice of representative, we have

$$\overline{\mathcal{M}}_\Gamma = {}^{\omega^*}\overline{\mathcal{M}}_{\hat{\Gamma}} = \sqrt{\overline{\mathcal{M}}_{\hat{\Gamma}}} . \tag{7.16}$$
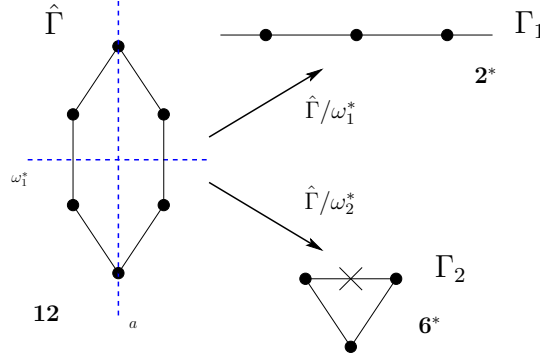
Figure 7.3: The cyclic graph $\hat{\Gamma} = C_6$ with two differently acting involutions ω_i^*. The involution ω_1^* yields a quotient graph Γ_1 with two half-edges contributing to $\tilde{n}_6^{(0,2)}$, while the involution $\omega_2^* = (a\omega_1^*)$ results in a graph Γ_2 with a Klein edge contributing to $\tilde{n}_6^{(1,0)_k}$. The bold-face number is $|\mathrm{Aut}(\hat{\Gamma})|$, while the bold-face numbers with star are the orders of the subgroups of $\mathrm{Aut}(\hat{\Gamma})$ that commute with ω_i^*.

The lesson we learn is the following. In order to avoid multiple countings we have to include in (7.9) only one representative of $\hat{\Gamma}/\omega^*$. In practice, this means that we have to perform an extended isomorphism test on the set of graphs $\{\Gamma\}$, *i.e.*, two graphs need to be considered as identical if they are firstly isomorphic after replacement of Klein edges with normal edges or if they secondly lift to the same covering graph.

Let us now take a closer look at the relation (7.14). As an illustrative example, consider the graph $\hat{\Gamma}$ with the two differently acting projections ω_i^* sketched in figure 7.3. We see that ω_1^* satisfies condition (7.14), while ω_2^* not. This raises the question whether $\mathbb{A}_\Gamma$ involves $\mathrm{Aut}(\Gamma)$ or $\mathrm{Aut}(\hat{\Gamma})^*$. Again, the equivariance condition implies that $\mathrm{Aut}(\hat{\Gamma})^*$ is the correct choice. Hence,

$$\mathbb{A}_\Gamma = \mathrm{Aut}(\hat{\Gamma})^* \ltimes \left(\prod_c \mathbb{Z}_{d_c} \prod_e \mathbb{Z}_{d_e} \prod_k \mathbb{Z}_{d_k} \prod_h \mathbb{Z}_{d_h} \right) , \tag{7.17}$$

where k runs over the set of Klein edges, h the set of half-edges and c the set of cross-caps, if present.

Finally, incorporating the tadpole condition of [17], which tells us that graphs involving disks with even degree cancel against graphs with cross-caps, we deduce that the set $\{\Gamma\}$ contributing to $\tilde{n}_d^{(g,h)}$ and $\tilde{n}_d^{(g,h)_k}$ includes all non-isomorphic and extended-non-isomorphic graphs Γ which fulfill the following criteria:

- d_h is odd for all half-edges.

- $2 \sum_e d_e + 2 \sum_k d_k + \sum_h d_h = d$.

- $1 - 2|v| + 2|e| + 2|k| + |h| + 2 \sum_v g_v = g$, where $|k|$ is the number of Klein edges and $|h|$ the number of half-edges.

- Edges connect only vertices with $i(e) \neq j(e)$.

- Half-edges are only attached to vertices with $i(v) = 1$ or 2.

- Klein edges only connect vertices with $i(k) = j(k)$ or with $i(k) = 1$ or 2 and $j(k) = 3$ or vice-versa.

Then, with $\Gamma = \hat{\Gamma}/\omega^*$ we obtain from (7.4):

$$\tilde{n}_d^\Sigma = (-1)^{3g-3+h} \sum_\Gamma \frac{(-1)^{|k|}}{|\mathbb{A}_\Gamma|} \int_{\overline{\mathcal{M}}_\Gamma} \sqrt{\frac{\mathbf{e}(i^* \mathcal{E}_d)}{\mathbf{e}(\mathcal{N}_{\hat{\Gamma}}^{vir})}} \ , \tag{7.18}$$

where the sum runs over the set $\{\Gamma\}$ specified above. Note that our discussion does not a priori fix the overall sign nor the sign of each individual graph. However, most of the sign factors in (7.18) can actually be borrowed from the tree-level discussion in [35]. The remaining signs were determined in [17] based on computations on compact models, comparison with the B-model, and integrality of Gopakumar-Vafa invariants. The existence of the sign $(-1)^k$ can also be inferred from the requirement that the contribution of a given class of equivariant graphs should be independent of the chosen quotient representative, see discussion around eq. (7.15).

The contribution of vertices, edges and Klein edges of the quotient space graph Γ to the integrand of (7.18) is as before accounted for by (7.5) and (7.6), and supplemented by the following modifications. For each half-edge ending on a vertex v, add a flag (v, h) to the set of flags of v. Define $i(h)$ as the image point p_i to which v maps in target space and $j(h)$ the image point p_j of the corresponding mirror-vertex in the covering graph. We also multiply the integrand by the following factor accounting for the half-edges. (This is essentially just a squareroot of an ordinary edge contribution.)

$$D(\Gamma) = \prod_h \frac{(-1)^{\frac{d_h-1}{2}} d_h^{d_h}}{(d_h!)(\lambda_{i(h)} - \lambda_{j(h)})^{d_h}} \prod_{\substack{k \neq i(h), j(h) \\ a=0}}^{\frac{d_h-1}{2}} \frac{1}{\frac{a}{d_h} \lambda_{i(h)} + \frac{d_h-a}{d_h} \lambda_{j(h)} - \lambda_k}$$

$$\times \prod_h^{\frac{3d_h-1}{2}} \left[\Lambda_{i(h)} + \frac{m}{d_h} (\lambda_{i(h)} - \lambda_{j(h)}) \right] \ . \tag{7.19}$$

The Klein edges are treated like usual edges, however with $i(k)$ and $j(k)$ defined as $i(v)$ and $j(v)$ of the corresponding covering graph edge. At the very end, we need to identify in the integrand $\lambda_1 = -\lambda_2$. Then we cancel any common factors between numerator and denominator from each summand. These could cause ill-defined "$\frac{0}{0}$"-type expressions when we set $\lambda_3 = 0$ in the final expression for $\tilde{n}_d^\Sigma$.

We have developed a full computer implementation of the above prescription and used it to calculate the open and unoriented Gromov-Witten invariants up to $\chi = 9$ for various degrees. Despite the fact that the actual implementation is non-trivial, we restrain from giving here any technical details on the actual implementation, and rather just list the complete set of obtained data in appendix B. The real Gopakumar-Vafa invariants which we were able to deduce from the data can be found in appendix C. Finally, note that the Gromov-Witten invariants obtained will be used in chapter 9 to fix the holomorphic ambiguities of the B-model.

Chapter 8

The (real) topological vertex

In this chapter, we will derive the real Gopakumar-Vafa invariants of local $\mathbb{P}^2$ via the real topological vertex. In section 8.1 and 8.2 we will recall some basic background material needed to formulate the topological vertex, which will be introduced in section 8.3, following roughly [50, 16]. The (1-leg) real topological vertex will be derived in section 8.4 at hand of local $\mathbb{P}^2$, as in [18]. The results of our computations, in terms of real Gopakumar-Vafa invariants, are listed in appendix C.

8.1 Toric manifolds and GLSM

Since we will need later on the description of a (non-compact) toric Calabi-Yau manifold in terms of a symplectic quotient, which can be seen physically as the vacuum manifold of a gauged linear sigma model (GLSM for short), let us briefly recall some basics thereof. More details can be filled in from standard textbooks (see for instance [3]).

A non-compact toric Calabi-Yau manifold M can be described as a symplectic quotient

$$M = \mathbb{C}^{3+k}//G, \tag{8.1}$$

with $G = U(1)^k$. The quotient is obtained by imposing the k constraints (moment maps)

$$\sum_{i=1}^{3+k} Q_i^a |z_i|^2 = r^a, \tag{8.2}$$

and dividing by G

$$z^i \rightarrow z^{i\epsilon_a Q_i^a} z^i, \tag{8.3}$$

with z_i the coordinates of $\mathbb{C}^{3+k}$, $a = 1, \ldots, k$, and where r^a are Kähler parameters mea-suring the sizes of 2- and 4-cycles. The parameters Q_i^a are usually referred to as charges for reasons that will become clear momentarily. The Calabi-Yau condition (vanishing first chern class, i.e., $c_1(M) = 0$) is equivalent to vanishing of the total charge, that is

$$\sum_i Q_i^a = 0 \,. \tag{8.4}$$

The symplectic description of a toric Calabi-Yau naturally arises as the vacuum man-ifold (defined by the vacuum expectation values of scalar fields) of a gauged linear sigma model. In detail, the sigma model of relevance is a $\mathcal{N} = (2, 2)$ supersymmetric $U(1)^k$ gauge theory with $(k + 3)$ chiral fields X_i (whose scalar components are the z_k). The charges of the X_i under the $U(1)$ gauge factors are the Q_a^i. The vacuum manifold is obtained by imposing the D-term constraints

$$\sum_i Q_i^a |X_i|^2 = t^a \,, \tag{8.5}$$

where $t^a = r^a + i\theta^a$, with r^a the Fayet-Iliopoulos parameter and θ^a Theta-angle of the ath $U(1)$ gauge factor. In addition, we need to mod out by gauge equivalence. Comparing to the symplectic description given above, one can easily infer that the vacuum manifold is indeed equivalent to a toric Calabi-Yau, as long as the charges satisfy (8.4).

Let us conclude this section by giving two explicit examples:

Example I: local $\mathbb{P}^2$

The linear sigma model yielding local $\mathbb{P}^2$, i.e., $\mathcal{O}(-3) \to \mathbb{P}^2$, is a $U(1)$ gauge theory with 4 chiral fields X_i and charge vector $Q = (1, 1, 1, -3)$. There is a single parameter t corresponding to the complexified Kähler class of the base $\mathbb{P}^2$. We have a single D-term constraint which reads

$$|X_1|^2 + |X_2|^2 + |X_3|^2 - 3|X_4|^2 = t \,. \tag{8.6}$$

Clearly, the fields X_i with $i \in \{1, 2, 3\}$ parameterize the $\mathbb{P}^2$ forming the base, while X_4 is a coordinate on the $\mathcal{O}(-3)$ fiber.

Example II: local $\mathbb{P}^1 \times \mathbb{P}^1$

The sigma model for local $\mathbb{P}^1 \times \mathbb{P}^1$, *i.e.*, $\mathcal{O}(-2,-2) \to \mathbb{P}^1 \times \mathbb{P}^1$, involves a $U(1) \times U(1)$ gauge group with 5 chiral fields X_i. The charge vector Q_1 for the first gauge factor reads $Q_1 = (1,1,0,0,-2)$, while the charge vector for the second gauge factor is given by $Q_2 = (0,0,1,1,-2)$. The two parameters t_1 and t_2 correspond to the complexified Kähler parameters of the two $\mathbb{P}^1$ in the base. Furthermore, we have two D-term constraints

$$
\begin{aligned}
|X_1|^2 + |X_2|^2 - 2|X_5|^2 &= t_1 \ , \\
|X_3|^2 + |X_4|^2 - 2|X_5|^2 &= t_2 \ .
\end{aligned}
\tag{8.7}
$$

The X_i for $i \in \{1,2\}$ are identified with the coordinates of the first $\mathbb{P}^1$ and X_i for $i \in \{3,4\}$ with coordinates of the second $\mathbb{P}^1$ in the base, while X_5 parameterizes the fiber.

8.2 Vertex geometry

In this chapter, we want to compute the topological string partition function of a local toric Calabi-Yau background X via the topological vertex approach. The basic idea of the topological vertex is to obtain the full topological string amplitude via appropriately gluing open topological string amplitudes of $\mathbb{C}^3$ patches together. Thus, we first need a (convenient) decomposition of a background X into $\mathbb{C}^3$ patches. As it turns out, for this purpose it is most convenient to express X as a $\mathbb{T}^2 \times \mathbb{R}$ fibration over $\mathbb{R}^3$, which is always possible for a local toric background [50].

Let us see how the $\mathbb{T}^2 \times \mathbb{R}$ over $\mathbb{R}^3$ fibration structure arises at hand of the simplest toric manifold, *i.e.*, flat space. In this case, we parameterize the background via three complex coordinates z_i and introduce the Hamiltonians

$$
\begin{aligned}
r_\alpha &= |z_1|^2 - |z_3|^2 \ , \\
r_\beta &= |z_2|^2 - |z_3|^2 \ , \\
r_\gamma &= \mathrm{Im}(z_1 z_2 z_3) \ .
\end{aligned}
\tag{8.8}
$$

These Hamiltonians generate three flows on $\mathbb{C}^3$ via the Poisson brackets

$$
\partial_v z_i = \{r_v, z_i\}_\omega \ ,
\tag{8.9}
$$

with respect to the natural symplectic form $\omega = \sum_i dz_i \wedge d\bar{z}_i$ on $\mathbb{C}^3$ and where $v \in \{\alpha, \beta, \gamma\}$. Clearly, this yields a $\mathbb{T}^2 \times \mathbb{R}$ fibration over $\mathbb{R}^3$, where the base is parameterized by $(r_\alpha, r_\beta, r_\gamma) \subset \mathbb{R}^3$ and the fiber is defined via the flows (8.9). Especially, the $\mathbb{T}^2$ fiber is generated by the circle action

$$
e^{i(\alpha r_\alpha + \beta r_\beta)} : (z_1, z_2, z_3) \to \left(e^{i\alpha} z_1, e^{i\beta} z_2, e^{-i(\alpha+\beta)} z_3\right) \ .
\tag{8.10}
$$

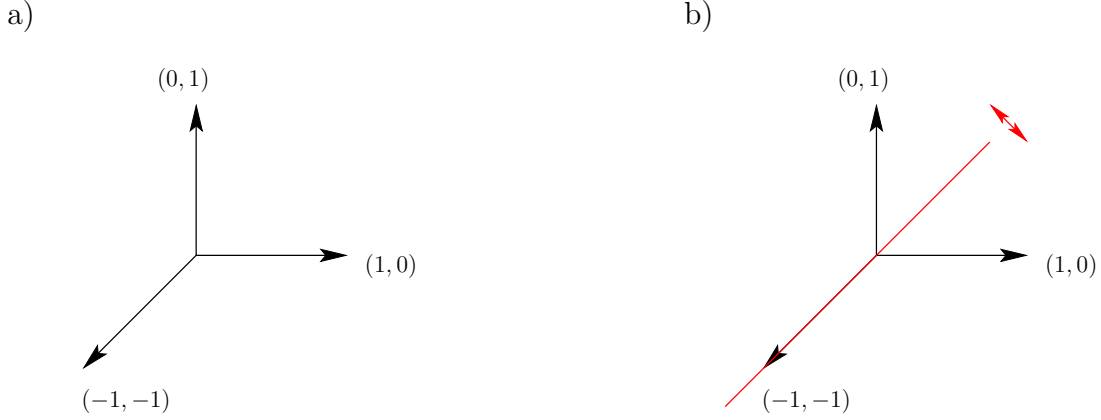a)   b)

Figure 8.1: a) Toric description of $\mathbb{C}^3$ as $\mathbb{T}^2 \times \mathbb{R}$ fibered over $\mathbb{R}^3$. The degeneration locus of the $\mathbb{T}^2$ fiber is given by the trivalent graph drawn in the $(r_\alpha, r_\beta, 0)$-plane of the base. The labels $(-p, q)$ correspond to the cycles of the $\mathbb{T}^2$ fiber which vanish over the corresponding edge. b) The anti-holomorphic involution of $\mathbb{C}^3$ under consideration acts on the trivalent graph as a reflection along the diagonal.

Observe that the $\mathbb{T}^2$ of the fibration degenerates over a trivalent graph in the $(r_\alpha, r_\beta, 0)$-plane in the base (which we will denote as Γ). This can be seen as follows: The 1-cycle of the $\mathbb{T}^2$ fiber generated by r_α degenerates over the subspace $z_1 = z_3 = 0$ of $\mathbb{C}^3$. Using (8.8), it is easy to see that this correspond to the $(0, r_\beta, 0)$ vector in the base with $r_\beta \geq 0$. Similar, the 1-cycle generated by r_β degenerates over the vector $(r_\alpha, 0, 0)$ with $r_\alpha \geq 0$. Finally, the 1-cycle generated by $r_\alpha - r_\beta$ degenerates over $z_1 = z_2 = 0$, which translates to the vector $(r_\alpha, r_\beta, 0)$ with $r_\alpha, r_\beta \leq 0$ and $r_\alpha = r_\beta$. Hence, the degeneration locus of the $\mathbb{T}^2$ clearly corresponds to a trivalent graph in the base. This is illustrated in figure 8.1a. Note that the $\mathbb{T}^2$ fiber over Γ has the topology of three infinite disks D_i (each disk arises as a S^1 fibered above one of the edges) meeting at the origin, where the full $\mathbb{T}^2$ shrinks to zero size.

Let us choose the generators of $H_1(\mathbb{T}^2)$ such that r_α generates the $(0, 1)$-cycle and r_β the $(1, 0)$-cycle. Then, one can correlate the degenerating cycles with the lines in the graph unambiguously by letting a $(-q, p)$-cycle degenerate over an edge that corresponds to $pr_\alpha + qr_\beta = 0$. However, one should keep in mind that due to the $SL(2, \mathbb{Z})$ symmetry of the $\mathbb{T}^2$ this choice is not unique.

For later reference, note that one can easily translate an anti-holomorphic involution of $\mathbb{C}^3$ to an action on the corresponding $\mathbb{T}^2 \times \mathbb{R}$ over $\mathbb{R}^3$ fibration by using (8.8). For example,

the anti-holomorphic involution I, acting on $\mathbb{C}^3$ as

$$I : (z_1, z_2, z_3) \rightarrow (\bar{z}_2, \bar{z}_1, \bar{z}_3) \,, \tag{8.11}$$

(with fixed-point locus given by $\mathbb{C} \times \mathbb{R}$) acts on the corresponding fibration as follows: I acts on the base as an exchange of r_α with r_β and a reflection of r_γ, as sketched in figure 8.1b. The explicit action on the fiber is for our purposes not relevant, however, if needed, it can be easily inferred from (8.10).

Another geometric property we will make use of later, is the fact that there exists a specific class of (special) Lagrangian 3-cycles of $\mathbb{C}^3$, which we will denote as L_i, with topology $\mathbb{C} \times S^1$ (Lagrangian means that the Kähler form restricted to L vanishes, while special means that the 3-cycle is calibrated, *i.e.*, volume minimizing) [5]. In particular, the L_i wrap in the description of $\mathbb{C}^3$ as a $\mathbb{T}^2 \times \mathbb{R}$ over $\mathbb{R}^3$ fibration the $\mathbb{T}^2$ part of the fiber and project to lines in the base [50]. In detail, the Lagrangians can be parameterized as

$$
\begin{aligned}
L_1 &: r_\alpha = 0, \; r_\beta = r_1^*, \; r_\gamma \geq 0 \,, \\
L_2 &: r_\beta = 0, \; r_\alpha = r_2^*, \; r_\gamma \geq 0 \,, \\
L_3 &: r_\alpha - r_\beta = 0, \; r_\alpha = r_3^*, \; r_\gamma \geq 0 \,,
\end{aligned}
\tag{8.12}
$$

where r_i^* is a modulus of L_i. Specifically, the L_i end on the graph Γ. This is illustrated in figure 8.2a. The reason why these Lagrangians are of particular interest, lies in the fact that they intersect the (infinite) disks D_i at position r_i^*, *i.e.*, we have non-trivial relative homology groups $H_2(\mathbb{C}^3, L_i)$. This is sketched in figure 8.2b.

The (special) Lagrangians 3-cycles L_i we have introduced are non-compact. However, they can be "compactified" by introducing an additional set of vectors $f_i = (p_{f_i}, q_{f_i})$ in the (p, q)-plane over which a corresponding 1-cycle, *i.e.*, $(-q, p)$-cycle, of the $\mathbb{T}^2$ fiber degenerates (see figure 8.2c). Let us denote the vectors spanning the trivalent vertex as $v_i = (p_{v_i}, q_{v_i})$. If the projection of the L_i hits one of the f_i, another 1-cycle of the $\mathbb{T}^2$ fiber degenerates. Thus, over the end-points of this line, *i.e.*, then it hits v_i, respectively f_i, we have that the $\mathbb{T}^2$ fiber degenerates to a S^1. If the pair (f_i, v_j) forms a oriented basis of $H_1(\mathbb{T}^2)$, that is

$$f_i \wedge v_i = p_{f_i} q_{v_i} - q_{f_i} p_{v_i} = 1 \,, \tag{8.13}$$

holds, the $\mathbb{T}^2$ fiber on the line is topologically a non-degenerate S^3, which we will denote as $\tilde{L}_i$. Note that if f_i fulfills (8.13), so does $f_i + n v_i$ for any integer n.

A convenient choice for the f_i is given by

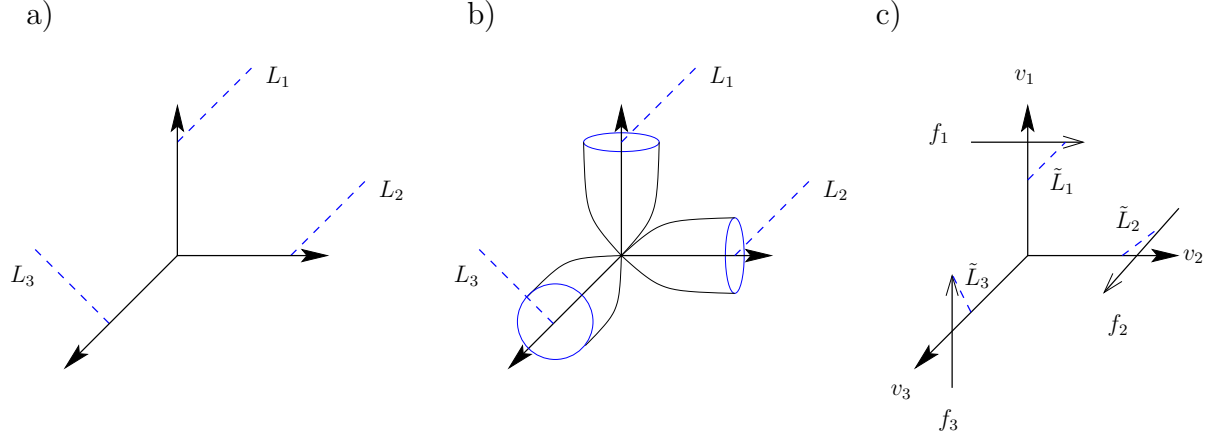$$(f_1, f_2, f_3) = (v_2, v_3, v_1) \,, \tag{8.14}$$

Figure 8.2: a) Toric diagram of $\mathbb{C}^3$ with the Lagrangians L_i. b) Sketch of the disks ending on the L_i. c) The compact three cycles $\tilde{L}_i$ in canonical framing.

which is called canonical framing and is illustrated in figure 8.2c.

We have now all basic ingredients at hand we will need later on. However, we still need to discuss how one can patch together the local pieces described above to form a (non-compact) toric Calabi-Yau manifold. For that, we use the symplectic description of a non-compact toric manifold introduced in section 8.1. First, one decomposes the $N = k+3$ complex coordinates z_i of the symplectic description into $\mathbb{C}^3$ patches. Then, one chooses one patch, say U_1, and introduces the Hamiltonians r_α and r_β as in (8.8) to generate the $\mathbb{T}^2$ fiber, while r_γ is taken to be the gauge invariant $r_\gamma = \text{Im}(\prod_i z_i)$. The translation of r_α and r_β to other patches can be achieved by using the momentum maps, *i.e.*, D-terms (see equation (8.2)), to express r_α and r_β in terms of the local coordinates used in the patch one wants to go to.

In this way we obtain a globally defined $\mathbb{T}^2$ fiber, to whose degeneration locus over the base spanned by r_α and r_β one can associate a graph Γ (consisting of local patches), fully encoding the global geometry. This receipt will become more clear in the explicit example given below.

However, there is a more convenient method to obtain the graph Γ of a non-compact toric Calabi-Yau, which we briefly mention here for completeness. In fact, one can argue that Γ is simply the graph dual of the toric diagram, which we will refer to as $\hat{\Gamma}$, of the Calabi-Yau under consideration! For a detailed discussion (including the relation to (p, q)-webs), we refer to [50].
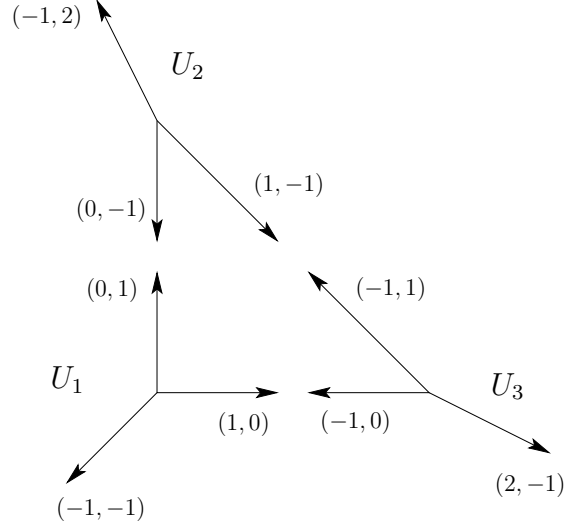
Figure 8.3: Graph Γ encoding local $\mathbb{P}^2$ constructed by patching three $\mathbb{C}^3$ patches U_i together.

Let us illustrate both ways of obtaining Γ via explicit examples:

Example I: local $\mathbb{P}^2$

As described in section 8.1, this model has four coordinates z_j and a D-term constraint given by (8.6). Thus, we have three $\mathbb{C}^3$ patches given by $z_i \neq 0$ for $i = 1, 2, 3$, where we will denote each respective patch by U_i. In detail, due to (8.6), one of the three z_i needs to be non-zero and we can solve for this z_i (the phase can be gauged away by dividing by the $U(1)$ action of the symplectic quotient), leaving the remaining coordinates z_j unconstrained, which therefore form a $\mathbb{C}^3$ patch U_i.

A corresponding globally defined $\mathbb{T}^2 \times \mathbb{R}$ over $\mathbb{R}^3$ fibration (which is fully encoded in a graph Γ in $\mathbb{R}^2$, see figure 8.3) can now be constructed as follows: We choose one of the patches U_i, let's say $U_1 = (z_2, z_3, z_4)$, and define on U_1 the fibration similar as for $\mathbb{C}^3$ via $r_\alpha = |z_2|^2 - |z_4|^2$ and $r_\beta = |z_3|^2 - |z_4|^2$, with the third direction given by the gauge invariant variable $r_\gamma = \text{Im}(z_1 z_2 z_3 z_4)$. The corresponding (local) graph is as in figure 8.1a. We can now use (8.6) to translate the two Hamiltonians r_α and r_β to the other patches. For example, in the patch $U_3 = (z_1, z_2, z_4)$, we have that r_α is defined as in U_1, while we have that r_β is given in U_3 by $r_\beta = t - |z_1|^2 - |z_2|^2 + 2|z_4|^2$. The corresponding action on
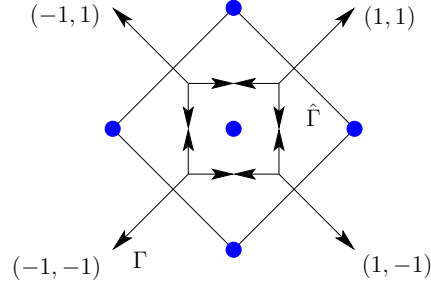
Figure 8.4: The toric diagram $\hat{\Gamma}$ of local $\mathbb{P}^1 \times \mathbb{P}^1$ with Γ (encoding the $\mathbb{T}^2$ fiber degeneration locus) being its graph-dual.

the $\mathbb{T}^2$ fiber over U_3 reads

$$e^{i(\alpha r_\alpha + \bar{r}_\beta)} : (z_1, z_2, z_4) \rightarrow \left(e^{-i\beta} z_1, e^{i(\alpha - \beta)} z_2, e^{i(2\beta - \alpha)} z_4\right). \tag{8.15}$$

The degeneration locus of the $\mathbb{T}^2$ fiber over U_3 can be easily inferred. We deduce that the 1-cycle generated by $r_\alpha + r_\beta$, that is the $(-1, 1)$-cycle, degenerates over $z_1 = z_4 = 0$. This translates in the base to the line with $r_\alpha \geq 0$ and $t \geq r_\beta \geq 0$. Further, the $(2, -1)$-cycle generated by $r_\alpha - 2r_\beta$ degenerates over the line with $r_\alpha \leq 0$, $2r_\alpha + r_\beta = t$ and $t \geq r_\beta \geq 0$. Finally, there is a $(-1, 0)$-cycle, generated by r_β, which degenerates over the line $r_\alpha = 0$ and $t \geq r_\beta \geq 0$.

The remaining U_2 patch can be derived similarly and one obtains the graph Γ shown in figure 8.3, encoding local $\mathbb{P}^2$.

Example II: local $\mathbb{P}^1 \times \mathbb{P}^1$

One can derive the corresponding graph Γ as in the previous example, however, it is far more convenient to just use the fact stated above that Γ simply corresponds to the (p, q)-web dual to the toric diagram $\hat{\Gamma}$. The corresponding graphs $\hat{\Gamma}$ and Γ for local $\mathbb{P}^1 \times \mathbb{P}^1$ are shown in figure 8.5.

8.3   The vertex

We have now all geometric ingredients at hand to state the topological vertex. As was shown in the last section, a non-compact toric Calabi-Yau can be decomposed into $\mathbb{C}^3$ patches. Furthermore, we associated to a patch a set of (special) Lagrangian 3-cycles L_i.

Let us now consider the (open) topological string A-model partition function for a $\mathbb{C}^3$ patch with N_i D-branes on L_i. As discovered in [29], the open topological string amplitudes on this geometry are not univocally defined in the sense that they depend on choice of an integer for each boundary. This is known as framing ambiguity. This ambiguity can be specified by replacing the non-compact L_i by compactified Lagrangians $\tilde{L}_i$ (defined by a set of framing vectors f_i, as introduced in the last section).

For canonical framing, the open topological string partition function will be given by

$$Z = \sum_{R_1, R_2, R_3} C_{R_1 R_2 R_3} \prod_{i=1}^{3} \mathrm{Tr}_{R_i} V_i \,, \tag{8.16}$$

where V_i is a matrix source associated to the i-th Lagrangian and each sum runs over the set of all Young diagrams (including the trivial diagram, which we will denote later on simply as $\bullet$). The amplitude $C_{R_1 R_2 R_3}$ is a function of the string coupling λ and contains information about holomorphic maps from (oriented) Riemannian surfaces into $\mathbb{C}^3$ with boundary on L_i. This amplitude is known as the topological vertex. An important property is its cyclic symmetry:

$$C_{R_1 R_2 R_3} = C_{R_3 R_1 R_2} = C_{R_2 R_3 R_1} \,. \tag{8.17}$$

One can show that the full three-legged vertex (in canonical framing) is given by [50]

$$C_{R_1 R_2 R_3} = q^{\kappa_{R_2}/2 + \kappa_{R_3}/2} \sum_{Q, Q_1, Q_3} N_{Q Q_1}^{R_1} N_{Q Q_3^t}^{R_3^t} \frac{W_{R_2^t Q_1} W_{R_2 Q_3^t}}{W_{R_2 \bullet}} \,, \tag{8.18}$$

where the $N_{Q Q_1}^{R_1}$ are the $U(\infty)$ tensor product coefficients, and $W_{R_1 R_2} = W_{R_1 R_2}(q)$ is a certain rational function of q ($q = e^\lambda$) that arises by taking a specific limit (in level and rank) of the Chern-Simons invariant of the Hopf link in S^3 decorated with R_1 and R_2. When one of the representations on the vertex is trivial, we have the more compact expression

$$C_{\bullet R_1 R_2} = q^{\kappa_{R_2}/2} W_{R_1 R_2} \,. \tag{8.19}$$

As discussed in section 8.2, every non-compact toric geometry can be obtained by appropriately gluing local $\mathbb{C}^3$ patches together. Naturally, one might wonder if one can similarly glue the patchwise defined open topological partition functions (8.16) together to obtain the closed topological string partition function of the glued geometry. This is indeed the case, as derived in [50]. Important preceding developments are [59, 60]. The basic (minimal) receipt is as follows:

As described in section 8.2, we can easily infer from the toric diagram of the background the graph Γ where the $\mathbb{T}^2$ fibration degenerates. The edges are labeled by integral vectors v_i that encode which cycle of the fiber degenerates over the edge. Further, to each edge we associate a representation R_i.

The graph can be partitioned to trivalent vertices, *i.e.*, $\mathbb{C}^3$ patches. This associates to each vertex an ordered triplet of vectors (v_i, v_j, v_k), where the ordering is taken to be clockwise. If all edges are outgoing, we associate to the vertex a factor $C_{R_i R_j R_k}$, otherwise we replace the corresponding representation (associated to the incoming edge) by its transpose times $(-1)^{l(R)}$.

Let a vertex with triple (v_i, v_j, v_k) share the i-th edge with another vertex whose triple is (v_i', v_j', v_k'), *i.e.*, $v_i' = -v_i$. In this case, we glue the two amplitudes by summing over the representations on the i-th edge:

$$\sum_{R_i} C_{R_j R_k R_i} e^{-l(R_i) t_i} (-1)^{(n_i+1) l(R_i)} q^{-n_i \kappa_{R_i}/2} C_{R_i^t R_j' R_k'} , \qquad (8.20)$$

with $n_i = v_k' \wedge v_k$ if v_k and v_k' have the same orientation and $n_i = -v_k' \wedge v_k$ else (where $\wedge$ is defined as in (8.13)). $l(Q)$ denotes the number of boxes in the young diagram R, *i.e.*, $l(R) = \sum_i l_i$ with l_i the number of boxes in the i-th row of the diagram, R^t denotes the transpose diagram and t is the size of the 2-sphere obtained by gluing the two edges (recall that we have associated a disk with each edge, and by gluing the two disks we obtain a 2-sphere). Further, we defined

$$\kappa_{R_i} = \sum_i l_i (l_i - 2i + 1) . \qquad (8.21)$$

Finally, note that non-compact edges of Γ carry only the trivial representation $R = \bullet$.

For completeness, we just mention that the vertex is more powerful than one might infer from the above (minimal) description. For example, it can be as well used to calculate open string amplitudes for D-branes on outer or inner legs [50].

Let us illustrate the above sketched gluing rules via the following example:

Example: local $\mathbb{P}^2$

The corresponding graph Γ can be found in figure 8.3. We associate representations to the edges of the graph as sketched in figure 8.5. Following the above receipt, we directly
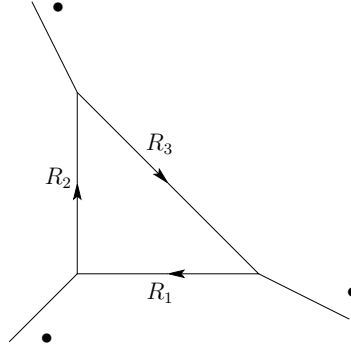
Figure 8.5: Diagram representing local $\mathbb{P}^2$ for the purpose of evaluating the topological vertex.

obtain the following expression for the total closed string topological partition function:

$$Z = \sum_{R_1,R_2,R_3} (-1)^{\sum_i l(R_i)} e^{-\sum_i l(R_i)t} q^{\sum_i \kappa_{R_i}} C_{\bullet R_2 R_3^t} C_{\bullet R_1 R_2^t} C_{\bullet R_3 R_1^t} , \qquad (8.22)$$

where t is the single Kähler parameter of local $\mathbb{P}^2$. In this sum, the R_i run over all Young diagrams (representations of $U(\infty)$). We can relate the free energy in those variables to the Gopakumar-Vafa invariants as follows [59]

$$\mathcal{F} = \log Z = \sum_{d,g,k} N_d^{(g)} \frac{1}{k} \big(q^{k/2} - q^{-k/2}\big)^{2g-2} e^{-tkd} . \qquad (8.23)$$

The invariants $N_d^{(g)}$ can be easily extracted (for an extensive list, see for instance [59]) and are in perfect agreement with the results obtained via other means (see for example [48], where some of the N_d^g were calculated via localization).

8.4 The real vertex

We are now in a position to present the formulas that express the real topological string amplitudes of local $\mathbb{P}^2$ in terms of the (real) topological vertex. The basic idea is the following. The topological vertex can be viewed as an all-genus resummation of the local contribution at each vertex on the toric diagram to the localization formulas for the topological string amplitude (see, *e.g.*, [61]). Going from the ordinary topological string to the real topological string amounts in the localization formalism to first restrict to the graphs fixed under the target space involution, and then take a squareroot of each individual contribution. The only conceptual difficulty is to understand which sign of the squareroot to

take. Taking these observations together, all we have to do to obtain a real vertex formalism is to identify the action of the target space involution on the toric diagram of figure 8.5 and on formulas (8.18) and (8.22), and then to take an appropriate squareroot. It is in fact not hard to see that the action on the representations is $R_1 \mapsto R_2$ and $R_3 \mapsto R_3$ (this can be derived similarly as the action on $\mathbb{C}^3$ shown in figure 8.1b). Using the symmetry of the topological vertex

$$C_{R_1 R_2 R_3} = q^{\sum \kappa_{R_i}/2} C_{R_1^t R_3^t R_2^t} , \tag{8.24}$$

we see that for the fixed configurations, $R_1 = R_2$, the summand in (8.22) is of the form.

$$(-1)^{2l(R_1)+l(R_3)} q^{-5\kappa_{R_1}/2 - \kappa_{R_3}/2} e^{-t(2l(R_1)+l(R_3))} \big(C_{\bullet R_3^t R_1} \big)^2 C_{\bullet R_1^t R_1} . \tag{8.25}$$

This is a perfect square except for the final term, which arises at the vertex fixed under the involution. Such a term will arise in general toric Calabi-Yaus with involution that leaves some vertices fixed, but permutes two of the legs ending on it. In that case, we will generally require a "real topological vertex" that might be obtained by taking an appropriate squareroot of the expression (8.3) for the topological vertex with $R_3 = R_1^t$, and $R_2 = R_2^t$. Indeed, we see that with this external data, and restriction of the sum to $Q_3 = Q_1^t$, the vertex is itself almost a sum of squares,

$$\big(N_{QQ_1}^{R_1} \big)^2 \frac{\big(W_{R_2^t Q_1} \big)^2}{W_{R_2 \bullet}} , \tag{8.26}$$

except for the $W_{R_2 0}$ in the denominator. We do not know at present how to take a squareroot of that last term. But luckily, for our application to local $\mathbb{P}^2$, we only need the two-legged vertex, and the real vertex only with trivial representation $R_2 = \bullet$ on the fixed leg. Based on the above observations, we propose the following expression for that real vertex amplitude

$$C_{R_1 \bullet}^{\text{real}} = q^{-\kappa_{R_1}/4} \sum_{Q,Q_1} N_{QQ_1}^{R_1} W_{Q_1 \bullet} . \tag{8.27}$$

Returning to the formula for local $\mathbb{P}^2$, we obtain for the partition function of the real topological string

$$Z^{\text{real}} = \sum_{R_1, R_3} (-1)^{l(R_1)} (-1)^{p(R_3)} e^{-t(l(R_1)+l(R_3)/2)} q^{-5\kappa_{R_1}/4 - \kappa_{R_3}/4} C_{R_1 \bullet}^{\text{real}} C_{\bullet R_3^t R_1} , \tag{8.28}$$

where $(-1)^{p(R_3)} = \pm 1$ is an a priori undetermined sign. Note that for symmetry reasons, this sign can only depend on R_3, as we have indicated. Some experimentation shows that

its correct value is determined by the *number of boxes in even columns*. In other words, if R_3^t consists of rows of length $l_1, \ldots l_r$, then

$$(-1)^{p(R_3)} = (-1)^{\sum_i l_{2i}} . \tag{8.29}$$

We are not aware that such a sign associated with 2d partitions has appeared before, nor does there seem to be any representation theoretic meaning. This would be worthy of clarification. In any event, we can now make contact with the other expressions for the amplitudes of real local $\mathbb{P}^2$. The real analogue of (8.23), see also (6.11), is

$$\log Z^{\text{real}} = \frac{1}{2}\mathcal{F} + \sum_{\substack{d \equiv \chi \bmod 2 \\ k \text{ odd}}} N_d'^{(\chi)} \frac{1}{k} \left(q^{k/2} - q^{-k/2}\right)^{\chi} e^{-tkd/2} \epsilon^{\chi} . \tag{8.30}$$

These formulas reproduce the localization results of the previous section, wherever the available data has allowed comparison, and also agree with the developments of the B-model to which we turn presently.

To close this section, we point out that we have merely scratched the surface of the real topological vertex. Starting with the derivation, but including its properties, applications, and connections with other theories, one can ask for a real counterpart of essentially everything that is known about the ordinary topological vertex. The central question in this endeavour is whether the signs can be understood in a uniform way. We have to leave this for the future.

Chapter 9

The B-model

In this chapter, we will calculate the real Gopakumar-Vafa invariants of local $\mathbb{P}^2$ in the mirror B-model. For this purpose, we will first recall some basics about topological field and string theory in sections 9.1, 9.2 and 9.3. A more detailed exposition of the necessary background material can be found for instance in [3]. We then give a sketch of the derivation of the (extended) holomorphic anomaly equations in sections 9.4 and 9.5, following [31, 30, 17]. Finally, in sections (9.6) and (9.7) we will use the (extended) holomorphic anomaly equations to derive real topological amplitudes of local $\mathbb{P}^2$. The results in terms of Gopakumar-Vafa invariants are listed in tables C.1 and C.2 of appendix C. A further major outcome of this chapter is the discovery of a new kind of "gap" structure of topological Klein-bottle amplitudes at the conifold point in moduli space.

9.1 Topological field theory basics

The starting point for the definition of a topological string theory is a two dimensional superconformal field theory with $\mathcal{N} = (2, 2)$ worldsheet supersymmetry. Such theories have four real supercharges: Two holomorphic charges $G^{\pm}$ and two anti-holomorphic charges $\bar{G}^{\pm}$ (all spin $\frac{1}{2}$). The superscript indicates the ± 1 charge under the $U(1)$ R-symmetries J and $\bar{J}$ (spin 1). Further, such theories possess a holomorphic, T, and anti-holomorphic, $\bar{T}$, stress-energy tensor (spin 2). We take the central charge to be $\hat{c} = 3$ and assume that all $U(1)$ charges are integer. The (holomorphic) supercharges satisfy the algebra

$$(G^{\pm})^2 = 0 \,, \ \{G^+, G^-\} = 2L_0 \,, \ [G^{\pm}, L_0] = 0 \,, \tag{9.1}$$

with L_0 the zero mode of the holomorphic stress-tensor. The anti-holomorphic version of this algebra is similar. From the nilpotency of the supercharges it follows that we can define some notion of G cohomology for fields and states. In order to obtain a finite dimensional space for the cohomology group, we need to consider suitable additions of holomorphic and anti-holomorphic supercharges. There are two inequivalent combinations (plus their conjugates):

$$Q_A = G^+ + \bar{G}^- \ \text{ and } \ Q_B = G^+ + \bar{G}^+ \,. \tag{9.2}$$

As far as the cohomology of states is concerned, Q_A, Q_B and their conjugates give all rise to the same space of states, *i.e.*, the supersymmetric ground states of the theory. However, the cohomology of fields generated by Q_A, Q_B and their conjugates, *i.e.*, fields ϕ which satisfy

$$[Q, \phi] = 0, \ \ \phi \sim \phi + [Q, \cdot] \,, \tag{9.3}$$

where $\cdot$ stands for any field ϕ' such that $[Q, \phi']$ is Q-exact, are not equivalent as operators. The cohomology operators for Q_A are called (chiral, anti-chiral) fields, for short (c, a), while the operators for Q_B are referred to as (chiral, chiral) fields, for short (c, c) or just chiral. Similar for the cohomology operators for the conjugates of Q_A and Q_B. In this thesis, we will only be concerned about Q_B (and its conjugate), hence we will drop the subscript from now on and implicitly always mean Q_B.

Let ϕ_i be a basis of Q-cohomology operators. Since such a basis forms a ring (the chiral ring), we can expand the product of two elements as

$$\phi_i \phi_j = \phi_k C_{ij}^k + [Q, \cdot] \,, \tag{9.4}$$

with C_{ij}^k the structure constants of the ring with respect to the basis ϕ_i. Similar for the cohomology of the conjugate of Q (forming the anti-chiral ring). [1] The R-symmetries provide the rings with two gradings, which we will denote by q and $\bar{q}$ (the $U(1)$ charges of the states). Chiral fields have $0 \leq q, \bar{q} \leq \hat{c}$, while anti-chiral fields have $0 \geq q, \bar{q} \geq \hat{c}$.

In order to construct a topological field theory, we need to perform a topological twist [62], that is, we redefine the worldsheet stress tensor via

$$T \rightarrow T \pm \frac{1}{2} \partial J \,, \tag{9.5}$$

plus an analog redefinition of $\bar{T}$. As there are four different chiral rings, we can perform four different twists (depending on choice of sign in (9.5) and its analog for $\bar{T}$). We will

---

[1]Naturally, this holds as well for the cohomologies of Q_A, (and its conjugate), hence we have four different chiral rings.

Figure 9.1: Doing the twisted path-integral on the hemisphere with insertion of the chiral field ϕ_i results in a state $|i\rangle$ at the boundary which is BRST equivalent to a ground state of the theory.

concentrate on the B-twist, that is, the twist with minus sign in (9.5), giving the topological B-model. The twisting has the effect of changing the spins of all operators by an amount proportional to their R-symmetry charge, *i.e.*, $s \to s - \frac{1}{2}q$. Thus, after the twist, half of the supercharges become scalar, the other half one-forms. Especially, after the twist we have a one-to-one correspondence between operators and states. In more detail, we identify the twisted path integral on a hemisphere with a chiral field ϕ_i inserted, with the ground state $|i\rangle$. This is illustrated in figure 9.1. Note that

$$|i\rangle = \phi_i |0\rangle + Q |\cdot\rangle \, , \tag{9.6}$$

where we have denoted the canonical ground state obtained without any insertion on the hemisphere by $|0\rangle$.

Under the conjugate twist (giving the anti-topological B-model), the same vacua are parameterized via the anti-chiral fields $\bar{\phi}_{\bar{\imath}}$. We will denote the arising states by $\langle \bar{\imath} |$. Since the spaces of vacua are the same, there must exist a change of basis relating the states, *i.e.*, $\langle \bar{\imath} | = \langle j | M_{\bar{\imath}}^{j}$ with $M \bar{M} = 1$. Thus, besides the natural topological inner products on the space of states,

$$\eta_{ij} = \langle j|i\rangle = \langle 0| \phi_j \phi_i |0\rangle = \langle \phi_j \phi_i \rangle_0 \, , \tag{9.7}$$

where $\langle \ldots \rangle_0$ denotes the topological field theory correlator on the sphere, we have in addition a hermitian inner product (also referred to as tt^*-metric)

$$g_{i\bar{\jmath}} = \langle \bar{\jmath} | i \rangle \, . \tag{9.8}$$

Note that the correlator on the sphere with three insertions (also known as the Yukawa coupling) encodes the structure of the chiral ring (cf. (9.4))):

$$C_{ijk} = \langle \phi_i \phi_j \phi_k \rangle_0 \, . \tag{9.9}$$

After the twist, the algebra (9.1) will coincide with the algebra satisfied by the BRST operator and anti-ghost in the critical bosonic string (we will discuss this in more detail

in section 9.2). Especially, the Hilbert space of the closed string physical states decomposes according to the grading of the chiral ring as (where we used the operator-state correspondence)

$$\mathcal{H}_{closed} = \bigoplus_{q,\bar{q}=0}^{3} \mathcal{H}^{q,\bar{q}}. \tag{9.10}$$

Chiral fields of charge $(1,1)$ are of particular interest, since they parameterize marginal deformations of the SCFT. Given such a chiral primary field ϕ_i (and its anti-chiral conjugate $\bar{\phi}_{\bar{i}}$), we can deform the theory by adding to the action

$$t^i \int \phi_i^{(2)} + \bar{t}^{\bar{i}} \int \bar{\phi}_{\bar{i}}^{(2)}, \tag{9.11}$$

where $\phi_i^{(2)} = dz d\bar{z} \{G^-, [\bar{G}^-, \phi_i]\}$ is the two-form descendant of the chiral primary field ϕ_i and t_i is a complex parameter. These deformations are all unobstructed and span a complex manifold $\mathcal{M}$ (locally parameterized by $(t^i, \bar{t}^{\bar{i}})$) of dimension $n = \dim \mathcal{H}^{1,1}$.

We are interested in how the structure of the theory changes as we perturb by marginal chiral fields ϕ_i, *i.e.*, how the set of vacuum states varies over $\mathcal{M}$, that is, as a function of the parameters $(t^i, \bar{t}^{\bar{i}})$. In other words, we would like to study the geometry of the vacuum bundle $\mathcal{V} \to \mathcal{M}$, where $\mathcal{V}$ decomposes at any point $m \in \mathcal{M}$ as follows (cf. (9.10)) [2]

$$\mathcal{V}_m = \mathcal{H}^{0,0} \oplus \mathcal{H}^{1,1} \oplus \mathcal{H}^{2,2} \oplus \mathcal{H}^{3,3}. \tag{9.12}$$

There exists a natural connection on $\mathcal{V}$ compatible with the holomorphic structure and the tt^*-metric. The connection satisfies the so-called tt^*-equations. These basically say that there exists an improved connection, the Gauss-Manin connection, which is flat. In the special case of $\hat{c} = 3$, the tt^*-equations can be formulated more intrinsically in terms of the geometry of $\mathcal{M}$, that is, where exists a special Kähler structure on $\mathcal{M}$. Especially, a metric on $\mathcal{M}$, known as the Zamolodchikov metric, can be defined via

$$G_{i\bar{j}} = \frac{g_{i\bar{j}}}{g_{0\bar{0}}}, \tag{9.13}$$

which, using the tt^*-equations, can be shown to be Kähler

$$G_{i\bar{j}} = \partial_i \partial_{\bar{j}} K, \tag{9.14}$$

with $K = -\log(g_{0\bar{0}})$.

---

[2] The space of vacua with $q = \bar{q}$ generated by the perturbation fit toegther over $\mathcal{M}$ into a holomorphic vector bundle, referred to as vacuum bundle.

Further, the curvature of the Zamolodchikov metric is given by

$$(R_{i\bar{j}})^k_l = [D_i, D_j]^k_l = C_{ilm}C_{\bar{j}\bar{m}\bar{k}}e^{2K}G^{\bar{m}m}G^{\bar{k}k} - \delta^k_l G_{i\bar{j}} - \delta^k_i G_{l\bar{j}}\,, \tag{9.15}$$

where D_i denotes the Zamolodchikov-Kähler connection. Note that we usually raise and lower indices with the tt^*-metric, for example

$$C^{jk}_{\bar{i}} = C_{\bar{i}\bar{j}\bar{k}}g^{\bar{j}j}g^{\bar{k}k} = C_{\bar{i}\bar{j}\bar{k}}e^{2K}G^{\bar{j}j}G^{\bar{k}k}\,. \tag{9.16}$$

In the remaining part of this section, let us briefly give some background on boundary conditions in $\mathcal{N} = (2,2)$ CFT. Details on basic concepts can be filled in from [3], while the main discussion mainly follows [30]. We will focus on boundary conditions for B-branes preserving $\mathcal{N} = 2$ supersymmetry, *i.e.*

$$(G^- + \bar{G}^-)|_{\partial\Sigma} = 0,\ (G^+ + \bar{G}^+)|_{\partial\Sigma} = 0,\ (J - \bar{J})|_{\partial\Sigma} = 0\,, \tag{9.17}$$

which are compatible with the topological B-model in the sense that we can define topological amplitudes with background D-branes which are BRST invariant. The discussion of chiral rings and their relation to supersymmetric ground states extends essentially unchanged to the open case (elements of the boundary chiral ring will be denoted in the following as ψ). The main difference is that the open string Hilbert space decomposes now as

$$\mathcal{H}_{open} = \bigoplus_{p=0}^{3} \mathcal{H}^p\,, \tag{9.18}$$

since we have only one R-charge to label states and fields. [3] Especially, deformations of the CFT are now parameterized by fields ψ_i with charge 1. However, the boundary deformations are not always unobstructed, *i.e.*, there can be a higher order superpotential $\mathcal{W}$, whose critical points determine the supersymmetric vacua of the theory. In detail, topological Hilbert spaces of strings between two B-type branes B and B' are identified as Ext-groups between the objects in the D-brane category:

$$\mathcal{H}^p_{B-B'} \cong \mathrm{Ext}^p(B, B')\,. \tag{9.19}$$

Infinitesimal deformations of a brane B correspond to $\mathrm{Ext}^1(B, B)$, while their obstructions are measured with $\mathrm{Ext}^2(B, B)$. In addition, there is a collection of higher-order obstruction maps, which can be identified with disk amplitudes with $n \geq 3$ boundary insertions,

---

[3]The relation between bulk and boundary R-charges is $p = q + \bar{q}$.

leading to a superpotential with critical locus given by the vanishing of the higher-order obstructions.

Note that the open string deformations can sometimes obstruct the bulk deformations, that is, there exists a bulk-to-boundary obstruction map, basically given by the disk correlator with one bulk and boundary insertion (for details, see for instance [30]).

Physically, all holomorphic information of the open string tree-level sector is expected to be captured by the superpotential for the massless fields on the brane. Let us restrict to $D5$-branes on a holomorphic curve C which carries no topological charge. The superpotential then arises as a domainwall between two $D5$-branes wrapped on two different holomorphic curves C_+ and C_- in the same class. As already discussed in detail in part II of this thesis (cf. chapter 2), in this case we have

$$\Delta \mathcal{W} = \mathcal{T} = \langle \Omega, \nu \rangle = \int_\Gamma \Omega \, , \tag{9.20}$$

where $\langle ., . \rangle$ is the standard symplectic pairing on $H^3(Y)$, Ω denotes the holomorphic three-form, ν the normal function defined via $C_+ - C_-$ and Γ is a three-chain with boundary $\partial \Gamma = C_+ - C_-$. In mathematics, it is well known that all the local information of ν is contained in Griffiths' infinitesimal invariant Δ_{ij}. One of the main results of [30] is that one can identify Δ_{ij} with the disk 2-point function. In more detail, using the expression

$$\Delta_{ij} = D_i D_j \mathcal{T} - C_{ijk} g^{\bar{k}k} D_{\bar{k}} \bar{\mathcal{T}} \, , \tag{9.21}$$

one can deduce the open-string holomorphic anomaly

$$\partial_{\bar{i}} \Delta_{jk} = -C_{jkl} g^{\bar{l}l} \Delta_{\overline{il}} \, , \tag{9.22}$$

which can be shown to be exactly satisfied by the disk 2-point function, therefore justifying the identification (modulo the holomorphic ambiguity). This will play a central role in section 9.5.

9.2　Topological string amplitudes

Topologically twisted $\mathcal{N} = (2,2)$ superconformal field theories, as described in the previous section, can be coupled to 2d topological gravity by identifying the supercharges (and their conjugates) with BRST operators and anti-ghosts of a critical bosonic string in which ghost and matter fields do not decouple. In this chapter we are mainly interested in the

topological B-model, for which the isomorphism is as follows (for simplicity we restrict to the holomorphic sector)

$$(G^+, J, T, G^-) \leftrightarrow (Q_{BRST}, J_{ghost}, T, b) \,, \tag{9.23}$$

where Q_{BRST} is BRST-current and b is the anti-ghost corresponding to the diffeomorphism symmetry on the bosonic string worldsheet. Further, $U(1)$ charges are identified with ghost numbers. There are however some distinctions to the usual bosonic string one should keep in mind. Namely, there is no ghost field, the cohomology of the anti-ghost is non-trivial and the BRST cohomology is finite dimensional (cf. (9.10)). One important consequence of this is the existence of a holomorphic anomaly, to be discussed in section 9.4.

The presence of anti-ghosts, the crucial element needed for the computation of correlation functions in the bosonic string, allows to define topological string amplitudes. For that, recall that in the bosonic string the anti-ghosts provide the link between CFT correlators on a fixed worldsheet and string correlators involving the integration over all metrics of the worldsheet. In detail, the Faddeev-Popov procedure reduces the integral over metrics to an integral over the moduli space of genus g surfaces with the anti-ghosts providing the measure. Then, in analogy to the bosonic string genus g free energy, and using the isomorphism (9.23), we can define the (closed and oriented) topological string amplitude at genus g ($g \geq 2$) by

$$\mathcal{F}^{(g)} = \int_{\mathcal{M}_g} [dm] \left\langle \prod_{a=1}^{3g-3} \left(\int \mu_a G^- \right) \left(\int \bar{\mu}_a \bar{G}^- \right) \right\rangle_{\Sigma^g} \,, \tag{9.24}$$

where $\langle \dots \rangle_{\Sigma^g}$ is the 2d field theory correlator on the worldsheet Σ^g, μ_a the Beltrami differentials, that are anti-holomorphic 1-forms on Σ^g with values in the holomorphic tangent bundle, and $\mathcal{M}_g$ is the moduli space of genus g Riemannian surfaces (with virtual complex dimension $3g - 3$). The measure reads

$$[dm] = \prod_{i=1}^{3g-3} dm_i d\bar{m}_i \,, \tag{9.25}$$

with $m_i, \bar{m}_i$ coordinates on $\mathcal{M}_g$. The definition of the topological string amplitude is a bit more subtile for $g \leq 1$, a detailed treatment can be found for instance in [3]. Note that $\mathcal{F}^{(g)}$ is a section of the line bundle $\mathcal{L}^{2g-2}$ over the CFT moduli space M.

Similarly, we can define the (open oriented) genus g topological amplitude $\mathcal{F}^{(g,h)}$ with h boundaries and $2g + h - 2 > 0$ as [30]

$$\mathcal{F}^{(g,h)} = \int_{\mathcal{M}^{(g,h)}} [dm][dl] \left\langle \prod_{a=1}^{3g+h-3} \left(\int \mu_a G^- \right) \left(\int \bar{\mu}_a \bar{G}^- \right) \prod_{b=1}^{h} \lambda_b (G^- + \bar{G}^-) \right\rangle_{\Sigma^{(g,h)}} \,, \tag{9.26}$$

where we made use of the fact that one can see the moduli space of a genus g curve with h boundaries, denoted as $\mathcal{M}^{(g,h)}$, as a fibration over the moduli space of genus g curves with h marked points $\mathcal{M}_{(g,h)}$. That is, we can isolate the variations which change only the length of the boundaries from variations which affect as well the bulk of the surface. Let us denote the coordinates on $\mathcal{M}_{(g,h)}$ by m^a and the real length moduli of the boundaries as l^b. The Beltrami differentials associated with the l^a are denoted as λ^a. Note that the λ^a are located near the boundary, and hence we contracted them with a combination of charges, *i.e.*, $(G^- + \bar{G}^-)$, that is preserved at the boundary. The measure $[dm]$ is as in (9.25), while $[dl]$ is defined as follows

$$[dl] = \prod_{i=1}^{b} dl_i \,. \tag{9.27}$$

For later reference, note that one can as well define a genus g (closed and oriented) topological amplitude with n insertions of chiral fields via (one can give a similar definition for $\mathcal{F}^{(g,h)}$)

$$\mathcal{F}^{(g)}_{i_1 i_2 \ldots i_n} = \int_{\mathcal{M}_g} [dm] \left\langle \int \phi_{i_1}^{(2)} \ldots \int \phi_{i_n}^{(2)} \prod_{a=1}^{3g-3} \left(\int \mu_a G^- \right) \left(\int \bar{\mu}_a \bar{G}^- \right) \right\rangle_{\Sigma^g} . \tag{9.28}$$

It is important to keep in mind that one can obtain $\mathcal{F}^{(g)}_{i_1 i_2 \ldots i_n}$ via covariant derivation

$$\mathcal{F}^{(g)}_{i_1 i_2 \ldots i_n} = D_{i_n} \mathcal{F}^{(g)}_{i_1 i_2 \ldots i_{n-1}} \,, \tag{9.29}$$

as shown in [31]. Here, D is the Zamolochikov-Kähler covariant derivative introduced in section 9.1.

So far we have only discussed oriented amplitudes. However, it is clear that one can similarly define (open and closed) unoriented topological amplitudes $\mathcal{K}^{(g,h)}$ and $\mathcal{R}^{(g,h)}$, where $\mathcal{K}^{(g,h)}$ are Klein-bottle type amplitudes with an even number of crosscaps and $\mathcal{R}^{(g,h)}$ are Möbius-strip type amplitudes with an odd number of crosscaps. Without going into any further details here, we just note that for these amplitudes one has to evaluate the CFT correlator on unoriented worldsheets $\Sigma^{(g,h)_\kappa}$, respectively $\Sigma^{(g,h)_r}$ and integrate over the corresponding moduli spaces, as for the oriented amplitudes.

9.3 Target space perspective

One might ask what the topological string computes in target space. As argued in [31] and carefully derived in [63] (see [64] for a short review), the closed topological string computes

certain higher derivative F-terms in the low-energy effective four dimensional ($\mathcal{N} = 2$) target space theory of the superstring. In more detail, the topological amplitudes compute gravitational terms of the form

$$\int d^4x d^4\theta \mathcal{W}^{2g} \mathcal{F}^{(g,0)} = \int d^4x \mathcal{F}^{(g,0)} R_+^2 F_+^{2g-2} + \dots , \tag{9.30}$$

where $\mathcal{W}$ is the 4-dimensional superfield multiplet containing as its top component the field strength of the gravitational multiplet and as its lowest component the graviphoton field strength (with F_+ being the self-dual part thereof) and R_+^2 is a contraction of the self-dual part of the Riemann tensor with itself.

Similarly, one can show that the open topological string computes the following terms in the target space effective theory [14]

$$\int d^4x d^2\theta \mathcal{F}^{(g,h)} \mathcal{W}^{2g} \mathcal{S}^{h-1} , \tag{9.31}$$

where $\mathcal{S} = \text{Tr}(W_\alpha W_\alpha)$ is the chiral superfield for the gauge field on N coincident branes. In particular, the genus zero partition functions $\mathcal{F}^{(0,1)}$ and $\mathcal{F}^{(0,2)}$ are related to the superpotential, respectively gauge kinetic function.

It is enlightening to understand the generation of these F-terms from a pure target-space point of view. Let us consider the F-terms which involve the closed amplitudes. The answer turns out to be that there are certain hidden degrees of freedom that have been integrated out to lead to the effective terms in equations (9.30) and (9.31). Specifically, solitons in form of D2-branes wrapped over elements of $H_2(X, \mathbb{Z})$ [12, 13].

This can be quantified by considering Schwinger type computations of integrating out a charged scalar field coupled to a constant $U(1)$ field strength $F_{\mu\nu} = \epsilon_{\mu\nu} F/2$ (details can be filled in from [12, 13, 3]). Let us first consider the two dimensional case. The path-integral is given by

$$e^{-S} = \int \mathcal{D}\phi \, e^{-\int |D_\mu \phi|^2 + m^2 |\phi|^2} , \tag{9.32}$$

with $D_\mu = (\partial_\mu - eA_\mu)$, ϕ the charged scalar field of mass m and charge e and A_μ denotes the $U(1)$ gauge field. We have

$$S = \text{Tr} \log(\Delta + m^2) = \int_\epsilon^\infty \frac{ds}{s} \text{Tr} e^{-s(\Delta + m^2)}, \tag{9.33}$$

where Δ is the Laplacian, and $\epsilon > 0$ a cutoff. The trace can be evaluated to

$$S = \int_\epsilon^\infty \frac{ds}{s} \frac{e^{-sm^2}}{2\sin(seF/2)} , \tag{9.34}$$

by using similarity of the problem to the (bosonic) harmonic oscillator. The step from two to four dimensions is easy, since the computation involving the four dimensional Laplacian splits into computations for two dimensional subspaces. Thus, we directly infer that in four dimensions

$$S = \int_\epsilon^\infty \frac{ds}{s} \frac{e^{-sm^2}}{2\sin(seF/2)^2} \, .$$

(9.35)

For a field transforming in a non-trivial representation of the four dimensional Lorentz group, the Laplacian possesses an additional term, *i.e.*,

$$\Delta \to \Delta + 2e\sigma_R^{\mu\nu} F_{\mu\nu} \, ,$$

(9.36)

with $\sigma_R^{\mu\nu}$ the Lie-algebra representation of the $SO(4) = SU(2)_L \times SU(2)_R$ Lorentz group acting on the field in representation R of the Lorentz group. Note that due to the self-dual field-strength, only the $SU(2)_L$ content of the representation will be of relevance. We then have

$$S = \int_\epsilon^\infty \frac{ds}{s} \frac{\text{Tr}(-1)^F e^{-sm^2\lambda/e} e^{-2s\sigma_L \lambda F}}{(2\sin(s\lambda F/2))^2} \, ,$$

(9.37)

where σ_L is the Cartan element of $SU(2)_L$ and we have rescaled $s \to s\lambda/e$.

Let us now go on and try to understand the generation of the terms (9.30) from the target-space viewpoint. As already noted above, the basic idea is that one needs to integrate out massive $D2$-branes wrapped around 2-cycles of the Calabi-Yau 3-fold X. For that, note that a $D2$-brane (in class $d \in H_2(X, \mathbb{Z})$) corresponds to a charged particle in four dimensions with charge d and mass given by

$$m = \frac{1}{\lambda} \int_d k = \frac{1}{\lambda} t_d \, ,$$

(9.38)

where k is Kähler form on X. The particle is furthermore charged under the graviphoton field with charge equal to its mass. However, there is one major difference between this case and the Schwinger type computation recalled above. Namely, here we have $\mathcal{N} = 2$ supersymmetry in contrast to the non-supersymmetric Schwinger type computation. Especially, the $SO(4)$ content of states preserving $\mathcal{N} = 2$ supersymmetry is of the form

$$[(1/2, 0) + 2(0, 0)] \otimes \mathcal{R} \, ,$$

(9.39)

where $\mathcal{R}$ is some representation of $SO(4)$. However, one can argue [12, 13] that the insertion of the R_+^2 term in the effective action absorbs the extra representation in front of (9.39), such that it suffices to stick to the non-supersymmetric Schwinger type computation with a

field in representation $\mathcal{R}$. Hence, substituting $e = m$ in (9.37), using (9.38) and absorbing F into λ, we deduce the following expression for $\mathcal{F}$ occuring in (9.30):

$$\mathcal{F} = \int_{\epsilon}^{\infty} \frac{ds}{s} \frac{\text{Tr}(-1)^F e^{-st_d} e^{-2s\sigma_L \lambda}}{(2\sin(s\lambda/2))^2} . \tag{9.40}$$

In order to evaluate this contribution, we need to know the degeneracy of the $D2$-branes as well as the $SO(4)$ content of the field they correspond to. To answer these questions, it turns out to be useful to consider the M-theory lift of our setup. For that, recall that Type IIA superstrings in ten dimensions on a background of the form $\mathbb{R}^4 \times X$ is equivalent to M-theory on $\mathbb{R}^4 \times X \times S^1$, where the radius of the circle factor becomes large as the string coupling of the Type IIA theory becomes strong. The $D2$-branes under consideration lift to $M2$-branes which are localized on the extra circle. Each can have an additional momentum of n units around the S^1. Thus, each $M2$-brane corresponds in the Type IIA limit to an infinite set of $D2$-branes indexed by n, whose mass is roughly $|t_d + 2\pi i n|$. This gives the degeneracy of the $D2$-branes. From the M-theory perspective, we can also easily deduce the $SO(4)$ content. Note first that $SO(4)$ is the natural Lorentz group of the five dimensional space-time occuring in the limit $\lambda \to \infty$, *i.e.*, the S^1 decompactifies in this limit and we have M-theory on $\mathbb{R}^5 \times X$. This gives rise to an unambiguous $SO(4)$ content for each particle. Let us label the left- and right- $SU(2)$ spins of $SO(4) = SU(2)_L \times SU(2)_R$ as j_L and j_R. Then, the $M2$-branes give rise to particles which transform in the five-dimensional rotation group as

$$[(1/2, 0) + 2(0, 0)] \otimes (j_L, j_R). \tag{9.41}$$

If we introduce the numbers $n^d_{(j_L, j_R)}$ which count the number of BPS $M2$-branes with charge d and transforming as in (9.41), it turns out that these numbers vary with the complex structure. In more detail, pairs of them can join to form a non-BPS multiplet. However, the numbers

$$n^d_{j_L} = \sum_{j_R} (-1)^{2j_R} (2j_R + 1) n^d_{(j_L, j_R)} , \tag{9.42}$$

are invariant under smooth deformations. The observation that only $n^d_{j_L}$ is invariant and thus enters in the topological computation, is as expected from the discussion above equation (9.37), where we argued that only the $SU(2)_L$ content of the representation will be of relevance for the Schwinger type computation. Having understood these things, let us now go back and compute (9.40) for all wrapped $D2$-branes.

Therefore, let us choose the following (non-standard) basis of $SU(2)_L$ representations

$$I_r = [(1/2) + 2(0)]^{\otimes r} , \tag{9.43}$$

with I_0 defined to be the trivial representation. Since the I_r form a basis with integer coefficients, we can define a new set of integer invariants $N_d^{(g)}$ via

$$\sum_{g=0}^{\infty} N_d^{(g)} I_g = \sum_{j_L} n_{j_L}^d [j_L] \,, \tag{9.44}$$

where $[j_L]$ denotes the spin-j_L representation. The invariants $N_d^{(g)}$ are usually referred to as Gopakumar-Vafa invariants. Then, using

$$\mathrm{Tr}_{I_g}(-1)^F e^{-2s\sigma_l \lambda} = [\mathrm{Tr}_{I_1}(-1)^F e^{-s\sigma_L \lambda}]^r = [s\sin(s\lambda/2)]^{2g} \,, \tag{9.45}$$

we deduce from (9.40) that we have for each $D2$-brane in the class d and representation I_g

$$\sum_n \int_\epsilon^\infty \frac{ds}{s} e^{-s(t_q + 2\pi i n)} (2\sin(s\lambda/2))^{2g-2} \,, \tag{9.46}$$

where the sum goes over the (infinite) set of momenta n around the M-theory circle. Using the identity

$$\sum_n e^{-2\pi i n s} = \sum_k \delta(s-k) \,, \tag{9.47}$$

the above expression can be recast into the form

$$\sum_{k\geq 0} \frac{1}{k} (2\sin(k\lambda/2))^{2g-2} e^{-kt_d} \,. \tag{9.48}$$

Finally, summing over classes and representations, we obtain

$$\mathcal{F} = \sum_{k,d,g} N_d^{(g)} \frac{1}{k} (2\sin(k\lambda/2))^{2g-2} e^{-kt_d} \,, \tag{9.49}$$

with $k, g \geq 0$ and $d \in H_2(X, \mathbb{Z})$, which expresses the closed topological string free energy in terms of Gopakumar-Vafa invariants $N_d^{(g)}$, up to classical terms and (for our purposes irrelevant) constant map contributions.

In a similar spirit, *i.e.*, via a Schwinger-type computation, one can give an analog space-time interpretation of the open topological string amplitude of equation (9.31). This has been worked out in [14] (see also [33]) to where we refer the interested reader for a detailed exposition.

Finally, one might ask how one should interpret the unoriented amplitudes $\mathcal{K}$ and $\mathcal{R}$, and as well the combined amplitude $\mathcal{G}'$ (cf. (6.3) and (6.8)) from a space-time point of view. This has not been worked out in detail yet in the literature. However, the existence of an integer expansion of $\mathcal{G}'$ (cf. (6.11)), which we used as a definition of real Gopakumar-Vafa invariants, suggests that one can give a more rigorous definition of these invariants, perhaps in a way similar as above.
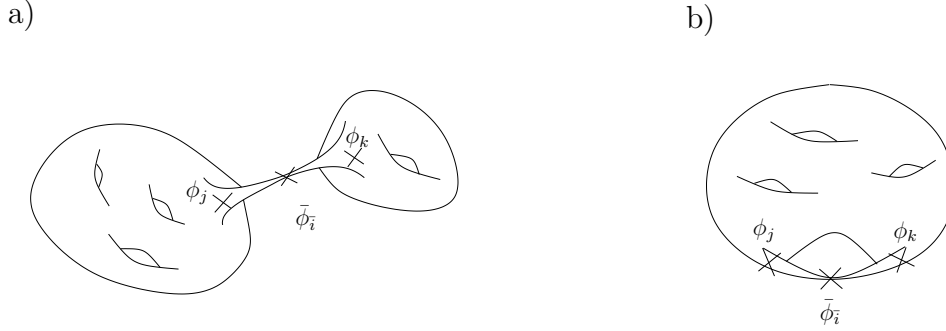
Figure 9.2: The two degenerations of a genus g Riemannian surface that contribute to the holomorphic anomaly. The crosses mark the positions of insertions of chiral, respectively anti-chiral fields. a) The surfaces splits into two components by developing a long tube. b) A handle of the surface pinches.

9.4 Holomorphic anomaly equation

Following [31], the holomorphic anomaly equation can be derived by considering an infinitesimal deformation of the action as in (9.11), combined with a derivation of (9.24) with respect to $\bar{t}_{\bar{i}}$. This leads to the insertion of the operator $\int \bar{\phi}_{\bar{i}}^{(2)}$ into (9.24). With some algebra, one then obtains (for a detailed derivation, see for instance [65])

$$\partial_{\bar{i}}\mathcal{F}^{(g)} = 4 \int_{\mathcal{M}_g} [dm] \sum_{a,b=1}^{3g-3} \frac{\partial^2}{\partial m^a \partial \bar{m}^b} \left\langle \int \bar{\phi}_{\bar{i}} \prod_{\substack{a' \neq a \\ b' \neq b}} \left(\int \mu_{a'} G^- \right) \left(\int \bar{\mu}_{b'} \bar{G}^- \right) \right\rangle_{\Sigma^g} , \qquad (9.50)$$

where $\partial_{\bar{i}} := \frac{\partial}{\partial \bar{t}_{\bar{i}}}$. Thus, the anti-holomorphic derivative yields a total derivative and naively this would mean that $\mathcal{F}^{(g)}$ is purely holomorphic. However, (fortunately) this is not correct, because $\mathcal{M}_g$ has boundaries where the Riemannian surface degenerates. In particular, the genus g surface can split into two surfaces of genus g_1 and g_2 with $g = g_1 + g_2$ by developing a long thin tube, or a handle of the surface can pinch, reducing the genus by one (again, one should see the pinching handle as a thin tube). These degenerations are depicted in figure 9.2. By carefully considering these boundary contributions, one can show that equation (9.50) can be rewritten as [31]

$$\partial_{\bar{i}}\mathcal{F}^{(g)} = \frac{1}{2} \sum_{g_1+g_2=g} C_{\bar{i}}^{jk} \mathcal{F}_j^{(g_1)} \mathcal{F}_k^{(g_2)} + \frac{1}{2} C_{\bar{i}}^{jk} \mathcal{F}_{jk}^{(g-1)} . \qquad (9.51)$$

This is the celebrated holomorphic anomaly equation (valid for $g \geq 2$). In the derivation, one has to be careful about the location of the anti-chiral fields. As it turns out, the whole

contribution comes from the region where the anti-chiral field sit on a long tube. Thus, one should see these degenerations rather as Riemannian surfaces which pinch at both ends of a tube. Each pinch is repaired by inserting a complete set of chiral fields ϕ_i on the lower-genus surface (see figure 9.2), yielding $\mathcal{F}_i$, respectively $\mathcal{F}_{ij}$, as defined in (9.28), while the tube is replaced with the three-point function on the sphere with insertions of three anti-chiral fields, *i.e.*, the anti-holomorphic Yukawa-coupling $C_{\bar{i}\bar{j}\bar{k}}$. The connection between the various pieces occurs via the metric $g^{\bar{i}i}$ (defined in 9.8), which is used to raise and lower indices (cf. (9.16)). This gives a more intuitive explanation of (9.51).

The holomorphic anomaly equation (9.51) allows to inductively solve for the $\mathcal{F}^{(g)}$ up to the holomorphic part (which one can argue to be determined by a finite set of constants). Besides using the Feynman graph techniques introduced in [31], one can as well solve the holomorphic anomaly equation via direct integration (which is based on an underlying polynomial structure of the $\mathcal{F}^{(g)}$ in terms of certain generators [66]). We will say more on that in section 9.6. The main obstacle to completely determine $\mathcal{F}^{(g)}$ via the holomorphic anomaly equation is to determine the holomorphic part, also referred to as holomorphic ambiguity. This is a notorious problem and the (so far) best technique to determine the unknown constants is to use certain information from special points in moduli space [53, 34]. We will come back to this in section 9.7 at hand of the model of our interest, namely local $\mathbb{P}^2$.

9.5   Extended holomorphic anomaly equations

In order to write down an extension of the holomorphic anomaly equation (9.51) to the (oriented) open string amplitudes, as defined in (9.28), we need to specify the boundary conditions, that is, the D-brane setup. We impose the following conditions: First of all, we assume that for generic values of the bulk (closed string) moduli, $\mathcal{F}^{(g,h)}$ does not depend on any continuous open string moduli. Secondly, we require that the topological charge of the D-brane configuration vanishes, similar to the charge cancellation in the superstring. Finally, we assume that bulk deformations are unobstructed by the branes.

These two assumptions directly lead to the following facts (cf. section 9.1): The disk amplitude with two bulk insertions is the analogue of the closed string Yukawa coupling. This can be deduced from the assumption of absence of open string moduli [30]. Similarly, this assumption tells us that the only open string degenerations of a genus g surface with h boundaries that can contribute to (9.51) are those where the length of a boundary
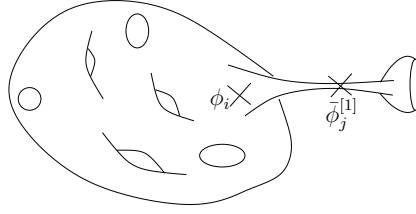
Figure 9.3: The only open string degeneration contributing to the holomorphic anomaly: A boundary component of a genus g Riemannian surface with h boundaries is separated by a long tube, or equivalently, shrinks to zero size.

component shrinks to zero size (with the only exception beeing the annulus amplitude) [30]. Such a degeneration is illustrated in figure 9.3.

A direct consequence of the second assumption is that we have to consider an orientifolded theory, and thus have to consider in addition unoriented topological amplitudes, as pioneered in [17]. (On a more technical level, this assumption also ensures the vanishing of disk 1-point functions, such that the disk 2-point function is indeed the simplest open string amplitude (see also [67])). However, before discussing unoriented amplitudes, let us first derive the extension of the holomorphic anomaly equation to the (oriented) amplitudes $\mathcal{F}^{(g,h)}$, following [30]. The derivation is similar to the derivation of the unextended equation sketched in section 9.4. The infinitesimal variation (9.11) combined with derivation in respect to $\bar{t}_i$ leads to the insertion of the operator $\int \bar{\phi}_i^{(2)}$ into the correlator. However, in contrast to (9.50), we obtain after some algebra the more complicated expression

$$
\partial_{\bar{i}} \mathcal{F}^{(g,h)} = \int_{\mathcal{M}_{(g,h)}} [dm][dl]
$$

$$
\left(4 \sum_{a,b=1}^{3g+h-3} \frac{\partial^2}{\partial m^a \partial m^b} \left\langle \int \bar{\phi}_j \prod_{\substack{a' \neq a \\ b' \neq b}} \left(\int \mu_{a'} G^- \right) \left(\int \bar{\mu}_{b'} \bar{G}^- \right) \prod_{b=1}^{h} \lambda_b (G^- + \bar{G}^-) \right\rangle_{\Sigma^{(g,h)}} \right.
$$

$$
\left. + 2 \sum_{b=1}^{h} \frac{\partial}{\partial l^b} \left\langle \int \bar{\phi}_i^{[1]} \prod_{a=1}^{3g+h-3} \left(\int \mu_a G^- \right) \left(\int \bar{\mu}_a \bar{G}^- \right) \prod_{b \neq b'} \lambda_{b'} (G^- + \bar{G}^-) \right\rangle_{\Sigma^{(g,h)}} \right),
$$

$$
(9.52)
$$

where $\bar{\phi}_i^{[1]} = \frac{1}{2}[G^+ - \bar{G}^-, \bar{\phi}_i]$. Note that in (9.52) we have already skipped some terms which lead to a vanishing boundary contribution (see [30, 31] for details). Similar as before, we observe that only contributions from the boundary of the moduli space, there

$\Sigma^{(g,h)}$ degenerates, are of relevance. In detail, the closed string degenerations depicted in figure 9.2 are essentially unaffected by the presence of boundaries. The only difference is that we need to keep track of the distribution of the boundaries under deformations that split the surface into two (figure 9.2a). This will lead in (9.50) to an additional sum over all possible boundary distributions. As we already mentioned, the only open string degeneration that contributes is the shrinking of a boundary (conformally equivalent to separating a disk via a long thin tube, as shown in figure 9.3). This can be seen as the pinching of a disk, there we repair the left over surface (with $h - 1$ boundaries) via the insertion of a complete set of chiral fields ϕ_i, while the disk becomes the anti-topological disk two-point function

$$\Delta_{\bar{i}\bar{j}} = \int_0^1 \left\langle \bar{\phi}_i^{[1]}(r) \bar{\phi}_j(0) \right\rangle_{\Sigma^{(0,1)}} . \tag{9.53}$$

Again, the metric connects the disk with the remaining surface, hence we directly infer the open string extension of (9.50) to be

$$\partial_{\bar{i}} \mathcal{F}^{(g,h)} = \frac{1}{2} \sum_{\substack{g_1+g_2=g \\ h_1+h_2=h}} C_{\bar{i}}^{jk} \mathcal{F}_j^{(g_1,h_1)} \mathcal{F}_k^{(g_2,h_2)} + \frac{1}{2} C_{\bar{i}}^{jk} \mathcal{F}_{jk}^{(g-1,h)} - \Delta_{\bar{i}}^j \mathcal{F}_j^{(g,h-1)} . \tag{9.54}$$

This is the so-called extended holomorphic anomaly equation.

Similarly, we can derive extended holomorphic anomaly equations for unoriented amplitudes [17]. In principle, one should follow the same route as before, however it is more convenient to take a shortcut by directly inferring the respective equations in analogy to the intuitive derivation of the holomorphic anomaly equation sketched in the previous section.

Let us start with unoriented amplitudes with a odd number of crosscaps, denoted as $\mathcal{R}^{(g,h)}$. We can have the following closed string degenerations of a surface $\Sigma^{(g,h)_r}$. The surface can split into two with at least one of the arising individual surfaces unoriented. Further, a handle or Klein-handle can pinch. Thus, we immediately deduce that

$$\partial_{\bar{i}} \mathcal{R}^{(g,h)} \supset \sum_{\substack{g_1+g_2=g \\ h_1+h_2=h}} C_{\bar{i}}^{jk} \mathcal{F}_j^{(g_1,h_1)} \mathcal{R}_k^{(g_2,h_2)} + \sum_{\substack{g_1+g_2=g \\ h_1+h_2=h}} C_{\bar{i}}^{jk} \mathcal{K}_j^{(g_1,h_1)} \mathcal{R}_k^{(g_2,h_2)}$$
$$+ \frac{1}{2} C_{\bar{i}}^{jk} \mathcal{R}_{jk}^{(g-1,h)} + \frac{1}{2} B_{\bar{i}}^{jk} \mathcal{R}_{jk}^{(g-1,h)} , \tag{9.55}$$

where $B_{\bar{i}}^{jk}$ is the parity twisted Yukawa-coupling. Similarly, the degenerations of a unoriented surface with an even number of crosscaps, $\Sigma^{(g,h)_k}$, are as follows. The surface can split into two, there the arising two individual surfaces are either both unoriented with an even or odd number of crosscaps, or one surface is oriented and the other is unoriented

with an even number of crosscaps. Again, either a handle or a Klein-handle can pinch. This leads to

$$\partial_{\bar{i}} \mathcal{K}^{(g,h)} \supset \frac{1}{2} \sum_{\substack{g_1+g_2=g-1 \\ h_1+h_2=h}} C_{\bar{i}}^{jk} \mathcal{R}_j^{(g_1,h_1)} \mathcal{R}_k^{(g_2,h_2)} + \frac{1}{2} \sum_{\substack{g_1+g_2=g \\ h_1+h_2=h}} C_{\bar{i}}^{jk} \mathcal{K}_j^{(g_1,h_1)} \mathcal{K}_k^{(g_2,h_2)}$$
$$+ \frac{1}{2} B_{\bar{i}}^{jk} \mathcal{F}_{jk}^{(g-1,h)} + \frac{1}{2} B_{\bar{i}}^{jk} \mathcal{K}_{jk}^{(g-1,h)} + \frac{1}{2} C_{\bar{i}}^{jk} \mathcal{K}_{jk}^{(g-1,h)} . \tag{9.56}$$

We have not included any open string degenerations in equations (9.55) and (9.56) so far. Similar as before, only the shrinking of a boundary, respectively crosscap, is of relevance. However, these two degenerations always arise as the common limit of two worldsheets of different topology. Namely, a real node (of the covering space surface) can be smoothed either to a disk or a crosscap in the quotient. Thus, we obtain

$$\partial_{\bar{i}} \left(\mathcal{F}^{(g,h)} + \mathcal{R}^{(g,h-1)} \right) \supset -2\Delta_{\bar{i}}^j \mathcal{F}_j^{(g,h-1)} ,$$
$$\partial_{\bar{i}} \left(\mathcal{K}^{(g,h)} + \mathcal{R}^{(g,h-1)} \right) \supset -2\Delta_{\bar{i}}^j \mathcal{K}_j^{(g,h-1)} , \tag{9.57}$$
$$\partial_{\bar{i}} \left(\mathcal{K}^{(g,h)} + \mathcal{R}^{(g-1,h+1)} \right) \supset -2\Delta_{\bar{i}}^j \mathcal{R}_j^{(g-1,h)} .$$

If one compares these equations with the ones presented in [17], one should keep in mind that we are using a different normalization, therefore the factor of 2 instead of $\sqrt{2}$ on the right-hand side.

Combining (9.54), (9.55) and (9.56), we can write down an extended holomorphic anomaly equation for the combined topological amplitude $\mathcal{G}^{(\chi)}$ (with $\chi \geq 0$) defined in (6.3):

$$\partial_{\bar{i}} \mathcal{G}^{(\chi)} = \frac{1}{2} \sum_{\chi_1+\chi_2=\chi-2} C_{\bar{i}}^{Pjk} \mathcal{G}_j^{(\chi_1)} \mathcal{G}_k^{(\chi_2)} + C_{\bar{i}}^{Pjk} \mathcal{G}_{jk}^{(\chi-2)} - \Delta_{\bar{i}}^{Pj} \mathcal{G}_j^{(\chi-1)} , \tag{9.58}$$

where C^P and Δ^P are the projections of the Yukawa coupling, respectively disk 2-point function, onto the parity invariant states. Again, due to the different normalization of (6.3), this equation differs slightly from the one presented in [17].

Similar as for the pure oriented closed string amplitude $\mathcal{F}^{(g)}$, the (extended) holomorphic anomaly equations allow to solve recursively for $\mathcal{F}^{(g,h)}, \mathcal{R}^{(g,h)}, \mathcal{K}^{(g,h)}$ and $\mathcal{G}^{(\chi)}$ up to holomorphic ambiguities. We will discuss this in more detail in the next section at hand of local $\mathbb{P}^2$.

9.6   Solving the (extended) holomorphic anomaly equations for local $\mathbb{P}^2$

The extended holomorphic anomaly equations given in equations (9.54) and (9.56), specialized to the local 1-parameter case, simplify to

$$\partial_{\bar{z}} \mathcal{F}^{(g,h)} = \frac{1}{2} \sum_{\substack{g_1+g_2=g \\ h_1+h_2=h \\ 2g_i+h_i>1}} C_{\bar{z}}^{zz} \mathcal{F}_z^{(g_1,h_1)} \mathcal{F}_z^{(g_2,h_2)} + \frac{1}{2} C_{\bar{z}}^{zz} \mathcal{F}_{zz}^{(g-1,h)} - \Delta_{\bar{z}}^z \mathcal{F}_z^{(g,h-1)} \ , \tag{9.59}$$

and

$$\partial_{\bar{z}} \mathcal{K}^{(g,h)} = \sum_{\substack{g_1+g_2=g \\ h_1+h_2=h \\ 2g_2+h_2>1 \\ g_1>0}} C_{\bar{z}}^{zz} \mathcal{K}_z^{(g_1,h_1)} \mathcal{F}_z^{(g_2,h_2)} + \frac{1}{2} \sum_{\substack{g_1+g_2=g \\ h_1+h_2=h \\ g_i>0}} C_{\bar{z}}^{zz} \mathcal{K}_z^{(g_1,h_1)} \mathcal{K}_z^{(g_2,h_2)}$$
$$+ C_{\bar{z}}^{zz} \mathcal{K}_{zz}^{(g-1,h)} + \frac{1}{2} C_{\bar{z}}^{zz} \mathcal{F}_{zz}^{(g-1,h)} - \Delta_{\bar{z}}^z \mathcal{K}_z^{(g,h-1)}, \tag{9.60}$$

where $\mathcal{F}_{z\cdots z}$ is defined as in (9.29), similarly for the $\mathcal{K}$, and z is a local coordinate on the space of complex structures, $\mathcal{M}_Y$, of Y. Further, C_{zzz} is the usual Yukawa-coupling, *i.e.*, the sphere three-point function, and Δ_{zz} is the disk two-point function (with bulk insertions). As usual, indices are raised and lowered via the Kähler metric on $\mathcal{M}_Y$. Note that we have here already implemented tadpole cancellation, so we can consistently set the $\mathcal{R}^{(g,h)}$ to zero.

Equations (9.59) and (9.60) can be solved recursively. Let us for the moment consider the simplified case without open strings, *i.e.*, $h = 0$. Then, recursively solved, the equations give an expression for $\mathcal{F}^{(g,0)}$ and $\mathcal{K}^{(g,0)}$ in terms of $\mathcal{F}^{(1,0)}$ and $\mathcal{K}^{(1,0)}$. These 1-loop amplitudes have the following holomorphic limits [31, 17]

$$\mathcal{F}^{(1,0)} = \frac{1}{2} \log (\tau) + a_{\mathcal{F}}^{(1,0)} \ ,$$
$$\mathcal{K}^{(1,0)} = \frac{1}{2} \log (\tau) + a_{\mathcal{K}}^{(1,0)} \ , \tag{9.61}$$

where we defined $\tau = \partial_t z(t)$ to be the derivative of z with respect to the preferred flat coordinate t at the large volume point of $\mathcal{M}_Y$. The 1-loop holomorphic ambiguities occurring in (9.61) are for local $\mathbb{P}^2$ given by

$$a_{\mathcal{F}}^{(1,0)} = -\frac{1}{2} \log(z) - \frac{1}{12} \log(-z) - \frac{1}{12} \log(1 - 27z) \ ,$$
$$a_{\mathcal{K}}^{(1,0)} = -\frac{1}{2} \log(z) - \frac{1}{8} \log(1 - 27z) \ . \tag{9.62}$$

To proceed, we define the non-holomorphic objects (propagators in Feynman diagram language) S^{zz} and K^{zz} as

$$
\begin{aligned}
S^{zz} &= 2\,\frac{\mathcal{F}_z^{(1,0)}}{C_{zzz}}\;, \\
K^{zz} &= 2\,\frac{\mathcal{K}_z^{(1,0)}}{C_{zzz}}\;,
\end{aligned}
\tag{9.63}
$$

where the Yukawa coupling $C_{zzz} = \mathcal{F}_{zzz}^{(0,0)}$ reads for local $\mathbb{P}^2$

$$
C_{zzz} = -\frac{1}{3}\frac{1}{z^3(1-27z)}\;.
\tag{9.64}
$$

Comparing with (9.61), we see that K^{zz} and S^{zz} differ only by a holomorphic function

$$
K^{zz} = S^{zz} + 2\frac{\partial_z a_{\mathcal{KF}}}{C_{zzz}}\;,
\tag{9.65}
$$

with

$$
a_{\mathcal{KF}} = a_{\mathcal{K}}^{(1,0)} - a_{\mathcal{F}}^{(1,0)}\;.
\tag{9.66}
$$

Hence, we can express both $\mathcal{F}_z^{(1,0)}$ and $\mathcal{K}_z^{(1,0)}$ in terms of the single non-holomorphic propagator S^{zz}, up to holomorphic terms. Furthermore, (using the special geometry relation (9.15)) it is easy to deduce that one can re-express the covariant derivative of S^{zz} in terms of S^{zz}, *i.e.*,

$$
D_z S^{zz} = -C_{zzz}\left(S^{zz}\right)^2 + (a_{DS})_z^{zz}\;,
\tag{9.67}
$$

and that a similar condition holds for the connection coefficient Γ_{zz}^z,

$$
\Gamma_{zz}^z = -C_{zzz}S^{zz} + (a_{\Gamma})_{zz}^z\;.
\tag{9.68}
$$

Here, a_{DS} and a_{Γ} are global holomorphic functions. For local $\mathbb{P}^2$, and our definition of the propagator (9.63), we have

$$
a_{\Gamma} = 2\,\partial_z a_{\mathcal{F}}^{(1,0)} = -\frac{7 - 216z}{6z(1-27z)}\;,
\tag{9.69}
$$

$$
a_{DS} = -\frac{z}{12(1-27z)}\;.
\tag{9.70}
$$

Thus, we conclude that all $\mathcal{F}^{(g,0)}$ and $\mathcal{K}^{(g,0)}$ can be expressed as polynomials in the single propagator S^{zz}, with coefficients given by holomorphic functions in z. This idea originated in [66], to which we refer for more details about the $\mathcal{F}^{(g,0)}$ case.

Let us now include the open string sector. With assumptions detailed in section 9.5, the only new ingredient that enters the recursive solution is the disk amplitude with two bulk insertions. In the holomorphic limit, this is given by (cf. (9.21))

$$\Delta_{zz} = \mathcal{F}_{zz}^{(0,1)} = \partial_z \partial_z \mathcal{T},$$ (9.71)

where $\mathcal{T}$ is the domain-wall tension. As for the closed string case, we can define a non-holomorphic object (terminator in Feynman diagram language)

$$\Delta^z = -\frac{\mathcal{F}_{zz}^{(0,1)}}{C_{zzz}},$$ (9.72)

which for local $\mathbb{P}^2$ satisfies

$$D_z \Delta^z = \frac{3}{4}\sqrt{z}.$$ (9.73)

As a consequence, the amplitudes $\mathcal{F}^{(g,h)}$ and $\mathcal{K}^{(g,h)}$ can be expressed in terms of the two non-holomorphic objects S^{zz} and Δ^z, with holomorphic coefficients. A detailed discussion of the (oriented) $\mathcal{F}^{(g,h)}$ case can be found in [68, 69]. Then, using the relations [31, 30]

$$C_{\bar{z}}^{zz} = \partial_{\bar{z}} S^{zz}, \ \ \Delta_{\bar{z}}^z = \partial_{\bar{z}} \Delta^z,$$ (9.74)

one can re-express the above extended holomorphic anomaly equations as

$$\partial_{S^{zz}} \mathcal{F}^{(g,h)} = \frac{1}{2} \sum \mathcal{F}_z^{(g_1,h_1)} \mathcal{F}_z^{(g_2,h_2)} + \frac{1}{2} \mathcal{F}_{zz}^{(g-1,h)},$$
$$\partial_{\Delta^z} \mathcal{F}^{(g,h)} = -\mathcal{F}_z^{(g,h-1)},$$ (9.75)

and

$$\partial_{S^{zz}} \mathcal{K}^{(g,h)} = \sum \mathcal{K}_z^{(g_1,h_1)} \mathcal{F}_z^{(g_2,h_2)} + \frac{1}{2} \sum \mathcal{K}_z^{(g_1,h_1)} \mathcal{K}_z^{(g_2,h_2)} + \mathcal{K}_{zz}^{(g-1,h)} + \frac{1}{2} \mathcal{F}_{zz}^{(g-1,h)},$$
$$\partial_{\Delta^z} \mathcal{K}^{(g,h)} = -\mathcal{K}_z^{(g,h-1)}.$$ (9.76)

These equations can be easily solved by direct integration, up to the holomorphic ambiguities to which we will return momentarily.

Before that, recall that in (6.1) we have identified the total topological string amplitude $\mathcal{G}^{(\chi)}$ as a combination of $\mathcal{F}$'s and $\mathcal{K}$'s (see (6.3), with $\mathcal{R}^{(g,h)} \equiv 0$). As already stated in the previous section, one can write down a combined holomorphic anomaly equation, directly for the total amplitude $\mathcal{G}^{(\chi)}$, see (9.58), which reduces for local 1-parameter models to

$$\partial_{\bar{z}} \mathcal{G}^{(\chi)} = \frac{1}{2} \sum_{\substack{\chi_1 + \chi_2 = \chi - 2 \\ \chi_i \geq 0}} C_{\bar{z}}^{zz} \mathcal{G}_z^{(\chi_1)} \mathcal{G}_z^{(\chi_2)} + C_{\bar{z}}^{zz} \mathcal{G}_{zz}^{(\chi-2)} - \Delta_{\bar{z}}^z \mathcal{G}_z^{(\chi-1)}.$$ (9.77)

It is obvious that just as the individual amplitudes $\mathcal{F}$ and $\mathcal{K}$, $\mathcal{G}^{(\chi)}$ can be written as a polynomial in the non-holomorphic propagator S^{zz} and terminator Δ^z, with holomorphic coefficients. Thus, we can re-express (9.77) as

$$
\begin{aligned}
\partial_{S^{zz}} \mathcal{G}^{(\chi)} &= \frac{1}{2} \sum \mathcal{G}_z^{(\chi_1)} \mathcal{G}_z^{(\chi_2)} + \mathcal{G}_{zz}^{(\chi-2)} \ , \\
\partial_{\Delta^z} \mathcal{G}^{(\chi)} &= -\mathcal{G}_z^{(\chi-1)} \ ,
\end{aligned}
\tag{9.78}
$$

which again can be simply solved by integration, yielding a polynomial in S^{zz} and Δ^z with holomorphic functions in z as coefficients.

9.7 Fixing the holomorphic ambiguities of local $\mathbb{P}^2$

In order to evaluate the polynomials in S^{zz} and Δ^z that we have obtained by integrating the holomorphic anomaly equation, $i.e.$, to obtain explicit expansions of $\mathcal{F}$, $\mathcal{K}$ and $\mathcal{G}$, we have to specify the coordinate z. That is, we have to chose a point in moduli-space around which to expand these amplitudes. Furthermore, the holomorphic ambiguities of these amplitudes, which we will denote as $a_{\mathcal{F}/\mathcal{K}}^{(g,h)}$ and $a_{\mathcal{G}}^{(\chi)}$, have to be fixed.

The natural point of interest in moduli space is the large-volume point with flat coordinate t corresponding to the Kähler parameter of $\mathbb{P}^2$. At this point, we can compare with our results from localization and the real topological vertex to fix the ambiguities $a_{\mathcal{F}/\mathcal{K}}^{(g,h)}$ and $a_{\mathcal{G}}^{(\chi)}$. The mirror map $z(t)$ and the domain-wall tension $\mathcal{T}$ that enters into $\Delta^z(t)$ can be obtained from the (inhomogenous) Picard-Fuchs equation (we have taken the liberty to multiply the inhomogeneous part with an additional factor of $-i(2\pi)^2$ in comparison with [17])

$$
\left(\theta^3 - 3z\theta(3\theta + 1)(3\theta + 2)\right) \mathcal{T} = -\frac{1}{4}\sqrt{z} \ ,
\tag{9.79}
$$

with $\theta = z\partial_z$. The solutions of the homogenous equation near $z = 0$ yield the well-known closed string periods (leading to the mirror map $z(t)$), while the solution of the inhomogeneous equation gives the domain-wall tension interpolating between the two open string vacua (recall that we have a discrete $\mathbb{Z}_2$ valued Wilson-line on the brane).

$$
\mathcal{T} = 2i\ \Gamma(3/2)^2 \sum_{n=0}^{\infty} \frac{\Gamma(3n + 3/2)}{\Gamma(n + 3/2)^3} z^{n+1/2} \ .
\tag{9.80}
$$

Using the definitions (9.63) and (9.72), we obtain the following large-volume expansions of

the $z(t)$, $S^{zz}(t)$ and $\Delta^z(t)$

$$
\begin{aligned}
z(t) &= -q - 6q^2 - 9q^3 - 56q^4 + 300q^5 - 3942q^6 + 48412q^7 - \cdots , \\
S^{zz}(t) &= \tfrac{1}{2}q^2 + 15q^3 + 135q^4 + 785q^5 + \tfrac{4473}{2}q^6 + 18333q^7 - \cdots , \\
-i\Delta^z(t) &= -\tfrac{3}{2}q^{3/2} - \tfrac{39}{2}q^{5/2} - \tfrac{117}{2}q^{7/2} - \tfrac{765}{2}q^{9/2} + 1881q^{11/2} - \cdots ,
\end{aligned}
\tag{9.81}
$$

with $q = e^{2\pi i t}$. Note that

$$
S^{zz}(t) = \tau^2 S^{tt}, \ \ S^z(t) = \tau \Delta^t .
\tag{9.82}
$$

where $\tau = \partial_t z(t)$. Plugging these expansions into the polynomial expressions for $\mathcal{F}$ and $\mathcal{K}$ and comparing with our localization results allows us to fix the holomorphic ambiguities up to a certain order. We here report our observations.

First of all, the holomorphic ambiguities of $\mathcal{F}^{(0,h)}$, $\mathcal{F}^{(1,h)}$ and $\mathcal{K}^{(1,h)}$ take a very simple form. More precisely, in our scheme, the ambiguities $a_{\mathcal{F}}^{(0,h)}$ and $a_{\mathcal{K}}^{(1,h)}$ all vanish, whereas we find for the ambiguity $a_{\mathcal{F}}^{(1,h)}$ of $\mathcal{F}^{(1,h)}$

$$
a_{\mathcal{F}}^{(1,h)} = \begin{cases} -\tfrac{1}{24}z^{1/2} & h = 1 \\ (-1)^h \tfrac{3^{(h-1)}}{2^{(2h+2)h}} \, z^{h/2} & h > 1 \end{cases} .
\tag{9.83}
$$

Secondly, one may note that the open string degenerations alone completely generate all Feynman diagrams for $\mathcal{F}^{(0,h)}$, $\mathcal{F}^{(1,h)}$, and $\mathcal{K}^{(1,h)}$ for all h. This means that using a flat coordinate t, we have the following simple expressions for these amplitudes, which can be evaluated even for very large h most economically:

$$
\begin{aligned}
\mathcal{F}^{(0,h)} &= \int d\Delta^t \partial_t \mathcal{F}^{(0,h-1)} = \left[\int d\Delta^t \partial_t \right]^{h-2} \mathcal{F}^{(0,2)}(t) , \\
\mathcal{K}^{(1,h)} &= \int d\Delta^t \partial_t \mathcal{K}^{(1,h-1)} = \left[\int d\Delta^t \partial_t \right]^{h} \mathcal{K}^{(1,0)}(t) , \\
\mathcal{F}^{(1,h)} &= \int d\Delta^t \partial_t \mathcal{F}^{(1,h-1)} + a_{\mathcal{F}}^{(1,h)} \\
&= \left[\int d\Delta^t \partial_t \right]^{h} \mathcal{F}^{(1,0)}(t) + \sum_{i=1}^{h} \left[\int d\Delta^t \partial_t \right]^{(h-i)} a_{\mathcal{F}}^{(1,i)} .
\end{aligned}
\tag{9.84}
$$

For higher genus, things become more involved, and there does not appear to be a simple structure as in (9.83). For illustration, we give here the following oriented open string

amplitudes

$$\mathcal{F}^{(2,1)} = -\frac{7\sqrt{q}}{2880} + \frac{79q^{3/2}}{2880} - \frac{59q^{5/2}}{128} + \frac{2597q^{7/2}}{720} - \frac{205151q^{9/2}}{240} + \frac{31659529q^{11/2}}{640} + \cdots \, ,$$

$$\mathcal{F}^{(2,2)} = \frac{11q}{3072} + \frac{41q^2}{12288} + \frac{10663q^3}{2560} - \frac{389561q^4}{30720} + \frac{13173223q^5}{3072} - \frac{5413756009q^6}{20480} + \cdots \, ,$$

$$\mathcal{F}^{(2,3)} = -\frac{87q^{3/2}}{20480} - \frac{3259q^{5/2}}{10240} - \frac{476291q^{7/2}}{20480} - \frac{465417q^{9/2}}{20480} - \frac{348949197q^{11/2}}{20480} + \cdots \, ,$$

$$\mathcal{F}^{(2,4)} = \frac{407q^2}{81920} + \frac{57861q^3}{32768} + \frac{2103243q^4}{20480} + \frac{15796159q^5}{32768} + \frac{4897896903q^6}{81920} + \cdots \, .$$

$$(9.85)$$

and the following unoriented amplitudes.

$$\mathcal{K}^{(2,0)} = \frac{5q}{128} + \frac{33q^2}{16} - \frac{10953q^3}{64} + \frac{223495q^4}{32} - \frac{13926207q^5}{64} + \frac{379810917q^6}{64} + \cdots \, ,$$

$$\mathcal{K}^{(2,1)} = -\frac{9q^{3/2}}{128} - \frac{12723q^{5/2}}{1024} + \frac{270585q^{7/2}}{256} - \frac{13282137q^{9/2}}{256} + \frac{1951535727q^{11/2}}{1024} + \cdots \, ,$$

$$\mathcal{K}^{(2,2)} = \frac{99q^2}{2048} + \frac{48897q^3}{1024} - \frac{4235175q^4}{1024} + \frac{120073203q^5}{512} - \frac{20153395269q^6}{2048} + \cdots \, ,$$

$$\mathcal{K}^{(2,3)} = \frac{747q^{5/2}}{4096} - \frac{4921425q^{7/2}}{32768} + \frac{215009073q^{9/2}}{16384} - \frac{27419944149q^{11/2}}{32768} + \cdots \, ,$$

$$\mathcal{K}^{(2,4)} = -\frac{34749q^3}{32768} + \frac{6909435q^4}{16384} - \frac{1208349657q^5}{32768} + \frac{21269586123q^6}{8192} + \cdots \, .$$

$$(9.86)$$

In all these cases, we have parameterized the holomorphic ambiguities of $\mathcal{F}^{(g,h)}$ and $\mathcal{K}^{(g,h)}$ via the function

$$a_{\mathcal{F}/\mathcal{K}}^{(g,h)} = \sum_{i=0}^{n-1} a_i \frac{z^{i+h/2}}{(1-27z)^{2g-2}} \, , \qquad (9.87)$$

where a_i are rational numbers and

$$n = \begin{cases} 2g-1 & \text{for } \mathcal{F}^{(g,0)} \\ 3g-2 & \text{else} \end{cases} . \qquad (9.88)$$

We have then compared the coefficients of the q-expansion in low degree with our localization results in order to determine the coefficients of the holomorphic ambiguity a_i. Note that the number of coefficients that needs to be fixed is larger for $h \neq 0$ than in the purely closed string case. This can be traced back to the existence of the tensionless domain wall at the orbifold point and the resulting singularity of the $\mathcal{F}$ and $\mathcal{K}$ at this point. On the other hand, it is mildly comforting that the number of unknown coefficients does not grow with h. (Naively, one might expect $n \sim 3g + h$ or something similar.) This could suggest that there is additional structure that we have so far not identified. However, hopes of finding a very simple expression as in (9.83) for $g > 1$ have so far not materialized.

The (individual) amplitudes we have determined so far are only sufficient to obtain $\mathcal{G}^{(\chi)}$ via relation (6.3) up to $\chi = 3$ (which has been already achieved in [17]). In order to go beyond we need more information. A prime candidate to look at is the conifold point in moduli space, where it is known that the expansion of the closed string amplitudes

$\mathcal{F}^{(g,0)}$ possesses a "gap". This structure, whose existence can be understood physically, gives enough information to completely determine these amplitudes for all g [53, 34, 54]. It is natural to ask whether there is as well some systematics in the expansion of the real topological string amplitudes at the conifold point.

To exhibit the gap, we first need the appropriate flat coordinate. To this end, we solve the Picard-Fuchs equation (9.79) after the variable transformation $z \to z' = \frac{1-\Delta}{27}$, where Δ is the discriminant $\Delta = 1 - 27z$. Thus, $\theta \to \theta' = (\Delta - 1)\partial_\Delta$ and we obtain the known closed string periods at the conifold. In particular, we deduce the local flat coordinate at the conifold t_c to be,

$$t_c = \sqrt{3}\Delta + \frac{11\Delta^2}{6\sqrt{3}} + \frac{109\Delta^3}{81\sqrt{3}} + \frac{9389\Delta^4}{8748\sqrt{3}} + \frac{88351\Delta^5}{98415\sqrt{3}} + \frac{823187\Delta^6}{1062882\sqrt{3}} + \frac{68584051\Delta^7}{100442349\sqrt{3}} + \cdots . \quad (9.89)$$

The additional solution $\mathcal{T}_c$ of the inhomogeneous equation corresponds to the domain-wall tension at the conifold (up to a rational closed string period),

$$\mathcal{T}_c = \frac{\Delta^2}{24\sqrt{3}} + \frac{121\Delta^3}{2592\sqrt{3}} + \frac{3197\Delta^4}{69984\sqrt{3}} + \frac{4372889\Delta^5}{100776960\sqrt{3}} + \frac{222720689\Delta^6}{5441955840\sqrt{3}} + \frac{79384773199\Delta^7}{2057059307520\sqrt{3}} + \cdots . \quad (9.90)$$

As before, we can then easily infer the expansions of $z(t_c)$, $S^{zz}(t_c)$, and $\Delta^z(t_c)$ at the conifold point. We obtain

$$\begin{aligned}
z(t_c) &= \frac{1}{27} - \frac{t_c}{27\sqrt{3}} + \frac{11t_c^2}{1458} - \frac{145t_c^3}{39366\sqrt{3}} + \frac{6733t_c^4}{12754584} - \frac{120127t_c^5}{573956280\sqrt{3}} + \cdots , \\
S^{zz}(t_c) &= -\frac{1}{1458} + \frac{4t_c}{2187\sqrt{3}} - \frac{103t_c^2}{118098} + \frac{317t_c^3}{354294\sqrt{3}} - \frac{254887t_c^4}{1033121304} + \frac{8144183t_c^5}{46490458680\sqrt{3}} + \cdots , \\
\Delta^z(t_c) &= -\frac{t_c}{324} + \frac{53t_c^2}{11664\sqrt{3}} - \frac{817t_c^3}{629856} + \frac{346487t_c^4}{408146688\sqrt{3}} - \frac{17312837t_c^5}{110199605760} + \cdots .
\end{aligned} \quad (9.91)$$

Observe that while the coordinate rescaling $t_c \to \sqrt{3}t_c$ can be used to make the expansions of (the closed string quantities) $z(t_c)$ and $S^{zz}(t_c)$ rational, the open string quantity $\Delta^z(t_c)$ stays irrational, therefore in comparison to the oriented closed string case, we do not perform such a rescaling. (Although, the rescaling would still make the expansion of the amplitudes with an even number of boundaries rational.) Using these expansions, we obtain the following conifold expansions of the amplitudes given above.

$$\begin{aligned}
\mathcal{F}^{(2,1)} &= -\frac{7}{466560\sqrt{3}} + \frac{1621t_c}{22394880} - \frac{97207t_c^2}{906992640\sqrt{3}} + \frac{18202763t_c^3}{587731230720} - \frac{71727601t_c^4}{3526387384320\sqrt{3}} + \cdots , \\
\mathcal{F}^{(2,2)} &= -\frac{227t_c}{1492992\sqrt{3}} + \frac{954653t_c^2}{8707129344} - \frac{5012287t_c^3}{39182082048\sqrt{3}} + \frac{4892098657t_c^4}{135413275557888} + \cdots , \\
\mathcal{F}^{(2,3)} &= \frac{545t_c}{8957952} - \frac{15095299t_c^2}{87071293440\sqrt{3}} + \frac{4878199531t_c^3}{56422198149120} - \frac{92953690463t_c^4}{1015599566684160\sqrt{3}} + \cdots , \\
\mathcal{F}^{(2,4)} &= -\frac{2735t_c}{53747712\sqrt{3}} + \frac{520278533t_c^2}{8358844170240} - \frac{6588078971t_c^3}{56422198149120\sqrt{3}} + \frac{1013092981t_c^4}{20061226008576} + \cdots ,
\end{aligned} \quad (9.92)$$

in the oriented sector and

$$
\begin{aligned}
\mathcal{K}^{(2,0)} &= -\frac{27}{128t_c{}^2} - \frac{47}{13824} + \frac{191t_c}{279936\sqrt{3}} + \frac{17693t_c{}^2}{201553920} - \frac{41893t_c{}^3}{408146688\sqrt{3}} + \cdots , \\
\mathcal{K}^{(2,1)} &= \frac{19}{9216\sqrt{3}} - \frac{15955t_c}{35831808} - \frac{12149t_c{}^2}{161243136\sqrt{3}} + \frac{29671433t_c{}^3}{313456656384} - \frac{54115555t_c{}^4}{626913312768\sqrt{3}} + \cdots , \\
\mathcal{K}^{(2,2)} &= -\frac{1003}{2654208} + \frac{9529t_c}{17915904\sqrt{3}} - \frac{330943t_c{}^2}{7739670528} - \frac{10573571t_c{}^3}{104485552128\sqrt{3}} + \cdots , \\
\mathcal{K}^{(2,3)} &= \frac{491}{2654208\sqrt{3}} - \frac{25373t_c}{161243136} + \frac{615487t_c{}^2}{5159780352\sqrt{3}} + \frac{280904809t_c{}^3}{30091839012864} + \cdots , \\
\mathcal{K}^{(2,4)} &= -\frac{193}{7077888} + \frac{191993t_c}{1719926784\sqrt{3}} - \frac{74663195t_c{}^2}{1486016741376} + \frac{690070327t_c{}^3}{30091839012864\sqrt{3}} + \cdots ,
\end{aligned}
\tag{9.93}
$$

in the unoriented sector. We observe that the open string amplitudes are all regular and $\mathcal{K}^{(g,0)}$ possesses similarly to $\mathcal{F}^{(g,0)}$ a gap at the conifold. Namely, as $t_c \to 0$, the amplitudes are of the general form

$$
\begin{aligned}
\mathcal{F}^{(g,0)} &= \frac{\Phi_g}{t_c^{2g-2}} + \mathcal{O}(t_c^0) , \\
\mathcal{K}^{(g,0)} &= \frac{\Psi_g}{t_c^{2g-2}} + \mathcal{O}(t_c^0) ,
\end{aligned}
\tag{9.94}
$$

the important point being that except for the leading singularity, the coefficients of the other singular terms all vanish. Furthermore, the order of the leading singularity at the conifold (of the amplitudes without fixed holomorphic ambiguities) can be easily parameterized in terms of g. Since we expect that this structure of the amplitudes is general, the holomorphic ambiguities parameterized by (9.87) need to preserve this structure. Each vanishing coefficient imposes one condition on $a_{\mathcal{F}/\mathcal{K}}^{(g,h)}$, *i.e.*, fixes one coefficient a_i. Hence, we deduce that the conifold gives the following number of conditions which can be used to (partly) fix the ambiguities of the amplitudes:

$$
\#_c = \begin{cases} 2g - 3 & \text{for } \mathcal{K}^{(g,0)} \\ 2g - 2 & \text{for } \mathcal{K}^{(g,h)} \text{ and } \mathcal{F}^{(g,1)} \\ 2g - 1 & \text{for } \mathcal{F}^{(g,h)} \ (h > 1) \end{cases} .
\tag{9.95}
$$

Nevertheless, $\sim g$ conditions remain undetermined. In particular, the leading singularities of the Klein bottle amplitudes $\mathcal{K}^{(g,0)}$ at the conifold, which we have denoted as Ψ_g, needs to be understood. We will briefly come back to this point below.

One might hope that the left-over conditions can be fixed via some additional systematics at the orbifold point. However, performing similarly as above the expansions of the amplitudes at the orbifold point, we have to conclude that there is no apparent such systematics which could aid in fixing the remaining ambiguities. Therefore, for the time

being we have to rely on localization to fix the $\sim g$ remaining conditions. With the data at hand, we have completely determined $\mathcal{G}^{(\chi)}$ from the individual amplitudes up to $\chi = 6$.

If we instead directly compute the combined amplitude $\mathcal{G}^{(\chi)}$ via (9.78), we can go a bit further since the real topological vertex provides data for higher χ. Similarly as for the individual amplitudes, we parameterize the holomorphic ambiguity of $\mathcal{G}^{(\chi)}$ via

$$a_{\mathcal{G}}^{(\chi)} = \sum_{i=0}^{n} a_i \frac{z^{i+\delta}}{(1 - 27z)^{\zeta}} \ , \tag{9.96}$$

with $n = \frac{3}{2}\zeta$, $\delta = (\chi \bmod 2)/2$ and

$$\zeta = \begin{cases} \chi & \text{for } \chi \text{ even} \\ \chi - 1 & \text{for } \chi \text{ odd} \end{cases} . \tag{9.97}$$

The conifold expansion shows that $\mathcal{G}^{(\chi)}$ possesses a gap for χ even and is regular for χ odd (this is as expected from the behavior of the individual amplitudes $\mathcal{F}$ and $\mathcal{K}$ at the conifold described above). Similarly as for the individual amplitudes $\mathcal{F}$ and $\mathcal{K}$, we can easily deduce that the gap leads to

$$\#_c = \begin{cases} \chi - 1 & \text{for } \chi \text{ even} \\ \chi & \text{for } \chi \text{ odd} \end{cases} , \tag{9.98}$$

conditions to fix the $(n + 1)$ coefficients a_i of $a_{\mathcal{G}}^{(\chi)}$ (if one can understand Ψ_g, the conifold gives exactly χ conditions). Using the data from the real topological vertex given in table C.3 of appendix C, we can fix the left-over conditions for some higher χ and in this way completely determined the amplitudes $\mathcal{G}^{(\chi)}$ up to $\chi = 9$. [4] The resulting real Gopakumar-Vafa invariants are listed in table C.1 and C.2 in appendix C.

Finally, let us spend a few words on the leading singularity of the $\mathcal{K}^{(g,0)}$ at the conifold (9.94). It is well known that the coefficient of the leading singularity of the oriented closed string amplitudes $\mathcal{F}^{(g,0)}$ at the conifold is given by [70, 71]

$$\Phi_g = \frac{B_{2g}}{2g(2g - 2)} \ , \tag{9.99}$$

where B_{2g} are the Bernoulli numbers. The universality of the relationship (9.99) has been understood from many perspectives over the years. Among other things, Φ_g gives the Euler characteristic of the moduli space of genus g complex curves. The gap structure was

---

[4] The data at hand is sufficient to go up to $\chi = 12$.

g	1	2	3	4	5	6
Ψ_g	$-\frac{1}{8}\log(t_c)$	$-\frac{9}{128}$	$\frac{81}{512}$	$-\frac{4239}{4096}$	$\frac{221859}{16384}$	$-\frac{48938499}{163840}$

Table 9.1: Ψ_g for low g (note that we have rescaled $t_c \to \sqrt{3}t_c$).

discovered in [53, 34], and explained physically in terms of the existence of a single light BPS state associated with the vanishing period at the conifold [72]. It behooves us to ask for a similar interpretation of the gap structure in $\mathcal{K}^{(g,0)}$. The coefficients Ψ_g have a good chance of being equally universal as the Φ_g. For future reference, we list the values of Ψ_g for low g in table 9.1 and leave a detailed understanding to subsequent work. Note that Ψ_g can be conveniently extracted from $\mathcal{G}'(x)$, as defined in (6.9), expanded at the conifold point. This can be easily inferred from (6.3) combined with the regularity of the individual amplitudes with boundaries at the conifold point.

Part IV

Appendices

Appendix A

Inhomogeneous Picard-Fuchs equation via Griffiths-Dwork

In the following, we will give some more details of the main computation of section 4.2, *i.e.*, the evaluation of (4.7). In order to be able to evaluate (4.7), we first need to derive the exact parts $\tilde{\beta}^{(k)}$ of the inhomogeneous Picard-Fuchs equations covering the (extended) periods of $Y^{(k)}$. We will achieve this via the Griffiths-Dwork method (see for instance [19]):

A.1 Griffiths-Dwork method

The fundamental weighted homogeneous differential form of the ambient space is given by

$$\omega^{(k)} = \sum_{i=1}^{5} (-1)^{i-1} \nu_i x_i dx_1 \wedge ... \wedge \widehat{dx_i} \wedge ... \wedge dx_5 , \tag{A.1}$$

where ν_i are the weights and x_i the homogenous coordinates of the ambient weighted $\mathbb{P}^4$. For later convenience, we define $\omega_i^{(k)} := \partial_i \omega^{(k)}$.

The holomorphic 3-form is given by

$$\Omega = Res_{W^{(k)}=0} \tilde{\Omega} , \tag{A.2}$$

with $\tilde{\Omega} = \frac{\omega^{(k)}}{W^{(k)}}$. For simplicity, the $^{(k)}$ indices are implicitly understood in the following. Then, the fundamental period

$$w_0 = \int_\Gamma \Omega , \tag{A.3}$$

where Γ is usually a 3-cycle, here however we allow Γ to have a boundary $\partial\Gamma$, evaluates to

$$w_0 = \int_\Gamma Res_{W=0} \tilde{\Omega} = \int_{T_\epsilon(\Gamma)} \tilde{\Omega} , \tag{A.4}$$

where T_ϵ is a small tube around Γ. From that we obtain

$$\partial_\psi^l w_0 = l! \int_{T_\epsilon(\Gamma)} \frac{(x_1 x_2 x_3 x_4 x_5)^l}{W^{l+1}} \omega \ , \tag{A.5}$$

where we have implicitly assumed that there will be no contribution of derivatives acting on the chain. That this is indeed the case will be explicitly verified for the models under consideration.

For $l = 4$ we can express $\partial_\psi^l w_0$ in terms of lower derivatives using the equations of motion $\partial_i W = 0$ and "partial integration" (Griffith's reduction of pole order) and obtain in this way a differential equation of (inhomogeneous) Picard-Fuchs type satisfied by w_0. The calculation is lengthy, but straight-forward.

A.2 $Y^{(6)}$

Using the Griffiths-Dwork method as described above and the relation

$$\begin{aligned}
\psi^2(1 - \psi^6)(x_1^4 x_2^4 x_3^4 x_4^4 x_5^4) &= \psi^7(x_1^3 x_2^3 x_3^3 x_4^3 x_5^4)\partial_5 W + \psi^6(x_1^2 x_2^2 x_3^2 x_4^3 x_5^5)\partial_4 W \\
&\quad + \psi^5(x_1 x_2 x_3^2 x_4^7 x_5^4)\partial_3 W + \psi^4(x_2 x_3^6 x_4^6 x_5^3)\partial_2 W \\
&\quad + \psi^3(x_2^5 x_3^5 x_4^5 x_5^2)\partial_1 W + \psi^2(x_1^4 x_2^4 x_3^4 x_4^4 x_5^2)\partial_5 W \ ,
\end{aligned} \tag{A.6}$$

we obtain the inhomogeneous Picard-Fuchs equation

$$\tilde{\mathcal{L}}^{(6)} = \psi^2(1 - \psi^6)\partial_\psi^4 - 2\psi(1 + 5\psi^6)\partial_\psi^3 + (2 - 25\psi^6)\partial_\psi^2 - 15\psi^5\partial_\psi - \psi^4 = d\tilde{\beta} \ , \tag{A.7}$$

with exact part

$$\begin{aligned}
\tilde{\beta}^{(6)} = \frac{6}{W^4} &\left[\psi^7 x_1^3 x_2^3 x_3^3 x_4^3 x_5^4 \omega_5 + \psi^6 x_1^2 x_2^2 x_3^2 x_4^3 x_5^5 \omega_4 + \psi^5 x_1 x_2 x_3^2 x_4^7 x_5^4 \omega_3 \right. \\
&\left. + \psi^4 x_2 x_3^6 x_4^6 x_5^3 \omega_2 + \psi^3 x_2^5 x_3^5 x_4^5 x_5^2 \omega_1 + \psi^2 x_1^4 x_2^4 x_3^4 x_4^4 x_5^2 \omega_5 \right] \\
+ \frac{2}{W^3} &\left[3\psi^6 x_1^2 x_2^2 x_3^2 x_4^2 x_5^3 \omega_5 + 2\psi^5 x_1 x_2 x_3 x_4^7 x_5^2 \omega_5 + 3\psi^6 x_1^2 x_2^2 x_3^2 x_4^3 x_5^2 \omega_4 \right. \\
&\left. + \psi^4 x_3^6 x_4^6 x_5 \omega_5 + \psi^5 x_1 x_2 x_3^2 x_4^7 x_5 \omega_3 - 2\psi x_1^3 x_2^3 x_3^3 x_4^3 x_5 \omega_5 \right] \\
+ \frac{1}{W^2} &\left[6\psi^5 x_1 x_2 x_3 x_4^2 x_5 \omega_4 + \psi^4 x_3^6 x_4 \omega_4 + \psi^5 x_1 x_2 x_3^2 x_4 x_5 \omega_3 + x_1^2 x_2^2 x_3^2 x_4^2 \omega_5 \right] \\
+ \frac{1}{W} &\left[\psi^4 x_3 \omega_3 \right] \ .
\end{aligned} \tag{A.8}$$

The next step in the evaluation of (4.7) is to define a proper tube $T_\epsilon(\partial\Gamma)$, where we have for $Y^{(6)}$: $\partial\Gamma = C_+^{(6)} - C_-^{(6)}$ with $C_\zeta^{(6)}$ given in (4.1). For simplicity, we set $\alpha^{(6)} = i$ and

drop the $^{(6)}$ indices in the following. Observe that the curves C_ζ possess two components distinguished by $\gamma = \pm 1$, i.e. $C_\zeta = C_\zeta^+ + C_\zeta^-$ with

$$C_\zeta^\gamma = \{x_1 = i\zeta x_2, x_3 = ix_4, x_5 = i^{\frac{-\zeta-1}{2}}\gamma\sqrt{3\psi}x_1 x_3\} . \tag{A.9}$$

Note that the curves intersect in three points:

$$p_1^\zeta := \{x_1 = i\zeta x_2, x_3 = x_4 = x_5 = 0\}, \ p_2 := \{x_3 = ix_4, x_1 = x_2 = x_5 = 0\} . \tag{A.10}$$

For the same reasons as in the quintic case discussed in [9], only the neighborhood of the set of points $\{p_1^\zeta, p_2^\zeta := p_2\}$ gives a contribution to the integral over the tube $T_\epsilon(\partial\Gamma)$. Hence, the integral (4.7) splits up into

$$\int_{T_\epsilon(\partial\Gamma)} \tilde\beta = \sum_{\zeta,\gamma,i} \zeta \int_{T_\epsilon(C_\zeta^\gamma;p_i^\zeta)} \tilde\beta , \tag{A.11}$$

where we define the tubes $T_\epsilon(C_\zeta^\gamma; p_i^\zeta)$ around C_ζ^γ near p_i^ζ momentarily:

The region around the points p_i^ζ is best described in the following two local charts of the ambient weighted $\mathbb{P}^4$:

$$U_1: \ x_i \rightarrow \frac{x_j}{x_1^{\nu_j}} , \ U_2: \ x_j \rightarrow \frac{x_j}{x_3^{\nu_j}} , \tag{A.12}$$

where $p_i^\zeta \subset U_i$.

Let us start with the region around p_1^ζ: Changing to the inhomogeneous coordinates of (A.12), i.e.

$$T' := \frac{x_2}{x_1} , \ X' := \frac{x_3}{x_1} , \ Y' := \frac{x_4}{x_1} , \ Z' := \frac{x_5}{x_1^2} , \tag{A.13}$$

and performing subsequently the coordinate change

$$T' \rightarrow i\zeta T , \ Y' \rightarrow -iY , \ X' \rightarrow X + Y + Z , \ Z' \rightarrow i^{\frac{-\zeta-1}{2}}\gamma(1 + \sqrt{3\psi}(Y + Z)) , \tag{A.14}$$

we obtain a more convenient parameterization of C_ζ^γ and p_1^ζ:

$$\begin{aligned} C_\zeta^\gamma &= \{T = -1, X = -Z = \frac{1}{\sqrt{3\psi}}\} , \\ p_1^\zeta &= \{T = -1, X = -Z = \frac{1}{\sqrt{3\psi}}, Y = 0\} . \end{aligned} \tag{A.15}$$

Observe that the curves C_ζ^γ are parametrized in their respective coordinate systems by the single coordinate $Y = re^{i\phi}$, and intersects with the other curves at $r = 0$.

We now define tubes $T_\epsilon^{\zeta\gamma}$ around the curves C_ζ^γ by requiring that $T_\epsilon^{\zeta\gamma}$ lies outside of $Y^{(6)}$ inside a small neighborhood of p_1^ζ ($0 \le r < r^*$) and inside of $P^{(6)}$ else ($r \ge r^*$). Therefore, consider the normal vectors

$$v_{\zeta\gamma} = a_{\zeta\gamma}\partial_T - \gamma \frac{i^{\frac{-\zeta-1}{2}}}{2} e^{-2i\phi}\partial_X + \gamma \frac{i^{\frac{-\zeta-1}{2}}}{2} e^{-2i\phi}\partial_Z \ , \tag{A.16}$$

with

$$a := \frac{f(r)}{1 + \gamma i^{\frac{\zeta+1}{2}}\sqrt{3\psi^3 Y^3}} \ , \tag{A.17}$$

where $f(r)$ is a non-negative C^∞ function with $f(0) = 1$ and $f(r) = 0$ for $r \ge r^* > 0$. Clearly $v_{\zeta\gamma}$ point inside of $P^{(6)}$ for $r > r^*$. Note that the definition of $a_{\zeta\gamma}$ naturally fixes the point r^*. To see that, note if we define $r^* = (3\psi^3)^{-1/6}$, $f(r^*)$ must vanish, since otherwise $a_{\zeta\gamma}$ would have poles at r^*. For reasons that will become clear later, we require as well that the first derivative $f'(r)$ vanishes at $r \ge r^* > 0$.

One easily checks that

$$D_{v_{\zeta\gamma}}W|_{C_\zeta^\gamma} = f(r) + \sqrt{3\psi^3}r^2 > 0 \ , \tag{A.18}$$

hence $v_{\zeta\gamma}$ points outside of $Y^{(6)}$ and thus we can use $v_{\zeta\gamma}$ to define proper tubes $T_\epsilon^{\zeta\gamma}$. In detail, the tubes are parameterized in local coordinates by

$$T = -1 + \tilde{\epsilon}a \ , \ X = -Z = \frac{1}{\sqrt{3\psi}} - \gamma \frac{i^{\frac{-\zeta-1}{2}}}{2}\tilde{\epsilon}e^{-2i\phi} \ , \tag{A.19}$$

where $\tilde{\epsilon} = e^{i\chi}\epsilon$ and $\chi \in [0, 2\pi]$.

For the evaluation of (A.11) we need to express $\tilde{\beta}$ in the coordinates (A.14), restrict to the respective tubes and perform the integration over

$$\int_0^\infty dr \int_0^{2\pi} d\phi \int_0^{2\pi} d\chi \ . \tag{A.20}$$

Since the terms occurring in $\tilde{\beta}$ are proportional to $\frac{\omega_i}{W^l}$, we especially need $\omega_i|_{T_\epsilon^{\zeta\gamma}}$. After going to the chart U_1 and restricting to $X' = iY'$, we infer from (A.1) that $\omega_i = 0$ for $i \notin \{3, 4\}$ and

$$\omega_4 = -i\omega_3 = dT' \wedge dX' \wedge dZ' \ . \tag{A.21}$$

Changing to the coordinates (A.14) then yields

$$dT' \wedge dX' \wedge dY' = i^{\frac{-\zeta+1}{2}}\zeta\gamma\sqrt{3\psi}dT \wedge dX \wedge dY \ , \tag{A.22}$$

which restricts on the tubes $T_\epsilon^{\zeta\gamma}$ to

$$dT \wedge dX \wedge dY|_{T_\epsilon^{\zeta\gamma}} = -i^{\frac{-\zeta-1}{2}} \gamma e^{-i\phi} a \left(1 - \frac{rf'(r)}{2f(r)}\right) \tilde{\epsilon}^2 dr \wedge d\phi \wedge d\chi . \tag{A.23}$$

We have now everything at our disposal to infer the contribution of the integrals over the tubes $T_\epsilon(C_\zeta^\gamma; p_1^\zeta)$ to (A.11). For performing the explicit calculation, note that only terms which do not come in powers of $\tilde{\epsilon}$ can survive the integration over $d\chi$. Hence, the integration over $d\chi$ simply yields a factor of 2π. For the integration over $d\phi$ it is more convenient to perform the variable transformation $e^{i\phi} \to z$, with $z \in \mathbb{C}$. In this coordinate, the integral becomes a line integral around the unit circle in the complex plane and only terms can contribute that have poles in the unit disk. Combined with the property $f(r) = f'(r) = 0$ for $r \geq r^*$, it is easy to see that only terms can contribute which do not come in powers of z in the nominator.

Performing the explicit calculation we infer that there is no contribution from the integrals over the tubes $T_\epsilon(C_\zeta^\gamma; p_1^\zeta)$ to (A.11).

It remains to evaluate the contribution of $T_\epsilon(C_\zeta^\gamma; p_2)$ to (A.11): For that, we need to perform the same calculations as above in the coordinate chart U_2 which includes p_2. Hence, we take the inhomogeneous coordinates

$$T' := \frac{x_4}{x_3} \ , \ X' := \frac{x_1}{x_3} \ , \ Y' := \frac{x_2}{x_3} \ , \ Z' := \frac{x_5}{x_3^2} \ , \tag{A.24}$$

and perform the same coordinate redefinitions as in (A.14) in order to obtain (A.15). However, this time p_1^ζ corresponds to p_2. Due to the symmetry of W, the tubes $T_\epsilon^{\zeta\gamma}$ have the same parameterization and we can still use (A.16)-(A.23), if we replace

$$\omega_4 \to \omega_2 \ , \ \omega_3 \to \omega_1 . \tag{A.25}$$

Performing the explicit calculation similar as in chart U_1, we infer that we obtain contributions from the term

$$\int_{T_\epsilon(C_\zeta^\gamma; p_2)} \frac{6\psi^4 x_2 x_3^6 x_4^6 x_5^3 \omega_2}{W^4} = \zeta \frac{2}{3} \pi^2. \tag{A.26}$$

Note that we have taken an additional normalization factor of 6^{-1} due to G_{fix} given in table 4.1 into account (p_2 is a singular point).

It remains to show that the underlying assumption that we have no contribution from derivatives acting on $T_\epsilon(\Gamma)$ indeed holds. The argumentation is as in [9]. For that, note that the normal vectors implementing first order deformations of C_ζ^γ are given by

$$n_{\zeta\gamma} = -i^{\frac{\zeta+1}{2}} \gamma \frac{x_5}{\sqrt{3}\psi} \frac{1}{2\psi} (\partial_3 - i\partial_4) . \tag{A.27}$$

Hence, we have that

$$n_{\zeta\gamma}\omega = -i^{\frac{\zeta+1}{2}}\gamma\frac{x_5}{\sqrt{3\psi}}\frac{1}{2\psi}(\omega_3 - i\omega_4) = 0 \; , \tag{A.28}$$

where we used (A.21).

A.3 $Y^{(8)}$

The discussion of the remaining two models $Y^{(8)}$ and $Y^{(10)}$ is very similar to $Y^{(6)}$, hence we will be brief:

For $Y^{(8)}$ we use the relation

$$
\begin{aligned}
\psi^3(1 - \psi^8)(x_1^4x_2^4x_3^4x_4^4x_5^4) &= \psi^{10}(x_1^3x_2^3x_3^3x_4^3x_5^4)\partial_5 W + \psi^9(x_1^2x_2^2x_3^2x_4^3x_5^4)\partial_4 W \\
&+ \psi^8(x_1x_2x_3^2x_4^9x_5^3)\partial_3 W + \psi^7(x_2x_3^8x_4^8x_5^2)\partial_2 W \\
&+ \psi^6(x_2^7x_3^7x_4^7x_5)\partial_1 W + \psi^5(x_1^6x_2^6x_3^6x_4^6x_5)\partial_5 W \\
&+ \psi^4(x_1^5x_2^5x_3^5x_4^5x_5^2)\partial_5 W + \psi^3(x_1^4x_2^4x_3^4x_4^4x_5^3)\partial_5 W \; ,
\end{aligned}
\tag{A.29}
$$

to obtain the inhomogeneous Picard-Fuchs equation

$$\tilde{\mathcal{L}}^{(8)} = \psi^3(1-\psi^8)\partial_\psi^4 - \psi^2(6+10\psi^8)\partial_\psi^3 + 5\psi(3-5\psi^8)\partial_\psi^2 - 15(1+\psi^8)\partial_\psi - \psi^7 = d\tilde{\beta} \; , \tag{A.30}$$

with exact part

$$
\begin{aligned}
\tilde{\beta}^{(8)} =& \frac{6}{W^4}\Big[\psi^{10}x_1^3x_2^3x_3^3x_4^3x_5^4\omega_5 + \psi^9x_1^2x_2^2x_3^2x_4^3x_5^4\omega_4 + \psi^8x_1x_2x_3^2x_4^9x_5^3\omega_3 + \psi^7x_2x_3^8x_4^8x_5^2\omega_2 \\
&+ \psi^6x_2^7x_3^7x_4^7x_5\omega_1 + \psi^5x_1^6x_2^6x_3^6x_4^6x_5\omega_5 + \psi^4x_1^5x_2^5x_3^5x_4^5x_5^2\omega_5 + \psi^3x_1^4x_2^4x_3^4x_4^4x_5^3\omega_5\Big] \\
&+ \frac{2}{W^3}\Big[3\psi^9x_1^2x_2^2x_3^2x_4^2x_5^3\omega_5 + 2\psi^8x_1x_2x_3x_4^9x_5^2\omega_5 + 2\psi^9x_1^2x_2^2x_3^2x_4^{10}x_5\omega_5 \\
&+2\psi^{10}x_1^3x_2^3x_3^3x_4^4x_5\omega_4 - 2\psi^{10}x_1^3x_2^3x_3^3x_4^3x_5^2\omega_5 + \psi^7x_3^8x_4^8x_5\omega_5 + \psi^8x_1x_2x_3^9x_4^2x_5\omega_4 \\
&+\psi^9x_1^2x_2^2x_3^3x_4^2x_5^2\omega_3 - 6\psi^2x_1^3x_2^3x_3^3x_4^3x_5^2\omega_5 - 3\psi^3x_1^4x_2^4x_3^4x_4^4x_5\omega_5 - \psi^4x_1^5x_2^5x_3^5x_4^5\omega_5\Big] \\
&+ \frac{1}{W^2}\Big[4\psi^8x_1x_2x_3x_4^2x_5\omega_4 + 2\psi^9x_1^2x_2^2x_3^2x_4^3\omega_4 - 6\psi^9x_1^2x_2^2x_3^2x_4^2x_5\omega_5 + \psi^7x_3^8x_4\omega_4 \\
&+ 3\psi^8x_1x_2x_3^2x_4x_5\omega_3 + 15\psi x_1^2x_2^2x_3^2x_4^2x_5\omega_5 + 3\psi^2x_1^3x_2^3x_3^3x_4^3\omega_5\Big] \\
&+ \frac{1}{W}\Big[\psi^7x_3\omega_3 - 15x_1x_2x_3x_4\omega_5\Big] \; .
\end{aligned}
\tag{A.31}
$$

In order to evaluate (4.7), we need to define proper tubes around the curves $C_{\langle\mu,\zeta\rangle}^{(8)}$. For simplicity, in the following we will just discuss the $C_{\langle-,\zeta\rangle}^{(8)}$ part. The $C_{\langle+,\zeta\rangle}^{(8)}$ part can be

discussed similarly and the results just differ by an overall sign[1] (therefore the μ in (4.8)). Hence, let us consider the curves

$$C_{\langle -,\zeta \rangle} := \{x_1 = \alpha^\zeta x_2, x_3 = \alpha x_4, x_5 = 2\alpha^{-\zeta-1}\psi x_1^2 x_3^2\} . \tag{A.32}$$

In the following we will denote these curves simply as C_ζ and we will implicitly set $\alpha = e^{i\pi/8}$. The two curves intersect in the point

$$p := \{x_3 = \alpha x_4, x_1 = x_2 = x_5 = 0\} . \tag{A.33}$$

As a consequence, (A.11) reduces for $Y^{(8)}$ to

$$\int_{T_\epsilon(\partial\Gamma)} \tilde{\beta} = \sum_\zeta \zeta \int_{T_\epsilon(C_\zeta;p)} \tilde{\beta} . \tag{A.34}$$

For the evaluation of (A.34), we go to the local chart U_2 defined in (A.24) and perform the variable redefinitions

$$T' \to -\alpha^{-1}T , \; Y' \to \alpha^{-\zeta}Y , \; X' \to X+Y+Z , \; Z' \to \alpha^{-\zeta-1}(1+\sqrt{2\psi}(Y+Z))^2 . \tag{A.35}$$

Then, we have

$$\begin{aligned} C_\zeta &= \{T = -1, X = -Z = \frac{1}{\sqrt{2\psi}}\} , \\ p &= \{T = -1, X = -Z = \frac{1}{\sqrt{2\psi}}, Y = 0\} . \end{aligned} \tag{A.36}$$

The tubes T_ϵ^ζ around C_ζ are parameterized similar as for $Y^{(6)}$ via normal vectors v_ζ defined by

$$v_\zeta = a_\zeta \partial_T - \frac{i}{4}\alpha^{2(\zeta-1)}e^{-3i\phi}\partial_X + \frac{i}{4}\alpha^{2(\zeta-1)}e^{-3i\phi}\partial_Z , \tag{A.37}$$

with

$$a_\zeta := \frac{f(r)}{1 - 2i\zeta\alpha^{2(\zeta-1)}\psi^2 Y^4} . \tag{A.38}$$

This choice ensures that

$$D_{v_\zeta}W|_{C_\zeta} = f(r) + \psi^3 r^3 > 0 , \tag{A.39}$$

such that T_ϵ^ζ is well defined.

---

[1] In fact, this must be so since by general principles, the total intersection of the hypersurface with a plane should give a vanishing result.

Thus, the tubes T_ϵ^ζ are locally parameterized by

$$T = -1 + \tilde\epsilon a \ , \ X = -Z = \frac{1}{\sqrt{2\psi}} - \tilde\epsilon \frac{i}{4} \alpha^{2(\zeta-1)} e^{-3i\phi} \ , \tag{A.40}$$

where $\tilde\epsilon = e^{i\chi}\epsilon$.

As a last piece, we need the restriction of the forms ω_i to T_ϵ^ζ: Going to the chart U_2 and restricting to $X' = \alpha^\zeta Y'$, we directly infer that $\omega_i = 0$ for $i \notin \{1, 2\}$ and that

$$\omega_2 = -\alpha^\zeta \omega_1 = dT' \wedge dX' \wedge dZ' \ . \tag{A.41}$$

Changing to the coordinates (A.35) then yields

$$dT' \wedge dX' \wedge dZ' = -2\alpha^{-2-\zeta}\sqrt{2\psi}(1 + \sqrt{2\psi}(Y + Z))dT \wedge dX \wedge dY \ . \tag{A.42}$$

Further,

$$dT \wedge dX \wedge dY|_{T_\epsilon^\zeta} = -i\frac{3}{4}\alpha^{2(\zeta-1)}ae^{-2i\phi}\tilde\epsilon^2 \left(1 - \frac{rf'(r)}{3f(r)}\right)dr \wedge d\phi \wedge d\chi \ . \tag{A.43}$$

Thus,

$$\omega_2|_{T_\epsilon^\zeta} = -\alpha^\zeta \omega_1|_{T_\epsilon^\zeta} =$$
$$= i3\alpha^{-4+\zeta}a\psi e^{-2i\phi}\left(re^{i\phi} + \frac{i}{4}\alpha^{2(\zeta-1)}e^{-3i\phi}\tilde\epsilon\right)\tilde\epsilon^2\left(1 - \frac{rf'(r)}{3f(r)}\right)dr \wedge d\phi \wedge d\chi \ . \tag{A.44}$$

We have now everything at our disposal to calculate (A.34). After performing the calculations, we infer that we have a contribution from the term

$$\int_{T_\epsilon(C_\zeta;p)} \frac{6\psi^6 x_2^7 x_3^7 x_4^7 x_5 \omega_1}{W^4} = \zeta 3\pi^2 \psi^2 \ , \tag{A.45}$$

where we included an additional normalization factor of 4^{-1}, similar as in the $Y^{(6)}$ case.

Similar as for $Y^{(6)}$, we infer from the normal vector

$$n_\zeta = -\frac{\alpha^{\zeta+1}}{4\psi^2}\frac{x_5}{x_1}(\partial_1 + \alpha^{-\zeta}\partial_2) \ . \tag{A.46}$$

that

$$n_\zeta \omega = -\frac{\alpha^{\zeta+1}}{4\psi^2}\frac{x_5}{x_1}(\omega_1 + \alpha^{-\zeta}\omega_2) = 0 \ , \tag{A.47}$$

where we used (A.41). Hence, the underlying assumption that we have no contribution from derivatives acting on $T_\epsilon(\Gamma)$ holds.

A.4 $Y^{(10)}$

For $Y^{(10)}$ we use the relation

$$\psi^3(1-\psi^{10})(x_1^4x_2^4x_3^4x_4^4x_5^4) = \psi^{12}(x_1^3x_2^3x_3^3x_4^3x_5^4)\partial_5 W + \psi^{11}(x_1^2x_2^2x_3^2x_4^3x_5^4)\partial_4 W$$
$$+ \psi^{10}(x_1x_2x_3^2x_4^6x_5^3)\partial_3 W + \psi^9(x_2x_3^{10}x_4^5x_5^2)\partial_2 W$$
$$+ \psi^8(x_2^9x_3^9x_4^4x_5)\partial_1 W + \psi^7(x_1^8x_2^8x_3^8x_4^3x_5)\partial_5 W \qquad \text{(A.48)}$$
$$+ \psi^6(x_1^7x_2^7x_3^7x_4^2x_5^2)\partial_5 W + \psi^5(x_1^6x_2^6x_3^6x_4x_5^3)\partial_5 W$$
$$+ \psi^4(x_1^5x_2^5x_3^5x_5^4)\partial_5 W + \psi^3(x_1^4x_2^4x_3^4x_5^4)\partial_4 W ,$$

to obtain the inhomogeneous Picard-Fuchs equation

$$\tilde{\mathcal{L}}^{(10)} = \psi^3(1-\psi^{10})\partial_\psi^4 - 10\psi^2(1+\psi^{10})\partial_\psi^3 + 5\psi(7-5\psi^{10})\partial_\psi^2 - 5(7+3\psi^{10})\partial_\psi - \psi^9 = d\tilde{\beta} , \quad \text{(A.49)}$$

with exact part

$$\tilde{\beta}^{(10)} = \frac{6}{W^4}\left[\psi^{12}x_1^3x_2^3x_3^3x_4^3x_5^4\omega_5 + \psi^{11}x_1^2x_2^2x_3^2x_4^3x_5^4\omega_4 + \psi^{10}x_1x_2x_3^2x_4^6x_5^3\omega_3\right.$$
$$+ \psi^9x_2x_3^{10}x_4^5x_5^2\omega_2 + \psi^8x_2^9x_3^9x_4^4x_5\omega_1 + \psi^7x_1^8x_2^8x_3^8x_4^3x_5\omega_5 + \psi^6x_1^7x_2^7x_3^7x_4^2x_5^2\omega_5$$
$$\left.+ \psi^5x_1^6x_2^6x_3^6x_4x_5^3\omega_5 + \psi^4x_1^5x_2^5x_3^5x_5^4\omega_5 + \psi^3x_1^4x_2^4x_3^4x_5^4\omega_4\right]$$
$$+ \frac{2}{W^3}\left[3\psi^{11}x_1^2x_2^2x_3^2x_4^2x_5^3\omega_5 + 2\psi^{10}x_1x_2x_3x_4^6x_5^2\omega_5 + 2\psi^{11}x_1^2x_2^2x_3^2x_4^3x_5^2\omega_4\right.$$
$$+ \psi^9x_3^{10}x_4^5x_5\omega_5 + \psi^{10}x_1x_2x_3^{11}x_4^2x_5\omega_4 + \psi^{11}x_1^2x_2^2x_3^3x_4^2x_5^2\omega_3 + 7\psi^5x_1^6x_2^6x_3^6x_4x_5\omega_5$$
$$- 10\psi^2x_1^3x_2^3x_3^3x_4^3x_5^2\omega_5 - 10\psi^3x_1^4x_2^4x_3^4x_4^4x_5\omega_5 - 10\psi^4x_1^5x_2^5x_3^5x_4^5\omega_5$$
$$\left.- 10\psi^5x_1^6x_2^6x_3^6x_4^2\omega_4 - \psi^6x_1^7x_2^7x_3^7x_4^2\omega_5\right]$$
$$+ \frac{1}{W^2}\left[5\psi^{10}x_1x_2x_3x_4^2x_5\omega_4 + 2\psi^{10}x_1x_2x_3^2x_4x_5\omega_3 + 35\psi x_1^2x_2^2x_3^2x_4^2x_5\omega_5 + \psi^9x_3x_4^5\omega_3\right.$$
$$\left.+ 5\psi^2x_1^3x_2^3x_3^3\omega_5 + 5\psi^3x_1^4x_2^4x_3^4\omega_4 + 13\psi^4x_1^5x_2^5x_3^5\omega_5 + 10\psi^2x_1^3x_2^3x_3^3x_4^3\omega_5\right]$$
$$+ \frac{1}{W}\left[\psi^9x_4\omega_4 - 35x_1x_2x_3x_4\omega_5\right] .$$

(A.50)

It is easy to see that the curve for $Y^{(10)}$ given in (4.1) can be obtained by the intersection $P' \cap Y^{(10)}$, with the plane

$$P' := \{x_1 = \alpha^\zeta x_2, \frac{1}{\sqrt{5}}\alpha^5x_3^5 + x_5 - \psi x_1x_2x_3x_4 = 0\}. \qquad \text{(A.51)}$$

By the principle mentioned in the footnote on page 125, we can (up to a sign) use either of the components of $P' \cap Y^{(10)}$, *i.e.*, either (4.1) or the curve $x_4^2 = 0$. The latter curve is

however also contained in the intersection of $Y^{(10)}$ with some different planes, and for incidental reasons, we prefer to present the evaluation of the integral in one of these alternative planes. More explicitly, the curve from (4.1) is equivalent to the curve

$$C_\zeta^\gamma := \{x_1 = i\zeta x_2, x_5 = i\frac{1}{5^{1/2}}x_3^5, x_4^2 = \gamma\sqrt{\zeta}\sqrt{5^{1/2}\psi}x_1 x_3^3\} \ , \tag{A.52}$$

with $\gamma = \pm 1$, which we obtain from $P \cap Y^{(10)}$, where P is related to P' via the coordinate transformation $x_5 \to x_5 + \psi x_1 x_2 x_3 x_4$. Similar as the curve for $Y^{(6)}$, the C_ζ curve splits into two components, i.e. $C_\zeta = C_\zeta^+ + C_\zeta^-$.

The component curves meet in three points:

$$p_1^\zeta = \{x_1 = i\zeta x_2, x_3 = x_4 = x_5 = 0\}, \ p_2 = \{x_5 = i\frac{1}{5^{1/2}}x_3^5, x_1 = x_2 = x_4 = 0\} \ . \tag{A.53}$$

In order to evaluate (A.11), we go to the local chart U_1 given by (A.13) and perform the following variable redefinitions:

$$T' \to i\zeta T \ , \ Y' \to i5^{-1/2}Y^{10} \ , \ X' \to (X + Y + Z)^2 \ ,$$
$$Z' \to \gamma^{1/2}\zeta^{1/4}(1 + 5^{1/24}\psi^{1/12}(Y + Z))^3 \ . \tag{A.54}$$

Then,

$$C_\zeta^\gamma = \{T = -1, X = -Z = \frac{1}{\sqrt{5^{1/12}\psi^{1/6}}}\} \ ,$$
$$p_1^\zeta = \{T = -1, X = -Z = \frac{1}{\sqrt{5^{1/12}\psi^{1/6}}}, Y = 0\} \ . \tag{A.55}$$

We define the tubes $T_\epsilon^{\zeta\gamma}$ via the normal vectors

$$v_{\zeta\gamma} = a_{\zeta\gamma}\partial_T - \frac{\gamma^{3/2}\zeta^{5/4}}{12 \cdot 5^{-3/8}}e^{-14i\phi}\partial_X + \frac{\gamma^{3/2}\zeta^{5/4}}{12 \cdot 5^{-3/8}}e^{-14i\phi}\partial_Z \ , \tag{A.56}$$

with

$$a_{\zeta\gamma} := \frac{f(r)}{1 + \gamma^{1/2}\zeta^{3/4}5^{-3/8}\psi^{5/4}Y^{15}} \ . \tag{A.57}$$

Then, we have

$$D_{v_{\zeta\gamma}}W|_{C_\zeta^\gamma} = f(r) + \psi^{5/4}r^{14} > 0 \ , \tag{A.58}$$

such that the tubes $T_\epsilon^{\zeta\gamma}$ are well defined and locally parameterized by

$$T = -1 + \tilde\epsilon a \ , \ X = -Z = \frac{1}{\sqrt{5^{1/12}\psi^{1/6}}} - \frac{\gamma^{3/2}\zeta^{5/4}}{12 \cdot 5^{-3/8}}e^{-14i\phi}\tilde\epsilon \ , \tag{A.59}$$

where $\tilde{\epsilon} = e^{i\chi}\epsilon$.

Let us now consider the forms ω_i: Going to the chart U_1 and restricting to $Y' = i5^{-1/2}X'^5$, we directly infer that $\omega_i = 0$ for $i \notin \{3, 5\}$ and that

$$\omega_3 = -dT' \wedge dY' \wedge dZ' \, , \ \omega_5 = -dT' \wedge dX' \wedge dZ' \, . \tag{A.60}$$

Thus,

$$w_5 = -i5^{-1/2}X'^{-4}w_3 = -dT' \wedge dX' \wedge dZ' \, . \tag{A.61}$$

Changing to the coordinates (A.54) then yields

$$dT' \wedge dX' \wedge dZ' = i\gamma^{1/2}\zeta^{1/4}6 \cdot 5^{1/24}\psi^{1/12}(X + Y + Z)(1 + 5^{1/24}\psi^{1/12}(Y + Z))^2 dT \wedge dX \wedge dZ \, . \tag{A.62}$$

Further,

$$dT \wedge dX \wedge dZ|_{T_\epsilon^{\zeta\gamma}} = -\frac{7}{6}5^{3/8}\gamma^{3/2}\zeta^{5/4}ae^{-13i\phi}\tilde{\epsilon}^2 \left(1 - \frac{rf'(r)}{14f(r)}\right) dr \wedge d\phi \wedge d\chi \, . \tag{A.63}$$

Hence,

$$w_5|_{T_\epsilon^{\zeta\gamma}} = i7 \cdot 5^{3/24}\psi^{1/12}ae^{-13i\phi}Y(1 + 5^{1/24}\psi^{1/12}(Y + Z))^2 \left(1 - \frac{rf'(r)}{14f(r)}\right) \tilde{\epsilon}^2 dr \wedge d\phi \wedge d\chi,$$

$$w_3|_{T_\epsilon^{\zeta\gamma}} = 7 \cdot 5^{15/24}\psi^{1/12}ae^{-13i\phi}Y^9(1 + 5^{1/24}\psi^{1/12}(Y + Z))^2 \left(1 - \frac{rf'(r)}{14f(r)}\right) \tilde{\epsilon}^2 dr \wedge d\phi \wedge d\chi. \tag{A.64}$$

After performing the explicit integration, we infer that we obtain contributions from the following terms occurring in $\tilde{\beta}^{(10)}$:

$$\int_{T_\epsilon^{\zeta\gamma}} \frac{6\psi^6 x_1^7 x_2^7 x_3^7 x_4^2 x_5^2 \omega_5}{W^4} = \zeta\frac{2}{5}\sqrt{5}\pi^2\psi^3 \, ,$$

$$\int_{T_\epsilon^{\zeta\gamma}} \frac{14\psi^5 x_1^6 x_2^6 x_3^6 x_4 x_5 \omega_5}{W^3} = -\zeta\frac{7}{5}\sqrt{5}\pi^2\psi^3 \, , \tag{A.65}$$

$$\int_{T_\epsilon^{\zeta\gamma}} \frac{13\psi^4 x_1^5 x_2^5 x_3^5 \omega_5}{W^2} = \zeta\frac{13}{5}\sqrt{5}\pi^2\psi^3 \, ,$$

where we have included an additional normalization factor of 10^{-1}.

With similar computations as above one can show that for chart U_2 (which includes p_2) no contribution arises.

Summing the contributions given in (A.65), we infer

$$\int_{T_\epsilon(C_\zeta^\gamma; p_1^\zeta)} \tilde{\beta} = \zeta\frac{8}{5}\sqrt{5}\pi^2\psi^3 \, . \tag{A.66}$$

It remains to show that the underlying assumption is correct: We have

$$n_{\zeta\gamma} = \gamma^{-1}\zeta^{-1/2}\frac{1}{4}5^{-1/4}\psi^{-3/2}\frac{x_4^2}{x_3}\left(\partial_3 - i5^{1/2}x_3^4\partial_5\right) \ . \tag{A.67}$$

Hence,

$$n_{\zeta\gamma}\omega = \gamma^{-1}\zeta^{-1/2}\frac{1}{4}5^{-1/4}\psi^{-3/2}\frac{x_4^2}{x_3}\left(\omega_3 - i5^{1/2}x_3^4\omega_5\right) = 0 \ , \tag{A.68}$$

where we used (A.61) .

Appendix B

Localization invariants of orientifolded local $\mathbb{P}^2$

This appendix lists the complete set of data obtained via localization for an orientifold of local $\mathbb{P}^2$ (see chapter 7). More specifically, we list the invariants $\tilde{n}_d^{(g,h)}$, $\tilde{n}_d^{(g,h)_k}$ defined in equation (6.7) and their combination to real Gromov-Witten invariants $n_d'^{(\chi)}$, as defined in equation (6.9).

Table 1

d	$\tilde{n}_d^{(0,2)}$	$\tilde{n}_d^{(1,0)}{}_k$	$n_d'^{(\chi=0)}$
2	$\frac{3}{8}$	$-\frac{3}{8}$	0
4	$-\frac{21}{16}$	$\frac{117}{16}$	6
6	$\frac{59}{4}$	$-\frac{411}{4}$	-88
8	$-\frac{5781}{32}$	$\frac{48981}{32}$	1350
10	$\frac{48939}{20}$	$-\frac{472779}{20}$	-21192

Table 2

d	$\tilde{n}_d^{(0,3)}$	$\tilde{n}_d^{(1,1)}$	$\tilde{n}_d^{(1,1)}{}_k$	$n_d'^{(\chi=1)}$
1	0	$\frac{1}{12}$	0	$\frac{1}{12}$
3	$-\frac{3}{16}$	$-\frac{3}{8}$	$\frac{9}{16}$	0
5	$\frac{9}{8}$	$\frac{3}{2}$	$-\frac{171}{8}$	$-\frac{39}{4}$
7	$-\frac{333}{16}$	$\frac{839}{24}$	$\frac{7047}{16}$	$\frac{5455}{12}$
9	$\frac{5415}{16}$	$-\frac{9995}{8}$	$-\frac{139509}{16}$	$-\frac{38521}{4}$

Table 3

d	$\tilde{n}_d^{(0,4)}$	$\tilde{n}_d^{(1,2)}$	$\tilde{n}_d^{(1,2)}{}_k$	$\tilde{n}_d^{(2,0)}{}_k$	$n_d'^{(\chi=2)}$
2	0	$-\frac{5}{128}$	0	$\frac{5}{128}$	0
4	$\frac{9}{64}$	$\frac{41}{64}$	$-\frac{27}{32}$	$\frac{33}{16}$	2
6	$-\frac{135}{128}$	$-\frac{81}{128}$	$\frac{2997}{64}$	$\frac{10953}{64}$	-126
8	$\frac{945}{32}$	$\frac{1673}{16}$	$-\frac{20115}{32}$	$\frac{223495}{32}$	5652
10	$-\frac{38025}{64}$	$\frac{145145}{32}$	$\frac{993195}{32}$	$-\frac{13926207}{64}$	-182618

Table 4

d	$\tilde{n}_d^{(0,5)}$	$\tilde{n}_d^{(1,3)}$	$\tilde{n}_d^{(2,1)}$	$\tilde{n}_d^{(1,3)}{}_k$	$\tilde{n}_d^{(2,1)}{}_k$	$n_d'^{(\chi=3)}$
1	0	0	$-\frac{7}{2880}$	0	0	$-\frac{7}{2880}$
3	0	$\frac{3}{128}$	$\frac{79}{2880}$	0	$-\frac{9}{128}$	$-\frac{7}{360}$
5	$-\frac{135}{1024}$	$-\frac{309}{256}$	$-\frac{59}{128}$	$\frac{675}{512}$	$-\frac{12723}{32}$	$-\frac{413}{32}$
7	$\frac{1323}{1280}$	$-\frac{195}{128}$	$\frac{2597}{720}$	$-\frac{11907}{128}$	$\frac{270585}{256}$	$\frac{2783151}{2880}$
9	$\frac{10935}{256}$	$\frac{33111}{128}$	$-\frac{205151}{240}$	$\frac{387099}{128}$	$-\frac{13252137}{256}$	$-\frac{47518049}{960}$

Table 5

d	$\tilde{n}_d^{(0,6)}$	$\tilde{n}_d^{(1,4)}$	$\tilde{n}_d^{(2,2)}$	$\tilde{n}_d^{(1,4)}{}_k$	$\tilde{n}_d^{(2,2)}{}_k$	$\tilde{n}_d^{(3,0)}{}_k$	$n_d'^{(\chi=4)}$
2	0	0	$\frac{11}{3072}$	0	0	$-\frac{11}{3072}$	0
4	0	$-\frac{33}{4096}$	$\frac{41}{12288}$	0	$\frac{99}{2048}$	$\frac{63}{512}$	$\frac{1}{6}$
6	$\frac{729}{5120}$	$\frac{2457}{2560}$	$\frac{10663}{1024}$	$-\frac{2187}{1024}$	$\frac{48897}{1024}$	$-\frac{70053}{512}$	$-\frac{169}{2}$
8	$-\frac{81}{80}$	$\frac{20781}{2048}$	$-\frac{389561}{30720}$	$\frac{2835}{16}$	$-\frac{4235175}{1024}$	$\frac{13298129}{512}$	13353
10	$\frac{2025}{32}$	$\frac{583185}{1024}$	$\frac{13173223}{3072}$	$-\frac{212625}{32}$	$\frac{120073203}{512}$	$-\frac{581900049}{512}$	$\frac{5429209}{6}$

Table 6

d	$\tilde{n}_d^{(0,7)}$	$\tilde{n}_d^{(1,5)}$	$\tilde{n}_d^{(2,3)}$	$\tilde{n}_d^{(3,1)}$	$\tilde{n}_d^{(1,5)}{}_k$	$\tilde{n}_d^{(2,3)}{}_k$	$\tilde{n}_d^{(3,1)}{}_k$	$n_d'^{(\chi=5)}$
1	0	0	0	$\frac{31}{483840}$	0	0	0	$\frac{31}{483840}$
3	0	0	$-\frac{87}{20480}$	$-\frac{6523}{1935360}$	0	0	$\frac{261}{20480}$	$-\frac{31}{6048}$
5	0	$\frac{747}{40960}$	$\frac{3259}{10240}$	$\frac{4691}{15360}$	0	$\frac{747}{4096}$	$\frac{123311}{40960}$	$\frac{2665}{768}$
7	$-\frac{27783}{163840}$	$-\frac{401481}{81920}$	$-\frac{476291}{20480}$	$-\frac{667343}{69120}$	$\frac{583443}{163840}$	$-\frac{4921425}{32768}$	$\frac{212582451}{163840}$	$\frac{15384587}{13824}$
9	$\frac{531441}{573440}$	$-\frac{1515591}{40960}$	$-\frac{465417}{20480}$	$-\frac{239350813}{645120}$	$\frac{27103491}{81920}$	$\frac{215009073}{16384}$	$-\frac{14079900303}{81920}$	$-\frac{3675141313}{23040}$

Table 7

d	$\tilde{n}_d^{(0,8)}$	$\tilde{n}_d^{(1,6)}$	$\tilde{n}_d^{(2,4)}$	$\tilde{n}_d^{(3,2)}$	$\tilde{n}_d^{(1,6)}{}_k$	$\tilde{n}_d^{(2,4)}{}_k$	$\tilde{n}_d^{(3,2)}{}_k$	$\tilde{n}_d^{(4,0)}{}_k$	$n_d'^{(\chi=6)}$
2	0	0	0	$-\frac{101}{294912}$	0	0	0	$\frac{101}{294912}$	0
4	0	0	$\frac{407}{81920}$	$\frac{2683}{184320}$	0	0	$-\frac{1221}{40960}$	$\frac{3893}{245760}$	$\frac{1}{180}$
6	0	$\frac{11583}{163840}$	$\frac{57861}{32768}$	$\frac{594553}{122880}$	0	$-\frac{34749}{32768}$	$\frac{3926367}{163840}$	$-\frac{15301627}{245760}$	$-\frac{1961}{60}$
8	$\frac{243}{1120}$	$\frac{830871}{81920}$	$\frac{21059243}{20480}$	$\frac{850621349}{5160960}$	$-\frac{243}{40}$	$\frac{69909435}{16384}$	$-\frac{595150251}{81920}$	$\frac{2072508751}{73728}$	$\frac{215387}{10}$

Table 8

d	$\tilde{n}_d^{(0,9)}$	$\tilde{n}_d^{(1,7)}$	$\tilde{n}_d^{(2,5)}$	$\tilde{n}_d^{(3,3)}$	$\tilde{n}_d^{(4,1)}$	$\tilde{n}_d^{(1,7)}{}_k$	$\tilde{n}_d^{(2,5)}{}_k$	$\tilde{n}_d^{(3,3)}{}_k$	$\tilde{n}_d^{(4,1)}{}_k$	$n_d'^{(\chi=7)}$
1	0	0	0	0	$-\frac{127}{77414400}$	0	0	0	0	$-\frac{127}{77414400}$
3	0	0	0	$\frac{3001}{3440640}$	$\frac{42589}{77414400}$	0	0	0	$-\frac{3001}{1146880}$	$\frac{1651}{1382400}$
5	0	0	$-\frac{3063}{327680}$	$\frac{342169}{3440640}$	$-\frac{128899}{1720320}$	0	0	$\frac{3063}{32768}$	$-\frac{2981749}{6881280}$	$-\frac{450397}{450160}$
7	0	$-\frac{326295}{1835008}$	$-\frac{22995213}{3276800}$	$-\frac{29732123}{688128}$	$-\frac{342951779}{15482880}$	0	$\frac{978885}{262144}$	$\frac{1800922047}{1835008}$	$-\frac{166848327}{1310720}$	$\frac{60794346311}{77414400}$

Table 9

d	$\tilde{n}_d^{(0,10)}$	$\tilde{n}_d^{(1,8)}$	$\tilde{n}_d^{(2,6)}$	$\tilde{n}_d^{(3,4)}$	$\tilde{n}_d^{(4,2)}$	$\tilde{n}_d^{(1,8)}{}_k$	$\tilde{n}_d^{(2,6)}{}_k$	$\tilde{n}_d^{(3,4)}{}_k$	$\tilde{n}_d^{(4,2)}{}_k$	$\tilde{n}_d^{(5,0)}{}_k$	$n_d'^{(\chi=8)}$
2	0	0	0	0	$\frac{2801}{82575360}$	0	0	0	0	$-\frac{2801}{82575360}$	0
4	0	0	0	$-\frac{92219}{55050240}$	$-\frac{664337}{165150720}$	0	0	0	$\frac{92219}{9175040}$	$-\frac{58547}{13762560}$	$\frac{1}{10080}$
6	0	0	$\frac{210519}{6553600}$	$\frac{7386879}{9175040}$	$\frac{83671439}{34406400}$	0	0	$-\frac{631557}{1310720}$	$\frac{65748309}{9175040}$	$-\frac{246136403}{13762560}$	$-\frac{1269}{160}$

Table 10

d	$\tilde{n}_d^{(0,11)}$	$\tilde{n}_d^{(1,9)}$	$\tilde{n}_d^{(2,7)}$	$\tilde{n}_d^{(3,5)}$	$\tilde{n}_d^{(4,3)}$	$\tilde{n}_d^{(5,1)}$	$\tilde{n}_d^{(1,9)}{}_k$	$\tilde{n}_d^{(2,7)}{}_k$	$\tilde{n}_d^{(3,5)}{}_k$	$\tilde{n}_d^{(4,3)}{}_k$	$\tilde{n}_d^{(5,1)}{}_k$	$n_d'^{(\chi=9)}$
1	0	0	0	0	0	$-\frac{73}{1751777280}$	0	0	0	0	0	$-\frac{73}{1751777280}$
3	0	0	0	0	$-\frac{10439}{55050240}$	$\frac{2596829}{24524881920}$	0	0	0	0	$\frac{10439}{18350080}$	$\frac{29993}{10948608}$
5	0	0	0	$\frac{44767}{18350080}$	$\frac{293957}{27525120}$	$-\frac{1902379}{1362493440}$	0	0	0	$-\frac{44767}{1835008}$	$\frac{744361}{55050240}$	$-\frac{509857}{19464192}$

Table B.1: Localization invariants of an orientifold of local $\mathbb{P}^2$ and their summation to real Gromov-Witten invariants.

Appendix C

Real Gopakumar-Vafa invariants of local $\mathbb{P}^2$

In this appendix, we collect the real Gopakumar-Vafa invariants of local $\mathbb{P}^2$ calculated via the three complementary techniques outlined in part III of this thesis. The invariants obtained via the three different schemes are in perfect agreement. Note that there is an overall sign ambiguity in the invariants, which we were not able to fix with our considerations. This ambiguity might be fixed via a mathematical more rigorous localization calculation than we performed in chapter 7.

$d \setminus \chi$	-1	0	1	2	3	4
1	$-1^\diamond$		0^*		0^*	
2		0^*		0^*		0^*
3	$1^\diamond$		0^*		0^*	
4		3^*		1^*		0^*
5	$-5^\diamond$		-10^*		-6^*	
6		-44^*		-63^*		-37^*
7	$42^\diamond$		229^*		474^*	
8		675^*		2826^*		6641^*
9	$-429^\diamond$		-4833^*		-24547^*	
10		-10596^*		-91309^*		-444825^*
11	$4939^\diamond$		96823^*		$922904^\diamond$	
12		$169815^\diamond$		$2548446^\diamond$		$22222821^\diamond$
13	-61555		$-1890640^\diamond$		$-29568178^\diamond$	
14		$-2766312^\diamond$		$-65141982^\diamond$		$-907236837^\diamond$
15	811445		36355693		855398125	
16		45651033		1571061879		32383098135
17	-11154329		-692134092		-23061556312	
18		-761270252		-36357840387		-1049953473666
19	158387705		13085426739		590387680935	
20		12804181968		815896308217		31671654196277
21	-2308018713		-246141639751		-14527282829907	
22		216905448900		-17878517912137		-903161239605882
23	34350229129		4612322986757		346447571899667	
24		3696709999475		384413718899808		24622104921447319
25	-520291543850		-86171027900880		-8055204030496600	
26		-63329911074864		-8138918187959256		-646992872220979059
27	7998433661880		1606102217387496		183404890744633392	
28		1089804320192328		170128830773159693		16487461934782290071
29	-124530193132562		-29877825751921400		-4102926664405466446	
30		-18827327577603608		-3518103635914287426		-409393336266808069759

Table C.1: $\hat{N}_d^{(\chi)}$ for high d obtained from the B-model (numbers marked with $\diamond$ have been verified via the real topological vertex, numbers marked with * in addition via localization).

$d \setminus \chi$	5	6	7	8	9
1	0^*		0^*		0^*
2		0^*		0^*	
3	0^*		0^*		0^*
4		0^*		0^*	
5	-1^*		0^*		0^*
6		-10^*		-1^*	
7	497^*		286^*		$91^\diamond$
8		9688^*		$9909^\diamond$	
9	-76685^*		$-162007^\diamond$		$-240214^\diamond$
10		$-1490889^\diamond$		$-3622074^\diamond$	
11	$5689826^\diamond$		$24839317^\diamond$		$80024538^\diamond$
12		$138741207^\diamond$		$660614879^\diamond$	
13	$-309836946^\diamond$		$-2387676377^\diamond$		$-14155255239^\diamond$
14		$-9250663299^\diamond$		$-73688144692^\diamond$	
15	13813050354		167924131768		1606774464538
16		496417243815		6048297221530	
17	-536811735677		-9568553947097		-136513807781008
18		-22814962465032		-399056811636330	
19	18866208478280		467697511728963		9398297970384222
20		933580323856212		22370764847588270	
21	-613983765096754		-20339969314765719		-551685003357975980
22		-34902135604573377		-1105187697763665228	
23	18804234985799241		806808827756109811		28574033239468010587
24		1213849008767132251		49357611086785857295	
25	-548264953334411255		-29708534211072505345		-1337857466210942972595
26		-3979202838046156548		-2029790874827662119329	
27	15348471706637436099		1028783168774451701259		57640797365862616605714
28		1241733288505925189151		77934424856611454475555	
29	-415237415601455194036		-33835984504174543688472		$-2316194195443332049565232$
30		-37166974728897157340684		$-28235781495282461942595 86$	

Table C.2: $\hat{N}_d^{(\chi)}$ for high d obtained from the B-model (numbers marked with $^\diamond$ have been verified via the real topological vertex, numbers marked with * in addition via localization).

χ \ d	6	7	8	9	10	11	12	13	14
10			6882		-6527094		2470331689		-472060307393
11		-15	254935			-195123249		66336579865	
12			3214		-8853482		7384195595		-2473627288265
13		-1		195943		-366754317		250379339074	
14			988		-9136211		17862370096		-10728530219814
15				109614		-539107092		771890474372	
16			191		-7226144		35296981346		-38871359145408
17				44507		-626854392		1965636872695	
18			21		-4398773		57410786270		-118572379592483
19				12949		-581661131		4173449453891	
20			1		-2061527		77347818109		-306601937181157
21				2626		-433433895		7446682383581	
22					-740639		86771638286		-676198602671642
23				352		-260366065		11241439498902	
24					-201867		81398541770		-1279073229693409
25				28		-126238105		14438862544045	
26					-40953		64054115660		-2085518321405375
27				1		-49322461		15854057302183	
28					-5985		42371627534		-2944249848639372
29						-15453034		14938241580054	
30					-595		23582667480		-3613212254655871
31						-3847413		12114187918765	
32					-36		11038869636		-3867758515991016
33						-750175		8473209466017	
34					-1		4337601572		-3621885665305630
35						-111971		5118273430606	
36							1425576149		-2974100596675286
37						-12342		2671254703769	
38							389623263		-2145509291350998
39						-946		1204005379440	
40							87807601		-1361557832849019
41						-45		467997216591	
42							16121003		-760697816260927
43						-1		156480858834	
44							2369885		-374239613900020
45								44835729183	
46							272051		-162059929797276
47								10949573048	
48							23479		-61706256970277
49								2262530362	
50							1432		-20621959046012
51								391668488	
52							55		-6032986939113
53								56047228	
54							1		-1539443942273
55								6508822	
56									-340986604623
57								597618	
58									-65152049938
59								41728	
60									-10651137069
61								2081	
62									-1474076916
63								66	
64									-170289956
65								1	
66									-16111390
67									
68									-1215524
69									
70									-70301
71									
72									-2926
73									
74									-78
75									
76									-1
77									

Table C.3: $\hat{N}_d^{(\chi)}$ for high χ obtained via the real topological vertex.

Bibliography

[1] M. B. Green, J. H. Schwarz and E. Witten, "Superstring Theory Vol. 1 & 2," *Cambridge, Uk: Univ. Pr. (1987)*

D. Lüst and S. Theisen, Lect. Notes Phys. **346**, 1 (1989).

J. Polchinski, "String theory. Vol. 1 & 2," *Cambridge, UK: Univ. Pr. (1998)*

[2] R. Blumenhagen, B. Kors, D. Lüst and S. Stieberger, "Four-dimensional String Compactifications with D-Branes, Orientifolds and Fluxes," Phys. Rept. **445**, 1 (2007) [arXiv:hep-th/0610327].

[3] K. Hori *et al.*, "Mirror symmetry," *Providence, USA: AMS (2003) 929 p*

[4] W. Lerche, "Special geometry and mirror symmetry for open string backgrounds with N = 1 supersymmetry," arXiv:hep-th/0312326.

[5] M. Aganagic and C. Vafa, "Mirror symmetry, D-branes and counting holomorphic discs," arXiv:hep-th/0012041.

[6] W. Lerche, P. Mayr and N. Warner, "Holomorphic N = 1 special geometry of open-closed type II strings," arXiv:hep-th/0207259.

[7] W. Lerche, P. Mayr and N. Warner, "N = 1 special geometry, mixed Hodge variations and toric geometry," arXiv:hep-th/0208039.

[8] H. Jockers and W. Lerche, "Matrix Factorizations, D-Branes and their Deformations," Nucl. Phys. Proc. Suppl. **171** (2007) 196 [arXiv:0708.0157 [hep-th]].

[9] D. R. Morrison and J. Walcher, "D-branes and Normal Functions," arXiv:0709.4028 [hep-th].

[10] J. Walcher, "Opening mirror symmetry on the quintic," Commun. Math. Phys. **276**, 671 (2007) [arXiv:hep-th/0605162].

[11] D. Krefl and J. Walcher, "Real Mirror Symmetry for One-parameter Hypersurfaces," JHEP **0809** (2008) 031 [arXiv:0805.0792 [hep-th]].

[12] R. Gopakumar and C. Vafa, "M-theory and topological strings. I," arXiv:hep-th/9809187.

[13] R. Gopakumar and C. Vafa, "M-theory and topological strings. II," arXiv:hep-th/9812127.

[14] H. Ooguri and C. Vafa, "Knot invariants and topological strings," Nucl. Phys. B **577** (2000) 419 [arXiv:hep-th/9912123].

[15] A. Neitzke and C. Vafa, "Topological strings and their physical applications," arXiv:hep-th/0410178.

[16] M. Marino, "Chern-Simons theory and topological strings," Rev. Mod. Phys. **77** (2005) 675 [arXiv:hep-th/0406005].

[17] J. Walcher, "Evidence for Tadpole Cancellation in the Topological String," arXiv:0712.2775 [hep-th].

[18] D. Krefl and J. Walcher, "The Real Topological String on a local Calabi-Yau," arXiv:0902.0616 [hep-th].

[19] D. R. Morrison, "Picard-Fuchs equations and mirror maps for hypersurfaces," arXiv:hep-th/9111025.

[20] A. Klemm and S. Theisen, "Considerations of one modulus Calabi-Yau compactifications: Picard-Fuchs equations, Kahler potentials and mirror maps," Nucl. Phys. B **389** (1993) 153 [arXiv:hep-th/9205041].

[21] A. Font, "Periods and duality symmetries in Calabi-Yau compactifications," Nucl. Phys. B **391**, 358 (1993) [arXiv:hep-th/9203084].

[22] P. Candelas, X. C. De La Ossa, P. S. Green and L. Parkes, "A pair of Calabi-Yau manifolds as an exactly soluble superconformal theory," Nucl. Phys. B **359**, 21 (1991).

[23] R. Roiban, C. Romelsberger and J. Walcher, "Discrete torsion in singular G(2)-manifolds and real LG," Adv. Theor. Math. Phys. **6**, 207 (2003) [arXiv:hep-th/0203272].

[24] S. Kachru, S. H. Katz, A. E. Lawrence and J. McGreevy, "Open string instantons and superpotentials," Phys. Rev. D **62**, 026001 (2000) [arXiv:hep-th/9912151].

[25] K. Fukaya, Y.-G. Oh, H. Ohta and K. Ono, "Lagrangian intersection Floer theory—anomaly and obstruction", preprint (2000)

[26] J. Walcher, unpublished

[27] J. Walcher, "Stability of Landau-Ginzburg branes," J. Math. Phys. **46**, 082305 (2005) [arXiv:hep-th/0412274].

[28] I. Brunner, K. Hori, K. Hosomichi and J. Walcher, "Orientifolds of Gepner models," JHEP **0702**, 001 (2007) [arXiv:hep-th/0401137].

[29] M. Aganagic, A. Klemm and C. Vafa, "Disk instantons, mirror symmetry and the duality web," Z. Naturforsch. A **57** (2002) 1 [arXiv:hep-th/0105045].

[30] J. Walcher, "Extended Holomorphic Anomaly and Loop Amplitudes in Open Topological String," arXiv:0705.4098 [hep-th].

[31] M. Bershadsky, S. Cecotti, H. Ooguri and C. Vafa, "Kodaira-Spencer theory of gravity and exact results for quantum string amplitudes," Commun. Math. Phys. **165** (1994) 311 [arXiv:hep-th/9309140].

[32] M. Bershadsky, S. Cecotti, H. Ooguri and C. Vafa, "Holomorphic anomalies in topological field theories," Nucl. Phys. B **405**, 279 (1993) [arXiv:hep-th/9302103].

[33] J. M. F. Labastida, M. Marino and C. Vafa, "Knots, links and branes at large N," JHEP **0011** (2000) 007 [arXiv:hep-th/0010102].

[34] M. x. Huang, A. Klemm and S. Quackenbush, "Topological String Theory on Compact Calabi-Yau: Modularity and Boundary Conditions," arXiv:hep-th/0612125.

[35] R. Pandharipande, J. Solomon and J. Walcher, "Disk enumeration on the Quintic 3-fold," J. Am. Math. Soc. (2008) [arXiv:math/0610901]

[36] J. P. Solomon "Intersection theory on the moduli space of holomorphic curves with Lagrangian boundary conditions," arxiv:math.sg/0606429

[37] N. P. Warner, "Supersymmetry in boundary integrable models," Nucl. Phys. B **450** (1995) 663 [arXiv:hep-th/9506064].

[38] A. Recknagel and V. Schomerus, "D-branes in Gepner models," Nucl. Phys. B **531**, 185 (1998) [arXiv:hep-th/9712186].

[39] I. Brunner and V. Schomerus, "D-branes at singular curves of Calabi-Yau compactifications," JHEP **0004**, 020 (2000) [arXiv:hep-th/0001132].

[40] J. Fuchs, C. Schweigert and J. Walcher, "Projections in string theory and boundary states for Gepner models," Nucl. Phys. B **588**, 110 (2000) [arXiv:hep-th/0003298].

[41] K. Hori and J. Walcher, "D-branes from matrix factorizations," Comptes Rendus Physique **5**, 1061 (2004) [arXiv:hep-th/0409204].

[42] D. Orlov, "Derived categories of coherent sheaves and triangulated categories of singularities," arXiv:math-ag/0503632.

[43] M. Herbst, K. Hori and D. Page, "Phases Of N=2 Theories In 1+1 Dimensions With Boundary," arXiv:0803.2045 [hep-th].

[44] W. Fulton, "Intersection theory," Springer, 1998

[45] M. Kontsevich, "Enumeration Of Rational Curves Via Torus Actions," arXiv:hep-th/9405035.

[46] T. Graber and E. Zaslow, "Open string Gromov-Witten invariants: Calculations and a mirror 'theorem'," arXiv:hep-th/0109075.

[47] D. E. Diaconescu, B. Florea and A. Misra, "Orientifolds, unoriented instantons and localization," JHEP **0307** (2003) 041 [arXiv:hep-th/0305021].

[48] A. Klemm and E. Zaslow, "Local mirror symmetry at higher genus," arXiv:hep-th/9906046.

[49] P. Mayr, "Summing up open string instantons and N = 1 string amplitudes," arXiv:hep-th/0203237.

[50] M. Aganagic, A. Klemm, M. Marino and C. Vafa, "The topological vertex," Commun. Math. Phys. **254** (2005) 425 [arXiv:hep-th/0305132].

[51] V. Bouchard, B. Florea and M. Marino, "Counting higher genus curves with crosscaps in Calabi-Yau orientifolds," JHEP **0412** (2004) 035 [arXiv:hep-th/0405083].

[52] V. Bouchard, B. Florea and M. Marino, "Topological open string amplitudes on orientifolds," JHEP **0502** (2005) 002 [arXiv:hep-th/0411227].

[53] M. x. Huang and A. Klemm, "Holomorphic anomaly in gauge theories and matrix models," JHEP **0709** (2007) 054 [arXiv:hep-th/0605195].

[54] B. Haghighat, A. Klemm and M. Rauch, "Integrability of the holomorphic anomaly equations," JHEP **0810**, 097 (2008) [arXiv:0809.1674 [hep-th]].

[55] B. Eynard and N. Orantin, "Algebraic methods in random matrices and enumerative geometry," arXiv:0811.3531 [math-ph].

[56] D. A. Cox and S. Katz, "Mirror symmetry and algebraic geometry," *Providence, USA: AMS (2000) 469 p*

[57] T. Graber and R. Pandharipande, "Localization of Virtual Classes," arXiv:math-ag/9708001.

[58] C. Faber, "Algorithm for Computing Intersection Numbers on Moduli Spaces of Curves, with an Application to the Class of the Locus of the Jacobians," arXiv:math-ag/9706006.

[59] M. Aganagic, M. Marino and C. Vafa, "All loop topological string amplitudes from Chern-Simons theory," Commun. Math. Phys. **247** (2004) 467 [arXiv:hep-th/0206164].

[60] A. Iqbal, "All genus topological string amplitudes and 5-brane webs as Feynman diagrams," arXiv:hep-th/0207114.

[61] D. E. Diaconescu and B. Florea, "Localization and gluing of topological amplitudes," Commun. Math. Phys. **257** (2005) 119 [arXiv:hep-th/0309143].

[62] E. Witten, "Topological Sigma Models," Commun. Math. Phys. **118** (1988) 411.

[63] I. Antoniadis, E. Gava, K. S. Narain and T. R. Taylor, "Topological amplitudes in string theory," Nucl. Phys. B **413**, 162 (1994) [arXiv:hep-th/9307158].

[64] I. Antoniadis and S. Hohenegger, "Topological amplitudes and physical couplings in string theory," Nucl. Phys. Proc. Suppl. **171** (2007) 176 [arXiv:hep-th/0701290].

[65] M. Vonk, "A mini-course on topological strings," arXiv:hep-th/0504147.

[66] S. Yamaguchi and S. T. Yau, "Topological string partition functions as polynomials," JHEP **0407** (2004) 047 [arXiv:hep-th/0406078].

[67] P. L. H. Cook, H. Ooguri and J. Yang, "New Anomalies in Topological String Theory," arXiv:0804.1120 [hep-th].

[68] Y. Konishi and S. Minabe, "On solutions to Walcher's extended holomorphic anomaly equation," arXiv:0708.2898 [math.AG].

[69] M. Alim and J. D. Lange, "Polynomial Structure of the (Open) Topological String Partition Function," JHEP **0710**, 045 (2007) [arXiv:0708.2886 [hep-th]].

[70] D. Ghoshal and C. Vafa, "C = 1 String As The Topological Theory Of The Conifold," Nucl. Phys. B **453**, 121 (1995) [arXiv:hep-th/9506122].

[71] H. Ooguri and C. Vafa, "Worldsheet Derivation of a Large N Duality," Nucl. Phys. B **641**, 3 (2002) [arXiv:hep-th/0205297].

[72] C. Vafa, "A Stringy test of the fate of the conifold," Nucl. Phys. B **447**, 252 (1995) [arXiv:hep-th/9505023].

Curriculum Vitae

Daniel Krefl

born 26.01.1980 in Bergisch Gladbach, Germany.

Graduate studies

April 2009 - Aug. 2009   *Max-Planck-Institut für Physik* (Werner-Heisenberg Institut)
Munich, Germany

Oct. 2007 - April 2009   *Organisation européenne pour la recherche nucléaire* (CERN)
Genève, Switzerland
Advisor: Prof. Dr. Wolfgang Lerche

Nov. 2006 - Dec. 2006   *Organisation européenne pour la recherche nucléaire* (CERN)
Genève, Switzerland
Advisor: Prof. Dr. Angel M. Uranga

Oct. 2006 - Oct. 2007   *Max-Planck-Institut für Physik* (Werner-Heisenberg Institut)
Munich, Germany

Oct. 2006 - July 2009   PhD student at the *Arnold-Sommerfeld-Center* (ASC) der
Ludwig-Maximilians-Universität (LMU), Munich, Germany
Advisor: Prof. Dr. Dieter Lüst

Undergraduate studies

Aug. 2005 - Aug. 2006 Diplom student at the *Arnold-Sommerfeld-Center* (ASC) der
Ludwig-Maximilians-Universität (LMU), Munich, Germany
Advisors: Prof. Dr. Dieter Lüst and Prof. Dr. Hans-Peter Nilles

Feb. 2004 - Dec. 2004 *Australian National University* (ANU), Canberra, Australia
Studies in physics and mathematics
Advisor: Prof. Dr. Sergey Sergeev

Oct. 2001 - Aug. 2006 *Universität Bonn*, Germany
Studies in physics

Oct. 2000 - Aug. 2002 *Universität Bonn*, Germany
Studies in computer science

Fellowships and scholarships

Oct. 2007 - April 2009 *Marie-Curie* fellowship of the European Union

Feb. 2004 - Dec. 2004 Scholarship of the *Deutscher Akademischer Austauschdienst*

Acknowledgments